Spring 2014

Supramolecular catalysis, discrete aromatic stacks and sequential reactions in the organic solid state

Jelena Stojakovic
University of Iowa

SUPRAMOLECULAR CATALYSIS, DISCRETE AROMATIC STACKS AND SEQUENTIAL REACTIONS IN THE ORGANIC SOLID STATE

by

Jelena Stojakovic

A thesis submitted in partial fulfillment
of the requirements for the Doctor of
Philosophy degree in Chemistry
in the Graduate College of
The University of Iowa

May 2014

Thesis Supervisor: Professor Leonard R. MacGillivray

Graduate College
The University of Iowa
Iowa City, Iowa

CERTIFICATE OF APPROVAL

_____

PH.D. THESIS

_____

This is to certify that the Ph.D. thesis of

Jelena Stojakovic

has been approved by the Examining Committee
for the thesis requirement for the Doctor of Philosophy
degree in Chemistry at the May 2014 graduation.

Thesis Committee: _____
Leonard R. MacGillivray, Thesis Supervisor

_____
Daniel M. Quinn

_____
Geoff G. Z. Zhang

_____
F. Christopher Pigge

_____
Edward G. Gillan

To my mentors, family, friends and princess

I do not think there is any thrill that can go through the human heart like that felt by the inventor as he sees some creation of the brain unfolding to success... such emotions make a man forget food, sleep, friends, love, everything.

Nikola Tesla

ACKNOWLEDGMENTS

I would like to express gratitude to my advisor Len MacGillivray whose care and patience guided me through my studies and life over last five years. I was also fortunate to share my years as a PhD student with wonderful MacGillivray group members Kristin, Rebecca, Katie, Jake, Michael, Beth, John, Poonam, Saikat, Joe, Manza and Nam. A lot of work in this thesis was done by my hardworking and talented undergrads Brian, Avery, Jacob and Taylor. Unfortunately, I just recently started working with Shawna and Roxy and I already wish I had more time to spend with them in the lab. The one, who helped me the most during my first months in Iowa, was undoubtedly Krešo. I would also like to thank our collaborators Jonas, Geoff and Rodger, and our crystallographer Dr. Dale Swenson.

I would never find my way to Iowa, if it was not for prof. Judaš. I am grateful for my family that provided for me and gave me education. My friends gave me support and confidence when I needed it the most.

ABSTRACT

The organic solid state is becoming more widely utilized to synthesize molecules that are inaccessible or difficult to realize from the liquid phase. A solid-state synthesis provides strict control of both geometry and stereochemistry. While essential for efficient and sustainable organic syntheses, catalysis in the organic solid state is expected to be difficult to achieve due to low diffusion rates of molecules in the crystals. However, recently a ditopic receptor was used as a small-molecule supramolecular catalyst to direct a topochemical [2+2] photodimerization of an olefin. To achieve catalytic turnover, mechanochemistry, in the form of a manual mortar-and-pestle dry grinding, had to be employed. A main obstacle in the manual grinding method is the fact that the mechanochemistry and photoreaction are conducted separately. Thus, an automated method that enables simultaneous grinding and irradiation would be preferred. However, such technology is not commercially available. We have developed a simple, readily accessible, and automated method to achieve the mechanochemical preparation of supramolecular materials. Importantly, method enables simultaneous grinding and irradiation. In effect, the vortex grinding serves as a ball mill that is UV irradiation transparent. The vortex method has been applied to the preparation of cocrystal and metal organic frameworks, as well as supramolecular catalysis. When conducted using vortex method, supramolecular catalysis proceeds four time faster than when conducted using manual grinding. Accelerated rate of catalysis is attributed to combination of external stress exerted by grinding and internal stress arising from photoreaction.

The scope of supramolecular catalysis is expanded to reaction of 2,2’-bpe, catalyzed by a similar ditopic receptor res. Importantly, in this system catalytic turnover proceeds spontaneously. The mechanism of catalysis was investigated using X-ray diffraction studies and gas-phase DFT calculations. The studies uncovered that 2,2’-bpe

and 2,2'-tpcb undergo rotational motion to release accumulated stress akin to action of a supramolecular torsional spring.

We report an integration of aromatic stacks into discrete assemblies based on hydrogen bonds in the solid state. We used indolo[2,3-*a*]carbazole to organize aromatics into double, triple, and quadruple stacks within cocrystals. We also showed that aromatics within quadruple stack undergo topochemical [2+2] photodimerization to give a single photoproduct stereoselectively in up to maximal yield.

We reveal the first example of a product of a templated solid-state that acts as a template in subsequent reaction. Both reactions proceed in 100% yield and stereoselectively. We also report the unique case of polymorphism where both polymorphs are photoreactive and within one polymorph photoreaction proceeds in SCSC manner.

Due to effects of crystal packing, homology in solid state is difficult to achieve. We present the application of the template screening approach to solid-state photoreactivity among all olefins of a homologous series. To assess electronic effects of substituents on stability and hydrogen bonds of assemblies, we preformed gas-phase DFT calculations on a series of substituted assemblies. We found, that the strength of hydrogen-bonding varies and correlates with electronic nature of the substituents.

Lastly, we incorporated principles of supramolecular chemistry, solid-state reactivity, green chemistry and sustainability in undergraduate curriculum. In particular, students employ supramolecular chemistry to control photoreactivity in the organic solid state using the template approach. To form supramolecular assemblies, mechanochemistry, in form of mortar-and-pestle grinding, is used. To study reactivity in crystals, X-ray diffraction is used. Students are involved in all steps necessary to obtain crystal structure: growing suitable crystals, selection of the best crystals, data collection, solution, refinement and analysis of the crystal structures. Overall, students have hands-down experience in all aspects of crystallography. Although essential in chemical,

biochemical, pharmaceutical and materials science, crystallography is rarely taught in undergraduates laboratories.

TABLE OF CONTENTS

LIST OF TABLES

LIST OF FIGURES

CHAPTER 1. INTRODUCTION

1.1 Supramolecular chemistry

'*Chemistry beyond molecules*' is probably the most popular term used when describing supramolecular chemistry. However, the term is somewhat vague and supramolecular chemistry is better defined as "*the chemistry of the intermolecular bond, covering the structures and functions of the entities formed by association of two or more chemical species*" (J.-M. Lehn, 1987, Nobel Lecture).[1] While classical covalent chemistry focuses on formation and breaking of covalent bonds as a means to construct new chemical entities, supramolecular chemistry focuses on reversible non-covalent interactions between chemical entities that determine function of the whole assembly (Fig. 1). The goal of supramolecular chemistry is to control structural and dynamic properties of matter. To master supramolecular chemistry, all resources of classical molecular chemistry must be employed in combination with high-level control of non-covalent interactions.[2]

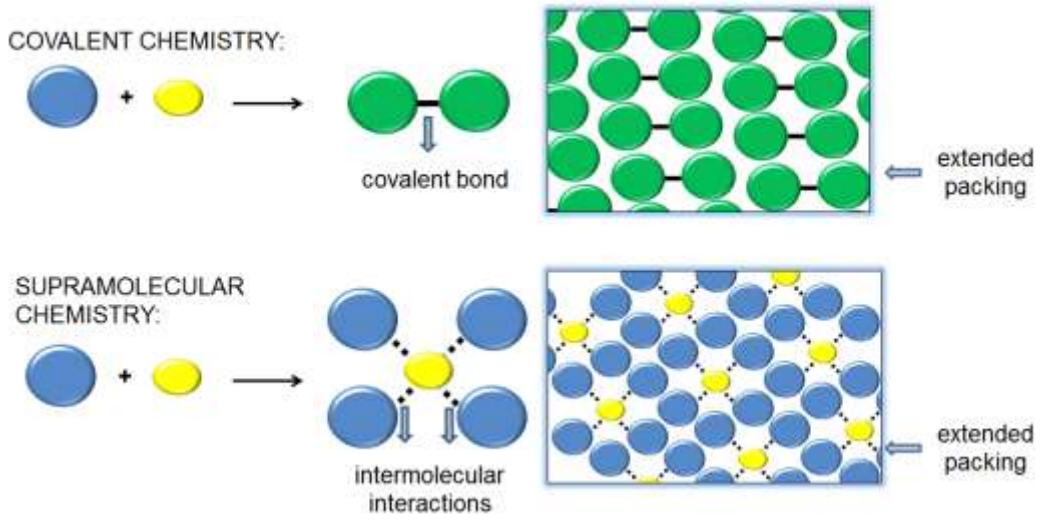

Figure 1 Covalent vs. supramolecular chemistry.

First one to propose existence of intermolecular forces was J. D. van der Waals in late 19th century.[3] Another leap in development of supramolecular chemistry was idea of "lock and key" enzyme-substrate interaction proposed by E. Fischer.[4] In 1930s, German term "*Übermoleküle*" (supermolecule) was coined to describe higher organization resulting from the association of coordinatively saturated species.[5] Development of ideas of intermolecular interactions lead to correct double helical structure of natural macromolecule DNA being reported in 1950s,[6] and in 1960s C. J. Pedersen worked on synthetic macrocyclic crown ethers.[7] Following the development of sophisticated and selective host-gest complexes, 1987 Nobel Chemistry Prize was awarded to D. J. Cram, J.-M. Lehn and C. J. Pedersen acknowledging their work and advances in the area of supramolecular chemistry. The next chapter in the field of supramolecular chemistry was marked by mechanically interlocked molecules, developed by J. F. Stoddart in 1990s, that are basis for molecular machinery.[8] Nowadays, supramolecular chemistry plays a critical role in development of advanced new materials, nanotechnology, catalysis, drug delivery, synthetic molecular logic gates and semi-synthetic DNA computers.[9]

As a consequence of subtleness of intermolecular interactions, supramolecular chemistry is intrinsically dynamic. In particular, non-covalent interactions are reversible and have very low or even zero, activation energy for formation. Thus, unlike in the case of covalent bond, rate of formation is not increased with temperature. In fact, high temperatures break supramolecular interaction. The thermodynamics of supramolecular chemistry is perhaps best illustrated in example of warm-blooded living organisms which can only survive in relatively narrow temperature range.

The dynamic nature of supramolecular chemistry is basis of self-organization. Self-organization refers to any system capable to form functional, well-defined, and often complex architectures upon self-assembly. The described process, combined with adaptive selection and variations gave rise to entire material universe, from simple atoms to living organisms.[10] More recently, these ideas and principles became a basis of what is

known as *Constitutional Dynamic Chemistry*. The dynamic approach of self-selection is in contrast to more traditional approach based on designed, target oriented self-assembly.[11]

Supramolecular interactions are basis of processes that occur in biology (e.g., highly specific substrate-protein recognition, translation and transcription of genetic code and signal induction of neurotransmitters).[12,13] Biologically processes display astonishing efficiency and precision and involve extremely complex architectures and systems. Such systems would be inconceivably difficult to design using only traditional covalent synthesis. For these reasons, supramolecular chemistry is seen as a route to mimicking Nature.[14,15]However, chemistry can design systems beyond those found in biology that meet currents needs of humanity such as high capacity for gas storage, anion sensing and development of organic electronics. In all these fields, supramolecular level is crucial, but often still lacking in understanding.

1.2 Crystal engineering

Crystal engineering is relatively young discipline that has experienced an exponential growth over last couple of decades. The reasons behind such increase in research activity are twofold. First, owning to rapid development of powerful computers, X-ray crystallographic analysis has become inexpensive, fast, and readily available. Second, crystal engineering is directly affected by advances in supramolecular chemistry and understanding of intermolecular interactions and structure-function relationships.[16] It was J. Dunitz that, now famously said, "Crystal is supermolecule *par excellence*!"[17] The physical and chemical properties of macroscopic solids depend upon spatial organization and intermolecular interactions within the crystal lattice as much as upon the properties of its individual molecular components.

The term "crystal engineering" was used as early as 1955 by R. Pepinsky to describe crystallization of chiral ionic species with metal-organic complexes in order to

determine absolute structure of ions.[18] Later on, term was used in the context of synthetic photochemistry: by Schmidt in 1971.[19] By the late 1980s, crystal engineering was shaped into a scientific discipline, largely due to extensive, systematic and creative studies of G. R. Desiraju.[10] Nowadays, crystal engineering emerged as a practical method to construct target functional architectures, with mechanistic, synthetic, and conceptual character.

A class of compounds that seems to be especially amenable to crystal engineering, and it is heavily studied in the work presented in this thesis, is cocrystals.[20] Although there seemed to be some disagreement in literature over the definition,[21] relatively practical and widely used definition of a cocrystal has been derived. In this work, the adopted definition of cocrystal is a structurally homogenous crystalline material that contains two or more neutral building blocks that are present in definite stoichiometric amounts. Additionally, each of components, as a pure substance, should be a solid at the room temperature, thus hydrates and solvates are excluded as cocrystals. Cocrystal engineering is especially active in production of pharmaceutical and energetic materials.

1.3 Supramolecular synthons and forces within organic crystals

Crystal engineering is in effect a rational design of supramolecular structure that necessarily relies upon self-assembly, or as one could refer to it, supramolecular synthesis. In same manner as classical covalent synthesis uses concept of synthons,[22] crystal engineering uses supramolecular synthons. Supramolecular synthons are structural units within supermolecule which can be assembled by known or plausible synthetic operations involving intermolecular interactions.[23]

In other words, the goal of crystal engineering is to recognize and design synthons that are reliable enough to be used from one structure to another and offer generality and predictability. Supramolecular synthons can be divided in two categories: homosynthons,

which are interactions between identical functional groups; and heterosynthons, which are interactions between two different functional groups (Fig. 2).

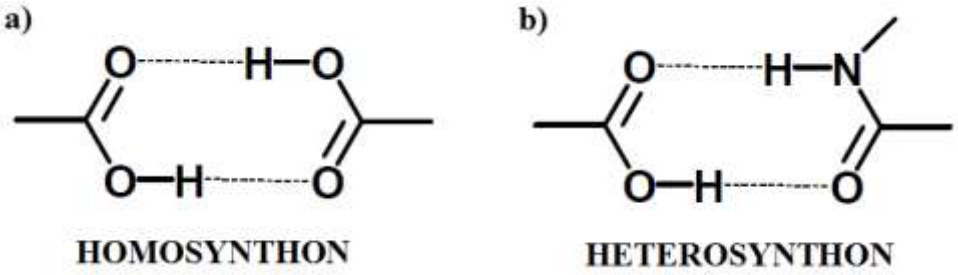

Figure 2 Schematic representation of: a) homosynthon, and b) heterosynthon.

The work of Desiraju and Etter in solid-state organic chemistry afforded the library of supramolecular synthons and, to some extent, hierarchy of synthons.[16,24] The most widely exploited non-covalent interaction in the context of crystal engineering is hydrogen bonding owing to its strength, ubiquity and directionality.[25] Hydrogen bonds vary in strength from conventional strong OH···O and NH···N (20-40 kJ/mol) to weaker ones like OH···π and CH···N (2-20 kJ/mol). Other supramolecular interactions include aromatic interactions and halogen bonding (Fig. 3). In general, molecules have tendency to form the strongest possible supramolecular interactions.[17] Such conclusion comes from analysis of thousands of crystal structures. For example, since hydrogen bonding is the strongest non-covalent interaction one would expect that all X-H groups will be engaged in hydrogen bonding. Indeed, structures with free X-H ends are extremely rare. However, these observations and conclusions should be regarded to more as guidelines than rules. In fact, an alternative model, advocated by Dunitz and Gavezzotti, accounts for close packing and tendency of crystals to minimize free space, as critical factors.[26] An oxygenated pyrimidine derivative, alloxan, although dense with hydrogen bond donor

and acceptor groups, does not form any strong hydrogen bonds. Instead, alloxan adopts high-density, low-energy structure with possibly some dipolar C···O interactions.[27] Overall, in majority of cases supramolecular synthons and their hierarchy are powerful design tools, as long as we keep in mind that "*any way of minimizing the free energy is a respectable way*."[28]

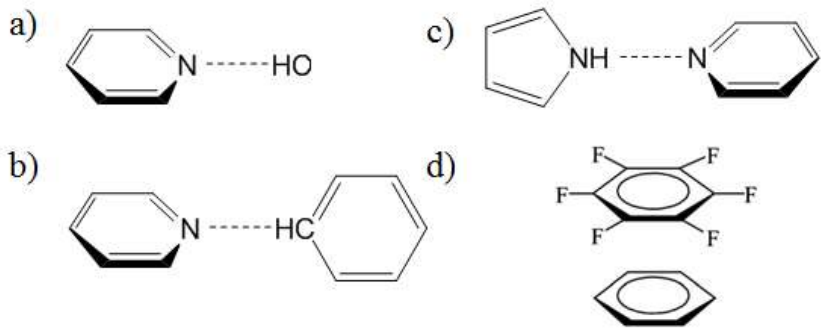

Figure 3 Examples of supramolecular synthons: a) OH···N hydrogen bond, b) CH···N hydrogen bond, c) NH···N hydrogen bond, d) pentafluorophenyl-phenyl interaction.

1.4 Crystal structure prediction

Crystal structure prediction (CSP) refers to calculation of the crystal structures from first principles.[29] Reliable CSP, based only on knowledge of molecular structure, has been an elusive goal of chemistry and physics for decades. Maddox emphasized difficulties associated with CSP in his opinion article: "*One of the continuing scandals in the physical sciences is that it remains in general impossible to predict the structure of even the simplest crystalline solids from knowledge of their chemical composition.*" A reliable CSP method would be greatly beneficial in all areas of science and industry that deal with preparation and properties of solid materials, and it would in particular benefit pharmaceuticals where polymorphism of molecular crystals poses a specific problem. Although certainly great advances have been achieved, the crystal structures of larger and

flexible organic compounds are still extremely difficult to predict.[30] The structures of organic solids are determined by subtle non-covalent interactions that are difficult to model. To overcome these issues, numerous approaches have been developed, including density functional theory (DFT), molecular mechanics (MM), data mining, evolutionary algorithms and simulated annealing. Modern CSP of organic crystals is based on crystal energy landscape search for the most thermodynamically stable crystal structure. An increased computational power enables search of impressively large structural landscape and pinning of global minimum. However, unsolved challenge remains understanding if the low energy structure is actually obtainable from crystallization process and, if it is, what the required crystallization conditions are. Considering inherent randomness in crystallization process it is still not certain that reliable crystal structure prediction is an obtainable goal.

1.5 Molecular motion in crystals and molecular motors

Owing to the restricted conformational and translational degrees of freedom of molecules in solids, crystalline state does not intuitively come to mind as a great environment to conduct reactions or support sophisticated molecular machinery. Indeed, diffusion rates of molecules in the crystalline state are at least six orders of magnitude less than in solution (10^{-15} m^2/ s).[31] However, when considering artificial macroscopic machines and biological machinery, like skeletal muscles, it becomes apparent that they are constructed in a highly ordered fashion with high packing densities within a finite volume, much like conventional crystals. In recent years, it became apparent that some crystals show surprising flexibility and ability to support direct molecular motion.[32] For example, Faringa[33] and Garcia-Garibay[34] were successful at designing the molecular systems that, as a response to external stimuli, transform input energy into mechanical

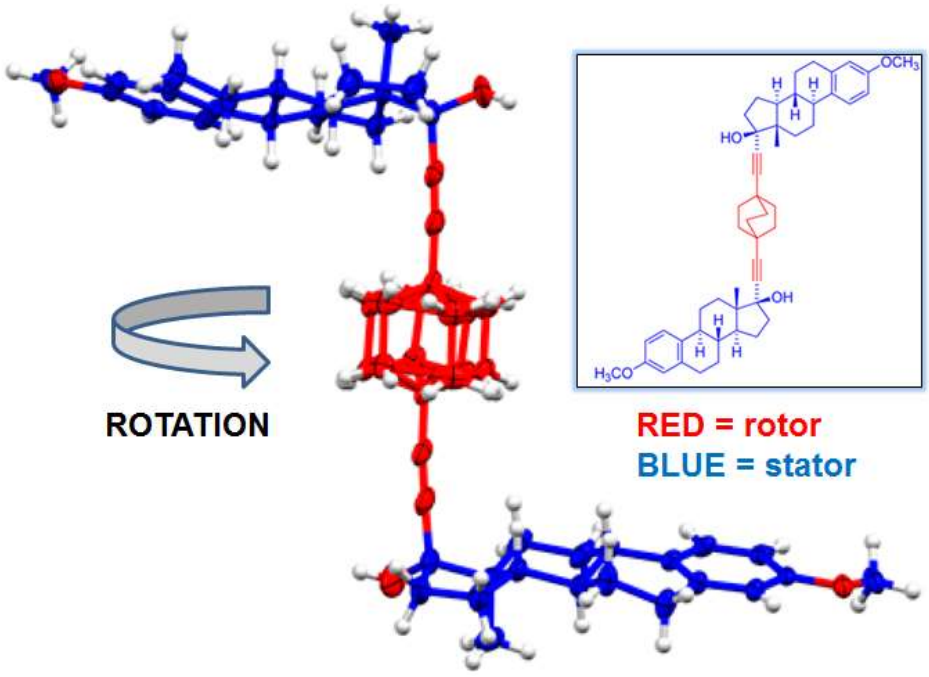

Figure 4 Example of a crystalline molecular motor. Blue = static fragment and Red = fast rotating fragment.

work. Effective crystalline molecular machines require molecular components forming an extended, rigid and highly-ordered network (*stators*) that are linked to the dynamic components (*rotors*) by covalent, supramolecular, or mechanical bonds (Fig. 4). Such crystals, that exhibit high degree of phase order and support high molecular mobility, are called amphidynamic crystals. To further advance the field of artificial molecular machines, our basic knowledge of molecular dynamics in condensed matter, and preparation and characterization of amphidynamic crystals has to be expanded.

1.6 Reactivity in crystals

While it was for long time assumed that reactions in crystals are forbidden, research over last fifty years has that notion disproven. Crystalline state has proved to be surprisingly flexible and able to support reactions in quite unique way. The homogeneous

and confined nature of molecular lattice provides often perfect control of stereochemistry and quantitative yields. Given that reactions occur in the absence of solvent, issues associate with organic solvent, such as solubility and environmental hazards, are eliminated. The number of different types of reactions that can occur in crystal is quickly increasing and nowadays described solid-state organic reactions include isomerization, polymerization, hydrogenation, halogenation, elimination, Diels-Alder cycloaddition and Wittig rearrangement.[35] In fact, back in 1972 it was proposed that roughly "*any reaction which occurs in an inert solvent at a reasonable rate at a temperature 60-100 °C below the melting points of the reactants can probably be made to occur in the solid.*"[36] The progress of solid-state organic synthesis may just prove this notion correct.

The most studied and used solid-state reaction is photodimerization of olefins, which also served as a model reaction in establishing crystal structure-chemical reactivity relationship. The 1921 report described two polymorph of *trans*-cinnamic acid which give different products upon irradiation with sunlight.[37] In 1943 Bernstein and Quimby proposed that relative position of phenyl groups affects outcome of photoreaction.[38] Later on, seminal work of Cohen and Schmidt generalized that outcome of photoreaction is determined by crystal structure of the starting materials.[39,40,41] The X-ray crystal structure analyses of a range of *trans*-cinnamic acids led to topochemical postulates. Specifically, topochemical postulates state that olefins will react upon irradiation to give cyclobutane product if double bonds (C=C) are parallel and separated by less than 4.2 Å. An excellent illustration of validity of structure-reactivity relationship is the case of *o*-ethoxy-*trans*-cinnamic acid. Three polymorphs of *o*-ethoxy-*trans*-cinnamic acid are known, namely, α-, β-, and γ-form. α-form adopts antiparallel orientation, related to the center of inversion with double bonds approximately 4 Å apart and upon UV-irradiation, gives the 'head-to-tail' *α*-truxillic acid dimer. β-form adopts parallel orientation with double bonds approximately 4Å apart, as well. Upon UV-irradiation, β-form gives the

'head-to-head' β-truxinic acid dimer. γ-form has double bonds more than 5 Å apart and is determined to be photostable upon UV-irradiation (Fig. 5).

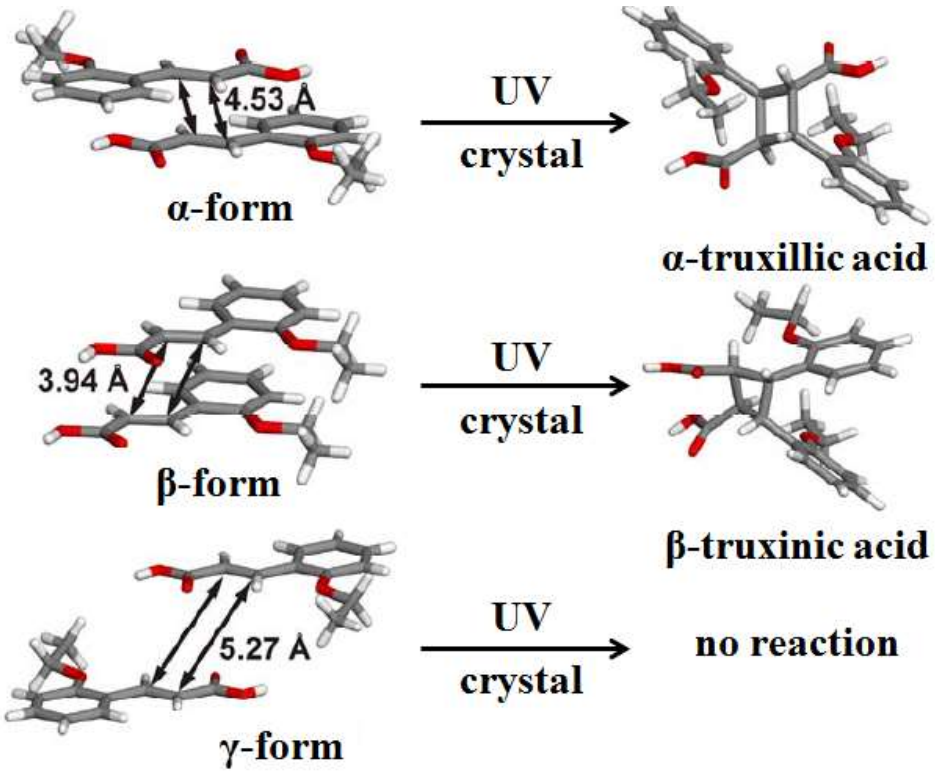

Figure 5 Solid-state reactivity of three polymorphs of *o*-ethoxy-*trans*-cinnamic acid.

Over years, other useful geometrical parameters were proposed. For example, the distance between two C=C bonds is defined as distance between the two centroids (*d*) and this parameter is often used in this thesis.[42] To describe the alignment of double bonds more accurately, the angles θ, θ_1 and θ_2 are used to assess rotational angle of one double bond with respect to the other, the obtuse angle of the parallelogram formed by the double bond carbons, and the angle between the plane of the reactive bonds.[43] Displacement parameters d_1 and d_2 that correspond to the displacement along the double

bond axis, and the displacement in the molecular plane, can be used, as well. Often overlooked factors that affect the reactivity of the crystals are the available free space surrounding the reactant molecules (the reaction cavity) and the lattice energy.[44,45] In conclusion, the topochemical postulates of Schmidt, are empirically derived, and as such, face some limitation. The postulates, can serve as a quick, practical and fairly accurate guidance when evaluating the propensity of a crystal to support reactivity. However, as in several examples that will be presented in this thesis, the postulates cannot explain all observed crystalline behavior. In such cases, more detailed studies and considerations are required to understand the behavior of the crystalline material.

1.7 Template approach

To steer crystal packing such to align C=C bonds to conform to topochemical postulates, several crystal engineering strategies were developed. For example, the starting material can be covalently decorated with chlorine to induce Cl⋯Cl and C-H⋯Cl contacts.[46,47] The halogen substitution can be also used in a more indirect way. For example, *para* substitution will not result in halogen-halogen interaction. Instead, the π- π interactions will be favored as a result of the electron-withdrawing nature of the halogen atoms, which reduces the electron density on the aromatic ring and enables a better offset of the aromatic rings.[48]

The other approach focuses on formation of the π- π interactions by introducing favorable electronic attraction between electron poor and electron rich rings. The classical example is the substitution of the aromatic rings with groups that have opposite electronic effects, such as -NO_2 and –OMe.[49] One of the strongest interactions is actually perfluorophenyl-phenyl interaction.[50]

In 2000, MacGillivray developed the template approach that is based on the use of an auxiliary small molecule as a template that uses reversible non-covalent interaction to assemble substrate in the suitable geometry.[51,52] In particular, the template is equipped

with two functional groups that are strategically positioned such to bring two substrates into close proximity (Fig. 6). The template approach was inspired by earlier works of Aoyama, Ito, and Feldman. In late 1980's, Aoyama used a resorcinol-decorated anthracene to direct stacking of quinones within 3.8 Å. The cocrystal is based on strong and directional O-H···N hydrogen bonds which later proved to be a reliable synthon in template-directed solid-state synthesis.[53] In 1990's, Ito forced stacking of cinnamates within diammonium salts.[54] Around same time, Feldman described a J-shaped dimer of naphthalene dicarboxylic acid based on complementary hydrogen-bonds.[55] Based on these reports, MacGillivray derived approach that decouples the reactivity of a solid from its long range packing.

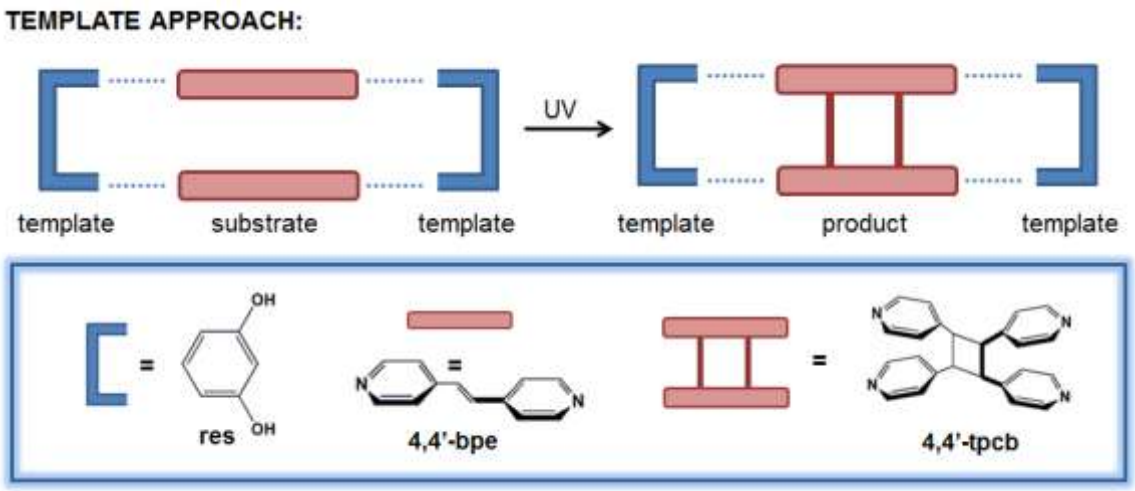

Figure 6 Template approach.

In particular, a small-molecule template, res (where res is resorcinol), is equipped with two strategically positioned functional –OH groups. The –OH groups act as a hydrogen-bond donor and interact with N-atoms of pyridyl groups positioned on the substrate *trans*-1,2-bis-(4-pyridyl)ethylene (4,4'-bpe) to form strong O-H···N hydrogen

bonds. As a result, a four membered assembly is formed. Within the assembly, the substrate is forced to stack in face-to-face manner and in close proximity and is, de facto, positioned to conform to the topochemical postulates. Upon UV-irradiation the substrate undergoes [2+2] photodimerization stereoselectively and in quantitative yields to give is *rctt*-tetrakis-1,2,3,4-(4-pyridyl)cyclobutane (4,4'-tpcb). The main advantage of template approach is that reactivity is correlated to localized geometry of rationally designed assemblies instead of incontrollable long range packing. In addition, no covalent modifications of the substrate are necessary, isolation of photoproduct is facile and modularity can be achieved in form of template-switching strategy.

Over the years, the modularity of the approach has been demonstrated, as well applicability to different substrates. The functional groups can be expanded to carboxylic acids instead of phenols,[56] the code can be reversed such that substrates are hydrogen-bond donors and template has hydrogen-bond accepting groups,[57] and, as demonstrated in this thesis, N-H···N hydrogen bonds can be used. The most impressive examples of efficiency of the template approach are stereoselective and quantitative synthesis of synthetically demanding ladderanes[58] and cyclophanes (Fig. 7).

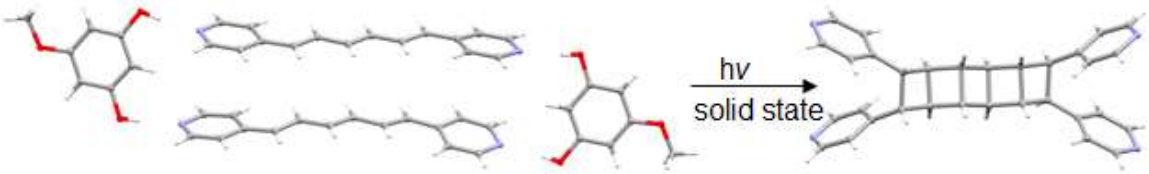

Figure 7 Solid state synthesis of ladderanes using the template approach.

The template approach has been expanded to coordinative bonds, as well. The first example of metal mediated [2 + 2] photodimerizations, dates back to the beginning of 20th century. Upon UV-irradiation, the uranyl chloride complex of dibenzylideneacetone is reported to yield a photodimer.[59] Later on, a $SnCl_4$ complex was

demonstrated to direct the photodimerization of ethylcinnamate.[60] In both cased, the carbonyl groups coordinate to the metal atoms. To expand the template approach to metal-organic materials, that exhibit unique magnetic and electronic properties, MacGillivray first turned to Zn(II) containing Schiff base. The complex stacks two molecules of 4,4′-bpe within 3.64 Å that upon UV-irradiation produced 4,4′-tpcb via a SCSC photodimerization in quantitative yield.[61] Next, argentophilic forces were used in Ag(I) complex to direct quantitative photodimerization of *trans*-1-(4-pyridyl)-2-(phenyl)ethylene (4-stilbz).[62] The products of above described and similar reactions were used to form metal-organic polyhedra and polygons,[63] support a thixotropic hydrogel[64] and to study softening and hardening of macro- and nano-sized organic crystals.[65]

More recently, template approach was used to achieve supramolecular catalysis.[66] Supramolecular catalysis in the solid state was expected to be difficult to achieve due to low diffusion rates of molecules in the crystals. However, MacGillivray group reported the first small-molecule catalyst that directs formation of covalent bonds in the solid state. The reaction directed by the catalyst occurs in a close-packed crystalline environment and results in stereospecific product formation in near quantitative yield. Specifically, in a stoichiometric amount, a ditopic supramolecular receptor, 4,6-diCl-res (4,6-dichlororesorcinol) directs a topochemical [2+2] photodimerization of 4,4’-bpe to yield 4,4’-tpcb. It was demonstrated that 4,6-diCl-res can operate in substoichiometric catalytic amounts, as well. When the catalyst, 4,6-diCl-res, was ground with excess of a substrate, 4,4’-bpe, using a dry mortar-and-pestle method, a solid mixture of a photoreactive assembly, 2(4,6-diCl-res)·2(4,4’-bpe) and free 4,4’-bpe was formed. Upon exposure to broadband UV radiation, 2(4,6-diCl-res)·2(4,4’-bpe) undergoes a stereospecific and quantitative photodimerization to form 2(4,6-diCl-res)·(4,4’-tpcb), consistent with established SCSC reactivity. The free 4,4’-bpe did not react. A second dry grind was used to achieve a catalytic turnover in which the photoproduct, 4,4’-tpcb, is released from 2(4,6-diCl-res)·(4,4’-tpcb), and new photoreactive 2(4,6-diCl-res)·(4,4’-

bpe) assemblies are formed. The process is repeated until all 4,4'-bpe is used. For catalysis to proceed to near quantitative yield, approximately 100/*n* (where: *n* = % catalyst loading) turnovers were required (Fig. 8).

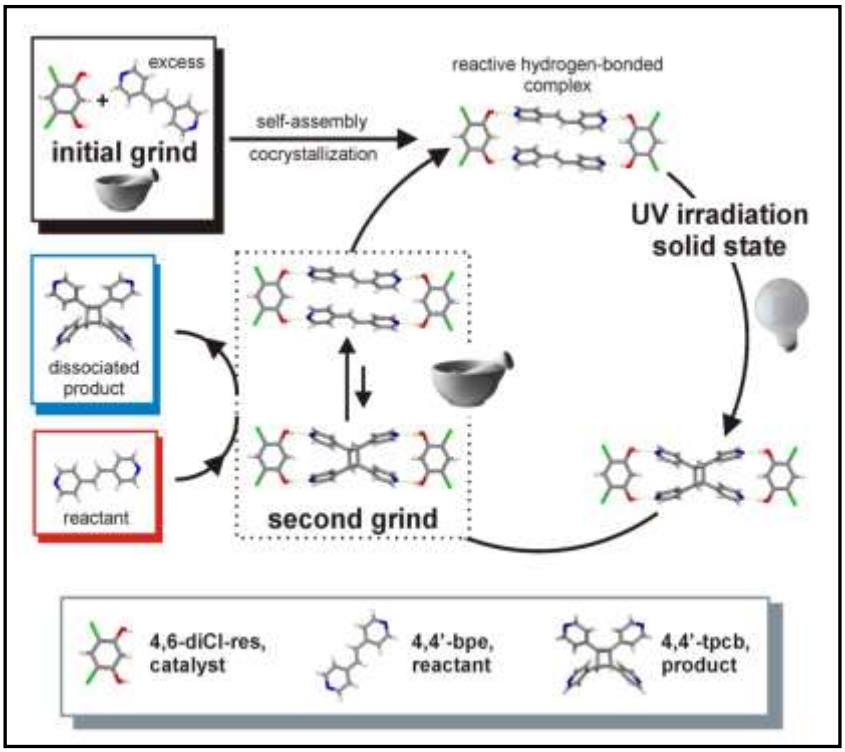

Figure 8 Supramolecular catalysis in the organic solid state.

1.8 Mechanochemistry

Mechanochemistry, in the broadest sense, can be defined as chemical synthesis induced by external mechanical energy, such as grinding two solids using a mortar-and-pestle.[67] A more restrictive definition, mainly argued by G. Kaupp, limits use of the term "mechanochemistry" only to reactions where mechanical energy directly ruptures strong bonds.[68] In the opinion of the majority of the scientific community with interest in mechanochemistry and ours, this definition is too restrictive, and, thus, the more inclusive definition is adopted in this thesis.

The history of mechanochemistry is long and rich. The reports dating back to 4th century B.C. describe the extraction of mercury by mechanochemical reduction of cinnabar achieved by grinding in a copper vessel in the presence of vinegar.[69] In the Middle Ages mechanochemistry was extensively used in mining and metallurgy.[70] However, throughout the history, mechanochemistry has been more of a secondary approach to organic synthetic chemistry as compared to mainstream liquid-phase synthesis. In 1980's, the increased interest in mechanochemistry was largely initiated by Tanaka and Toda who recognized grinding and milling as a means to conduct environmentally-friendly and solvent-free chemistry.[71] Their work mainly focused on host-guest inclusion compounds, which are based on molecular recognition and hydrogen bonding. Thus, modern mechanochemistry seems to be tightly bound to supramolecular chemistry. Recent years have witnessed a rapid development in the use of mechanochemistry to generate complex organic molecules, supramolecular assemblies and frameworks, such as 3D and 2D MOFs.

Mechanistic studies have not yet provided a full understanding of mechanochemical processes. Instead, several models have been developed, each applicable only to limited number of reaction. Hot spot theory accounts for small protuberance to cause plastic deformations that are result of dramatic increase in temperature (above 1000°C) for a very short period of time (`~10^{-4} s). The magma plasma theory proposes that direct impacts can result in temperatures above 10 000°C and, as a result energetic species are ejected. However, these two models seem to be unlikely applicable when describing the primary reactivity in molecular crystals. For molecular crystals proposed mechanisms can be grouped in following categories: i) molecular transport across surfaces, either through vapour or bulk of crystals ii) formation of liquid eutectic intermediate phases, and iii) reaction via an amorphous intermediate phase.[72] It is also important to recognize the physical effects of grinding on molecular crystals. These effects include reduction of particle size and continuous

exposure of fresh surfaces, intimate mixing of reactants, increase in crystalline defects and associate possible amorphization of the material, and frictional heating, both on local level and bulk material. The physical effects may enable or accelerate each of the three mechanisms described above.

In the light of recognized need for sustainability and ever-present aspirations for cost-reduction, the interest in industrial application of mechanochemistry has increased. Based on patent activity, especially active areas are medical/personal care, batteries, compounds of non-metallic elements and catalysis. Several processes that recently incorporated mechanochemical approach are going into production scale. In future, more activity is expected in areas under current research, such as synthesis of organic compounds, advanced inorganic materials and composites.

In conclusion, mechanochemistry has been recognized as a route that can offer more efficient, practical, and inherently safer approaches to synthesis. However, to fully employ mechanochemistry to generate molecular and supramolecular products of increasing complexity, as well as products connected to more mainstream chemistry, it is necessary to develop deeper understandings of underlying mechanisms, principles, and scopes of the approach.

1.9 Thesis overview

The work presented in this thesis reports new supramolecular architectures, processes and tools to conduct solid-state synthesis. More specifically, in second chapter, a solvent-free automated grinding method based on a vortex mixer that enables simultaneous grinding and UV irradiation, as well as *in situ* monitoring of solid-state reactivity is described. The method has been applied to mechanochemical preparation of supramolecular materials, *e.g.*, cocrystals, metal-organic framework. A recently reported supramolecular catalysis in the organic solid state, when performed using the vortex method, proceeds four times faster than when conducted through manual grinding. The

accelerated rate is attributed to the unique features of the vortex method that enables continued grinding while the photoreaction is occurring.

In Chapter 3, we report the expansion of supramolecular solid-state catalysis to a similar system 2(res)·2(2,2'-bpe) (where res is resorcinol and 2,2'-bpe is trans-1,2-bis-(2-pyridyl)ethylene). Catalysis yields *rctt*-1,2,3,4-tetrakis(2-pyridyl)cyclobutane (2,2'-tpcb) photoproduct in near to quantitative yields. Remarkably, the catalytic turnover proceeds spontaneously, that is, without extrinsic energy (e.g. mechanical energy) required, unlike in the case 2(4,6-diCl-res)·2(4,4'-bpe) where mechanochemistry was necessary to achieve turnover. To elucidate reasons behind such catalytic mechanisms, detailed gas-phase DFT and X-ray diffraction studies were performed. We concluded that rotamerism, that is not present in 4,4'-bpe, plays an important role in stability of assemblies that carry reactivity and, thus, affect macroscopic properties of solids and influence outcome of catalyzed photoreaction.

Chapter 4 focuses on aromatic stacking in solid state. we report a sequential integration of aromatics into discrete stacks based on hydrogen bonds in the solid state. Indolo[2,3-*a*]carbazole (IC) organizes aromatic 4,4'-bpe into discrete double, triple, and quadruple stacks within cocrystals of $(IC)_2(4,4'\text{-bpe})_2 \cdot 2(AcN)$, $(IC)_2(4,4'\text{-bpe})_3$ and $(IC)_2(4,4'\text{-bpe})_4$. IC interacts with 4,4'-bpe *via* N-H···N hydrogen bonds that enforce aromatic stacking exclusively in a face-to-face manner. Photoreactivity studies show that, upon UV irradiation, the quadruple-stacked $(IC)_2(4,4'\text{-bpe})_4$ undergoes a topochemical [2+2] photodimerization stereoselectively and in maximal theoretical yield.

In Chapter 5 a concept of using a product of a template-directed solid-state reaction as a template in subsequent reaction is demonstrated. The approach provides new tools to direct chemical reactivity in the solid state. In particular, *rctt*-cyclobutanetetracarboxylic acid (cbta) is product of the templated photodimerization of fumaric acid. We show that cbta can act as template for photodimerization of 4,4'-bpe.

We also report a unique form of cocrystal polymorphism where both polymorphs are photoreactive.

Next, homology of solid-state reactivity and modularity of template approach are studied in Chapter 6. we report a systematic crystallographic study of reactivity of six isomeric olefins within discrete hydrogen-bonded assemblies achieved using template approach. To assess performance of assemblies upon systematic electronic and steric changes, the detailed gas-phase DFT calculations have been performed.

Lastly, incorporation of principles of supramolecular chemistry, solid-state reactivity, green chemistry and sustainability in undergraduate curriculum is presented. We hope that introducing these concepts to young scientists at the earlier stage of education will help to change the traditional synthesis mind-set that relies only on liquid phase chemistry and heavy use of organic solvent. We also hope to stimulate interest in new areas such as crystal engineering, and associated well-established, but often overlooked areas, such as crystallography.

The research presented in this thesis explored new frontiers in supramolecular solid-state chemistry. The template approach was expanded to enable architectures beyond double stacks. To fill the need of scientist interested in mechanochemistry that was not met by commercially available technologies, a new technique was developed. The small-molecule supramolecular catalysts was found to have a greater reach in solid-state than previously reported. Collectively, these results demonstrate how rich and dynamic medium solid state is. To fully exploit solid state, we have to push forward concepts that are already in place, develop new technologies and ideas that will foster popularity and use within a large community of scientist, and place more effort in understanding underlying principles.

CHAPTER 2. VORTEX GRINDING METHOD AS A TOOL FOR MECHANOCHEMISTRY

A portion of this chapter was published as a communication and a paper and is adapted from *Chemical Communications* and *Faraday Discussion* [Stojakovic, J.; Farris, B. S.; MacGillivray, L. R. *Chem. Commun.* **2012**, *48*, 7958-7960. and [Stojakovic, J.; Farris, B. S.; MacGillivray, L. R. *Faraday Discuss.*, **2014**, Accepted Manuscript, **DOI:**10.1039/C4FD00006D].

2.1 Introduction

Supramolecular catalysis, where 4,6'-res is used as a small-molecule supramolecular catalyst to direct a topochemical [2+2] photodimerization of 4,4'-bpe in the organic solid state, was achieved using principles of mechanochemistry.[66] Mechanochemistry, in the form of a mortar-and-pestle dry grinding, was used to form catalyst-substrate complex and to achieve catalytic turnover. A main disadvantage of the grinding method is the fact that the mechanochemistry is performed manually and that the grinding and photoreaction are conducted separately. That grinding and irradiation are not conducted simultaneously is owing to a lack of instrumentation that enables such an experimental setup.

In this chapter, a method based on the use of a vortex mixer that enables automated grinding and simultaneous irradiation of a solid sample is described. A vortex mixer is a device commonly used to mix liquids in small vials with primary applications in the biosciences. A mixer consists of an electric motor vertically connected to a cupped rubber holder of vials. When the motor runs, the holder oscillates in circular motion with speeds up to several thousand rpm. The motion is transmitted to the vial and to a liquid inside the vial creating a vortex (Fig. 9).[73]

The inspiration to use a vortex mixer as a tool for mechanochemistry comes from sample preparations in the biosciences. The vortex mixer, which is common in most

laboratories, has been used to grind solid biological samples (e.g. leaf tissue) to afford fine powders within periods of minutes.[74,75] The vortex mixer has also been used for the solvent-free preparation of insoluble polymers for MALDI mass spectrometry.[76,77] The method involved adding dry components of a sample to a small glass vial with two metal balls (or BBs) made of steel and Zn plated. The contents were mixed using a vortex mixer for 30 to 60 s to yield samples that produce mass spectra of excellent quality. We hypothesized that such a method, with minor modifications, could replace manual mortar-and-pestle grinding, or ball-milling, whilst allow UV radiation to be transmitted to the solid reaction mixture. In other words, the vortex method could effectively serve as a ball mill that is transparent to UV-light. The aforementioned photocatalysis proceeds four

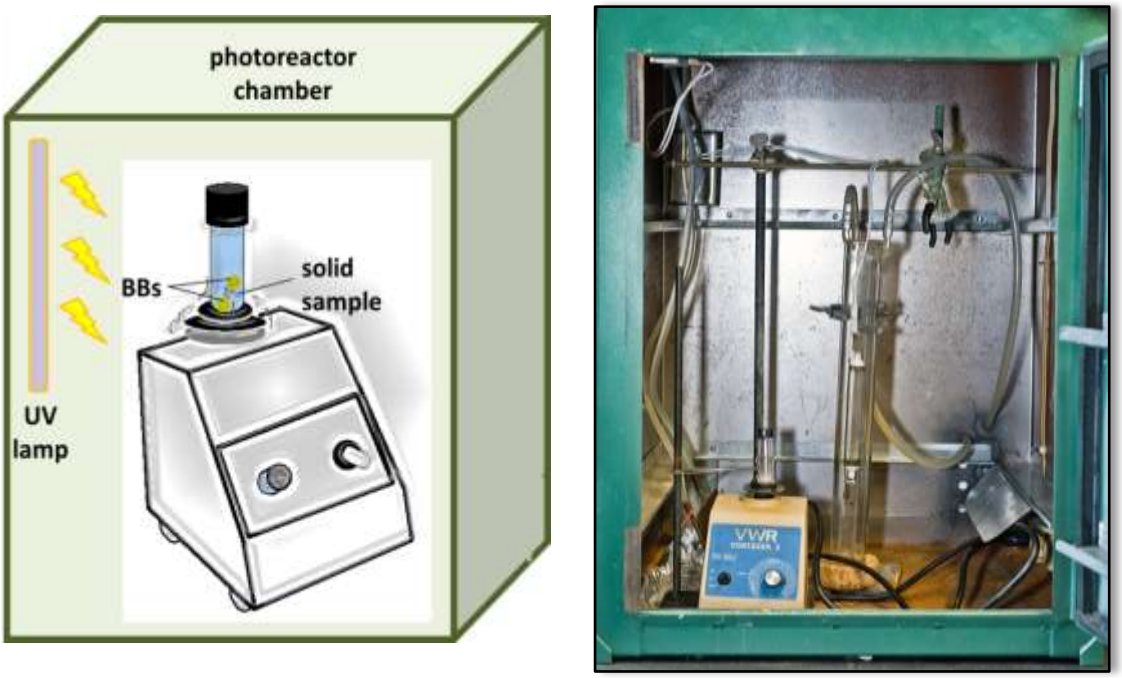

Figure 9 Vortex grinding apparatus with application of UV radiation a) schematic, and b) experimental set-up in our laboratory.

times faster than originally reported when preformed using the vortex grinding method. The increased rate of reaction may occur as a result of simultaneous exposure of the sample to mechanical stress, arising from collisions with BBs, as well as to internal stress originating from the photoreaction. The method has been also applied to solvent-free synthesis of metal-organic frameworks and cocrystals.

Given that ditopic templates can assemble higher olefins (e.g. dienes) that react to form higher cyclobutanes as photoproducts (e.g. cyclophanes, ladderanes), the vortex grinding has been considered as a means to generate *p*-[2.2]-cyclophane 1.[78] A small-molecule template 4-benz-res (4-benzyl-resorcinol) directs a diene 1,4-bpeb (*p*-di[2-(4-pyridyl)ethenyl]benzene) to give 1 in a photoreaction that involves monocyclobutane intermediate (Fig. 10). Herein present studies demonstrate a critical role of the use of a small amount of liquid phase to support the formation of 1 using the vortex method. It is well known that small amounts of liquid can be used to generate hydrogen-bonded cocrystals using mortar-and-pestle grinding. Compared to dry grinding, such liquid-

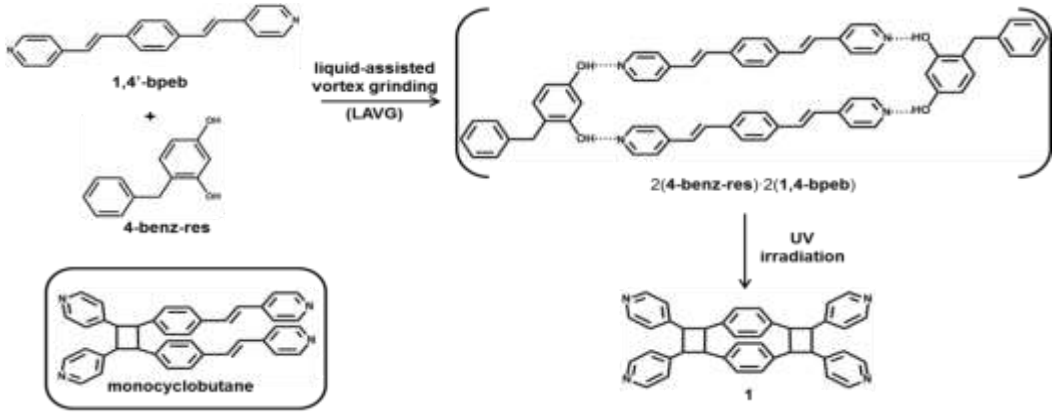

Figure 10 Solid state synthesis of 1 via LAVG combined with UV irradiation.

assisted grinding (LAG) can be faster, offer better yields, and generate solids of relatively high crystallinities. It has been suggested that the use of the liquid phase in LAG serves to enhance molecular diffusion without a dependence on solvent effects so as to essentially provide an ideal environment to explore molecular recognition and self-assembly.[79] Liquid-assisted vortex grinding (LAVG) was employed to generate 1 in a single step with outcomes that parallel the more conventional two-step solution growth approach.

2.2 Experimental

2.2.1 General remarks

All reagents were purchased from Sigma-Aldrich co. and used as is. ^{1}H NMR spectra were collected using a *Bruker* 300 MHz spectrometer and DMSO-d_6 as a solvent. Powder X-ray data were collected on a *Bruker* D-5000 diffractometer equipped with a *Bruker* SOL-X energy-sensitive detector using Cu K_α radiation (λ=1.54056 Å).Vortex grinding was performed using a *VWR* vortex mixer, type *Vortex Genie 2*. All photoreactions were carried out in a photoreactor chamber equipped with a broadband, low pressure UV lamp with the quartz mercury arc, *Hanovia* lamp, model number PC451.050. ACE glass inc. Power supply: 230 V, 50 Hz, 450 W. SEM images were collected using *Hitachi* S-4800 scanning electron microscope. Prior to imaging, samples were coated using *Emitech K550* sputter coater.

2.2.2 Cocrystallization *via* vortex grinding method

100 mg of 4,4’-bpe and 100 mg of 4,6-diCl-res (1:1 molar ratio) were placed in a borosilicate glass vial. The dimensions of the vial were 21 x 70 mm. Two premium grade steel BBs (5 mm diameter) were washed with soap, water and acetone, dried and placed in the vial together with the solid samples. The vial was mounted onto the vortex mixer, secured with the test tube holder attached to the ring stand rod and shaken using the

vortex mixer at the maximum speed. Motion of the vial was transmitted to the BBs which exhibited rapid, chaotic movement and collisions. The progress of cocrystallization was followed using powder X-ray diffraction. The morphology of obtained solid was investigated using SEM imaging. The obtained powder was exposed to UV-irradiation.

2.2.3 Supramolecular catalysis *via* vortex grinding method

100 mg of 4,4'-bpe and 50 mg of 4,6-diCl-res (1:0.5 molar ratio) were placed in the vial together with two BBs and set up for vortex grinding as described in Section 2.1.

To simultaneously conduct vortex grinding and UV irradiation, the vortex assembly was placed in the photochemical reactor, being approximately 15 cm from the UV lamp. The sample was simultaneously subjected to vortex grinding and UV irradiation in intervals of 2 h. The progress of catalysis was followed using ^{1}H NMR spectroscopy.

2.2.4 Model fitting and statistical analysis

From the ^{1}H NMR data, a yield of photoreaction (α) was calculated for each time point and plotted versus time (t). The data were compared to series of reported solid-state kinetic models based on the shape and statistical fit parameter R^2.

2.2.5 Synthesis of MOF *via* vortex grinding method

$Cu(OAc)_2 \cdot H2O$ (0.203 g, 1.0 mmol) and isonicotinic acid (0.252 g, 2.0 mmol) were placed in a vial together with two BBs and ground in a vortex mixer as described in Section 2.2.2 The progress of synthesis was followed using powder X-ray method.

2.2.6 Synthesis of *p*-[2.2]-cyclophane

In a typical manual grinding experiment, 50 mg of 1,4-bpeb and 35 mg of 4-benz-res (1:1 molar ratio) were placed in a mortar-and-pestle and ground for up to 1 h. The solid was analysed using XRPD. LAG experiments were conducted in the same manner save for a single drop of methanol (50 μl) being added to the solid mixture. The resulting

solid samples were then spread between glass plates and exposed to UV irradiation for a period of up to 120 h.

In a typical vortex grinding experiment, 50 mg of 1,4-bpeb and 35 mg of 4-benz-res (1:1 molar ratio) were placed in a capped sample vial with two metal BBs. The vial was mounted onto the vortex mixer and secured to a ring stand with a test tube holder. The samples were ground up to 1 h. The LAVG was conducted in the same manner except for a single drop of methanol (50 μl) being added to the sample vial. To simultaneously conduct LAVG and UV irradiation, the vortex assembly was placed in the photochemical reactor, being approximately 15 cm from the UV lamp. Upon initiation of the vortex mixer, the photochamber was closed and sample was exposed to UV radiation for a period of 10 h.

2.3 Results and discussion

2.3.1 Cocrystallization *via* vortex grinding method

To test the hypothesis that vortex grinding can substitute manual grinding, we focused on the photoreactive cocrystal 2(4,6-diCl-res)·2(4,4'-bpe) (where: 4,6-diCl-res = 4,6-dichlororesorcinol and 4,4'-bpe = *trans*-1,2-bis-(4-pyridyl)ethylene), that can be obtained either from solution or *via* dry mortar-and-pestle grinding.[66] After 1 min of vortex grinding, the sample appeared as fine homogenous powder. The X-ray powder pattern exhibited strong-intensity peaks that correspond to pure 4,6-diCl-res and 4,4'-bpe ($2\theta = 17^{\circ}$ and 19°, respectively) and low-intensity peaks at 20.5° that correspond to 2(4,6-diCl-res)·2(4,4'-bpe) (Fig. 11). After 10 min of vortex grinding, the intensity of the peaks changed. In particular, the peaks that correspond to 2(4,6-diCl-res)·2(4,4'-bpe) at 20.5° increased in intensity while the peaks that correspond 4,6-diCl-res and 4,4'-bpe at 17° and 19° decreased. Moreover, the X-ray powder pattern after 1 h corresponded to the simulated powder pattern of 2(4,6-diCl-res)·2(4,4'-bpe). Indeed, when the solid was exposed to UV irradiation, photoconversion of 4,4'-bpe to *rctt*-tetrakis-1,2,3,4-(4-

pyridyl)cyclobutane (4,4'-tpcb) proceeded in quantitative yield, confirming that vortex grinding is an alternative to manual grinding in solvent-free synthesis of a photoreactive cocrystal.

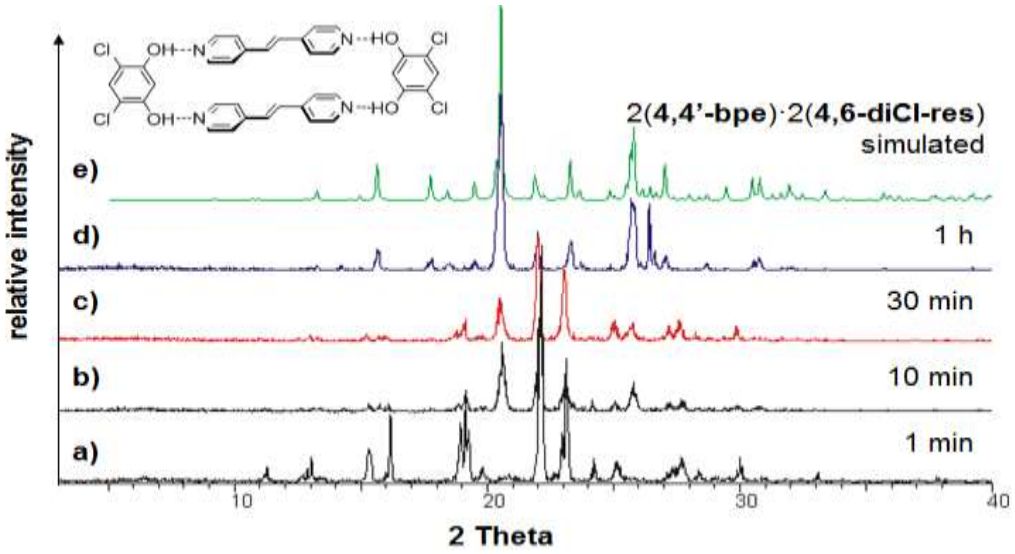

Figure 11 Progress of cocrystallization *via* the vortex method to give 2(4,6-diCl-res)·2(4,4'-bpe). XRPD patterns after grinding in vortex mixer: a) 1 min, b) 10 min, c) 30 min, d) 1 h, and e) simulated XRPD pattern of 2(4,6-diCl-res)·2(4,4'-bpe).

To gain insight into morphology and particle size of the solid subjected to the vortex mixer, a sample was studied using scanning electron microscopy (SEM) (Fig. 12). In particular, 2(4,6-diCl-res)·2(4,4'-bpe) obtained after 1 h of grinding in the mixer appeared as aggregates of poorly-defined shapes and nanoscale dimensions. The morphology compared favourably with a sample ground manually using a mortar-and-pestle, although the particles prepared using the vortex were consistently smaller, with sizes less than 100 nm. The SEM studies of MOFs prepared *via* a liquid-assisted grinding approach and the TEM studies of cocrystals prepared using the same approach, revealed that mechanochemical method can give nanosized particles. A recent 'mechano-assisted

reduction of size' (MARS) process of preparation of nanoparticles of C_{60} is the only SEM study of morphology and particle size of an organic crystalline solid achieved by manual grinding.[80] Crystals of nanosized dimensions were not expected to form by manual grinding. It was proposed that the generation of the C_{60} nanoparticles resulted from fast isotropic rotation of the spherical molecule and/or low cohesive energy. However, our results indicate that generation of nanosized particles may not be consequence of special properties of a compound, as proposed in the case of C_{60}. In fact, mechanochemistry may provide a more general route to nanosized particles.

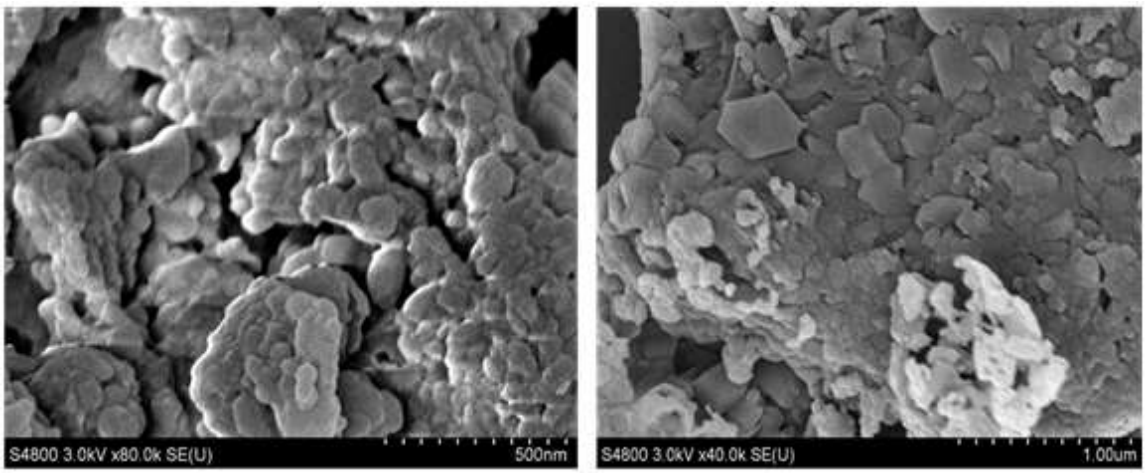

Figure 12 SEM images of 2(4,6-diCl-res)·2(4,4'-bpe) prepared by vortex grinding (500 nm scale) and manual grinding (1 μm scale).

2.3.2 Supramolecular catalysis *via* vortex grinding method

A recently reported supramolecular catalysis of a [2+2] photodimerization of 4,4'-bpe to give 4,4'-tpcb was achieved using a ditopic receptor as a small-molecule supramolecular catalyst. To achieve catalytic turnover, mechanochemistry, in the form of a mortar-and-pestle dry grinding, was employed. A main obstacle in the grinding method is the fact that the mechanochemistry is performed manually and that the grinding and photoreaction are conducted separately. we were prompt to investigate whether the vortex

method can substitute the manual grinding in supramolecular catalysis, and what effect will have simultaneous application of grinding and UV-irradiation on catalysis. The ^{1}H NMR data demonstrated the formation of a single photoproduct 4,4'-tpcb in 97% yield in a period of 24 h (Fig. 13a). For comparison, catalysis *via* manual grinding afforded 4,4'-tpcb in comparable yield after 90 h. The catalysis using the vortex mixer was, thus, four times faster than the catalysis *via* mortar-and-pestle grinding. The manual grinding also required the sample to be ground twice and transferred multiple times from mortar to glass plates. In contrast, in the vortex method, the reaction was completed in a single vial akin to a one-pot liquid-phase synthesis.

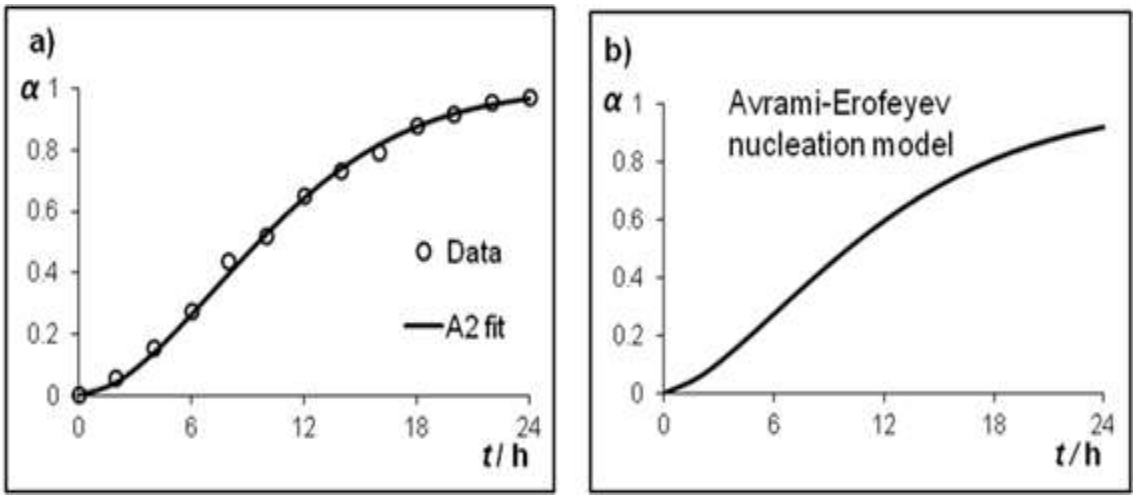

Figure 13 Supramolecular catalysis in a vortex from α-vs-*t* curve: a) experimental and b) simulated data for the A2 Avrami-Erofeyev model.

To understand the mechanism of supramolecular catalysis *via* vortex method and reasons behind dramatically increased rate, the obtained data were compared to reported kinetic models of solid-state reactions (Table 1).[81] Based on the sigmoidal shape of the *α*-vs-*t* curve and the highest statistical fit parameter R^2, the most reasonable fit to the data is A2 Avrami-Erofeyev nucleation model (Fig. 13b).[82,83] The nucleation models of solid-

state kinetic account both for nucleation, which involves the formation of crystalline phases at sites on surfaces (*e.g.*, imperfections from cracks, edges, point defects), and growth of product nuclei as the rate limiting steps. The continuous mechanical stress from the grinding in the vortex results in an increase of nucleation sites and, thus, can allow the catalysis to be accelerated in the mixer compared to manual grinding. Continued mechanical stress imparted by the BBs could also relieve any stress that builds up in the solid a result of the photoreaction.[84] It should be noted that such concomitant application of external stress able to promote the progress of photocatalysis (*i.e.*, turnover) is not readily achieved using manual mortar-and-pestle grinding or a commercially-available ball mill.

Table 1 Statistical analysis of various kinetic models of solid-state reactions.

Model	Integral form $g(\alpha)=kt$	R^2
P2	$\alpha^{1/2}$	0.8624
P3	$\alpha^{1/3}$	0.7597
P4	$\alpha^{1/4}$	0.6744
A2	$[-\ln(1-\alpha)]^{1/2}$	0.9936
A3	$[-\ln(1-\alpha)]^{1/3}$	0.9432
A4	$[-\ln(1-\alpha)]^{1/4}$	0.8714
D1	α^2	0.9770
D2	$((1-\alpha)\ln(1-\alpha))+\alpha$	0.9542
D3	$(1-(1-\alpha)^{1/3})^2$	0.8760
D4	$1-(2/3)\,\alpha-(1-\alpha)^{2/3}$	0.9336

2.3.3 Synthesis of MOF *via* vortex grinding method

To determine if the vortex grinding method can substitute commercial ball-mills, we turned to the preparation of a metal-organic framework (MOF). MOFs are garnering great interest owing to unique properties compared to more conventional porous materials.[85] As reported, the 3D MOF $[Cu(INA)_2]\cdot 2H_2O$ (where: INA = isonicotinate) can be prepared *via* either manual grinding or grinding in a shaker mill.[86,87] XRPD pattern collected after 30 min of vortex grinding, did not match the simulated pattern of target MOF (Fig. 14). Thus, the solid mixture of starting materials was subjected to vortex grinding for a longer period of time. After 45 min of vortex grinding, the formation of $[Cu(INA)_2]\cdot 2H_2O$ was indicated by a change in colour and a characteristic smell of acetic acid, released as a by-product. Indeed, the powder pattern collected after 45 min exhibited, in addition to peaks associated with starting materials, a set of low intensity peaks associated with $[Cu(INA)_2]\cdot 2H_2O$. After 1 h of vortex grinding, the XRPD pattern indicated that transformation to $[Cu(INA)_2]\cdot 2H_2O$ is complete.

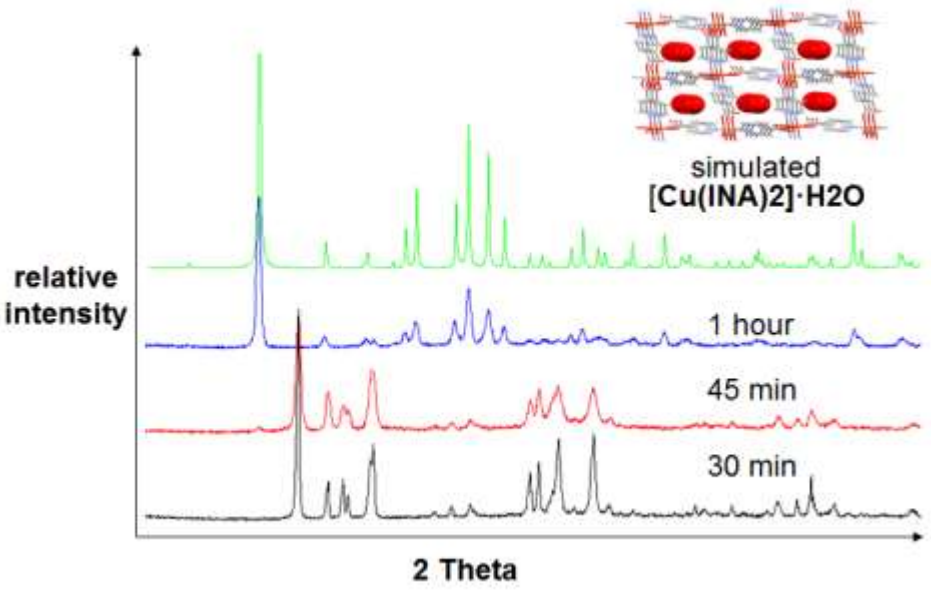

Figure 14 Progress of solvent-free synthesis of MOF.

2.3.4 Synthesis of *p*-[2.2]-cyclophane

The solid-state synthesis of 1 proved to be more challenging. Initially, we subjected a mixture of 4-benz-res and 1,4-bpeb (1:1 molar ratio) to dry mortar-and-pestle grinding for a period of 1 h. A powder XRD analysis demonstrated partial formation of the cocrystal 2(4-benz-res)·2(1,4-bpeb) along with crystalline phases consistent with 4-benz-res and 1,4-bpeb. Moreover, when the ground solid sample was exposed to broadband UV-radiation for a period of 60 h, the cyclophane 1 formed, along with intermediate monocycle (yield: 5 %), in relatively low yield (yield: 35 %). Neither 1 nor the monocyclized product formed in significantly greater amounts beyond 60 h of irradiation time (Table 2). For comparison, 1 forms stereoselectively and in up to quantitative yield when the cocrystal 2(4-benz-res)·2(1,4-bpeb) that is grown from solution is subjected to UV light for a period of 20 h. An application of LAG using methanol was also unsuccessful in affording 1 in appreciable amounts. Specifically, a powder XRD diffractogram with peaks similar to the solid obtained via dry mortar-and-pestle grinding was obtained when 4-benz-res and 1,4-bpeb were ground for a period of 1 h in the presence of methanol (50 μL). UV-irradiation of the solid for 60 h also generated a mixture of 1 (yield: 38 %) and the monocyclized photoproduct (yield: 8 %) in comparatively low yields.

Table 2 Mechanochemistry involving 4-benz-res to generate 1 from 1,4-bpeb.

grinding conditions	grinding time (h)	UV-irradiation time (h)	yield monocycle (%)	yield 1 (%)
dry mortar-and-pestle	1	60	5	35
LAG-methanol	1	60	8	38
dry vortex then UV	1	60	9	38
LAVG-methanol then UV	1	20	2	97

Since the manual grinding methods were not successful in preparation of 1, we next turned to test vortex grinding method. In particular, when 4-benz-res and 1,4-bpeb (1:1 molar ratio) were placed in a transparent sample vial along with two metal BBs and subjected to vortex grinding for a period of 1 h, a powder XRD pattern similar to the pattern from the manual grinding experiments was obtained. Moreover, exposure of the solid to broadband UV-radiation for a period of 60 h also generated 1 (yield: 38 %) and the monocyclized product (yield: 9 %) in relatively low yields.

While the dry and LAG conditions involving mortar-and-pestle grinding, as well as dry vortex grinding, to form 1 quantitatively were unsuccessful, an application of vortex grinding in the presence of a small amount of methanol was successful. In the experiment, a single drop of methanol was added to a solid mixture of 1,4-bpeb and 4-benz-res (1:1 molar ratio) in a capped sample vial containing the two BBs. The vial was then subjected to vortex grinding for a period of 1 h. Remarkably, in contrast to dry vortex grinding, the resulting powder XRD pattern matched the simulated pattern of the single-crystal X-ray structure of 2(4-benz-res)·2(1,4-bpeb) (Fig. 15). Exposure of the solid sample to UV-radiation for 20 h resulted in the stereoselective and near quantitative conversion of 1,4-bpeb to 1. The addition of the liquid phase, or application of liquid-assisted vortex grinding (LAVG), thus, served as a suitable mechanochemical method to generate 1 as compared to solution-grown 2(4-benz-res)·2(1,4-bpeb).

A successful application of LAVG was also achieved when the vortex grinding and application of UV light were performed simultaneously or in a single step. A mixture of 1,4-bpeb and 4-benz-res along with one drop of methanol were placed in a sample vial that was mounted on the vortex mixer. The assembly was then placed in the photochemical reaction chamber and the sample vial was exposed to UV-radiation under continuous vortex grinding. A ^{1}H NMR spectrum of the solid collected after a period of 4 h displayed peaks that correspond to the intermediate monocycle (yield: 16 %) and 1 (yield: 60 %). The formation of photoproducts is characterized by appearance of the

peaks at ~4.55 ppm, associated with cyclobutane ring, and disappearance of peaks at ~ 7.7 ppm, associated with C=C bonds. After a period of approximately 10 h, photoreaction generated 1 stereoselectively and in near quantitative yield (yield: 97%), which was evident from ^{1}H NMR spectra (Fig. 16). Spectra exhibited all peaks associated with 1, and trace amount of starting materials. Thus, in addition to providing access to 1 in a single step, the photoreaction involving LAVG proceeded two times faster than the irradiated solution-grown cocrystals. We ascribe success of LAVG compared to LAG to form 1 to external stress exerted by the BBs in the vortex mixer, which may be comparable to a vibrating ball mill (i.e. 'shakers'). Since the photoreaction is conducted in a capped vial, there may also be appreciable liquid vapour present in the vial during the grinding that may contribute to the formation of 1. However, that exact reasons behind dramatic effects of liquid on grinding, remain to be fully studied and understood.

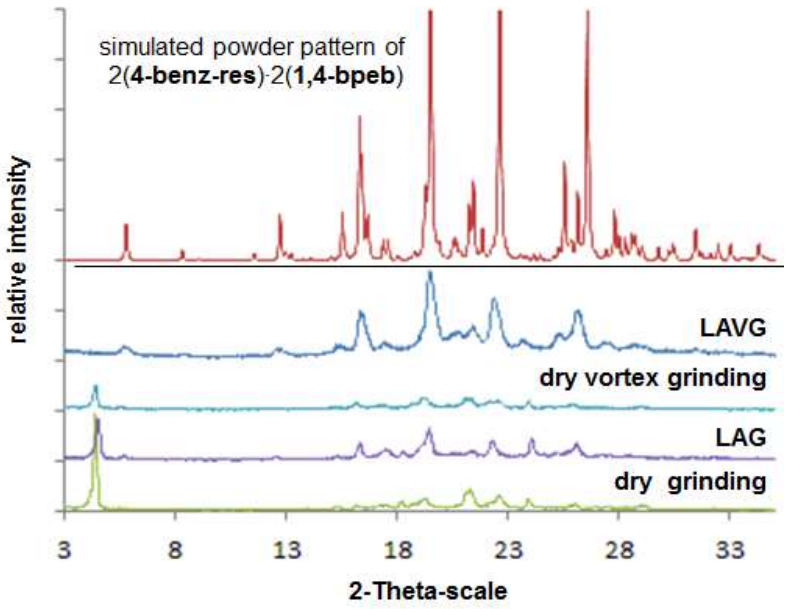

Figure 15 X-ray powder patterns of solid mixture of 4-benz-res and 1,4-bpeb after being subjected to different mechanochemical methods.

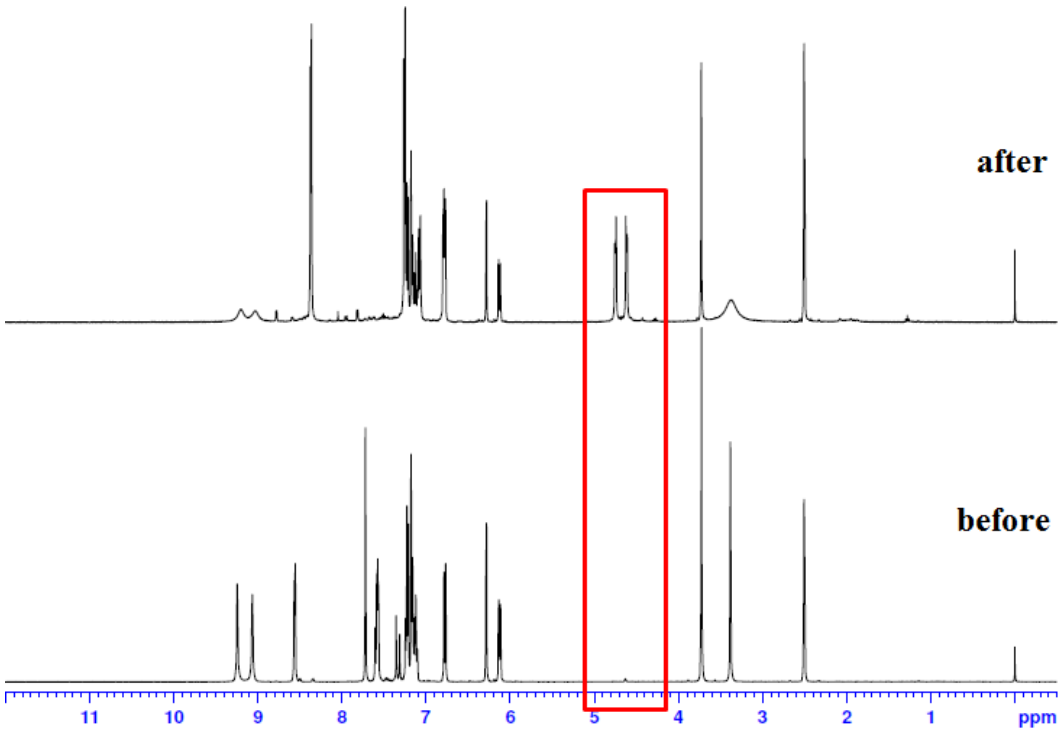

Figure 16 ^{1}H NMR spectra collected before and after 10 h of combined UV irradiation and LAVG. Red box highlights formation of peaks associated with cyclobutane rings.

2. 4 Summary

To summarize, a simple, readily accessible, and automated method that achieves the mechanochemical preparation of supramolecular materials has been developed. The vortex mixers are considered to be low-energy consumption devices and the relatively low cost of the constituent components means that the method is generally two orders of magnitude less expensive than those present in commercial ball mills. The combination of grinding and UV irradiation cannot be achieved using commercially-available instruments. However, it is easily achieved using the vortex grinding method. The vortex method has been applied to the preparation of solids sustained by hydrogen bonds and coordination bonds (MOF). Supramolecular catalysis via vortex grinding proceeds four time faster than previously reported as a result of a combination of stress exerted by grinding as well as internal stress coming from photoreaction. The scope of method was

expanded using a small amount of liquid in the form of LAVG. The molecular target 1 was prepared stereoselectively and in near quantitative yield using LAVG. The results demonstrate viability of LAVG as a practical approach to a complex organic molecule. Overall, such a versatile and resourceful method should appeal to a wide range of chemist, including green chemists and material scientists.

CHAPTER 3. SOLID-STATE SUPRAMOLECULAR CATALYSIS WHERE CATALYTIC TURNOVER PROCEEDS SPONTANEOUSLY

3.1 Introduction

The main task of synthetic chemistry is to design new molecules and materials and synthesize natural products. For efficient and sustainable organic syntheses, catalysis is essential. Chemical reactions are mediated by a wide variety of catalysts. Commonly used catalysts involve simple Brønsted acids or finely powdered metals, such as iron and palladium. In contrast to these simple catalysts, Nature uses much more elaborated and efficient enzymes to catalyze reactions. Enzymes are extremely complex and construction of functional enzyme mimics via classical covalent synthesis has proven to be extremely challenging. However, recent advances in the field of supramolecular chemistry have set a path for the development of molecular structures of enhanced complexity from modular components.[88] Supramolecular catalysts bind substrates using non-covalent interactions and may force spatial constraints on substrates to facilitate transformation to product. Compared to a classical catalysis, there is a binding step based on molecular recognition that precedes the reaction itself. Small-molecule supramolecular catalysts typically use hydrogen bonds to simultaneously assemble two substrates within a single molecular complex. In 1989, T. R. Kelly reported the first small-molecule ditopic receptor that accelerates S_N2 alkylation of an amine by alkyl halide (Fig. 17). To accelerate formation of the product by a factor of six, catalyst loading of 100% was required.[89] To control [2+2] photodimerization of cinnamic acid, M. Bassan designed a supramolecular hydrogen-bonded assembly based on the cinnamic acid ester covalently bound to diaminotriazine as a recognition unit, and a derivative of barbituric acid as a catalyst. In the presence of the catalys, up to 10-fold enhancement for the formation of dimers and up to 75-fold enhancement for the *E*-isomer were observed.[90] In general, supramolecular

catalysis requires relatively high catalyst loading owing to effects of entropy and comperatively weak intermolecular forces.

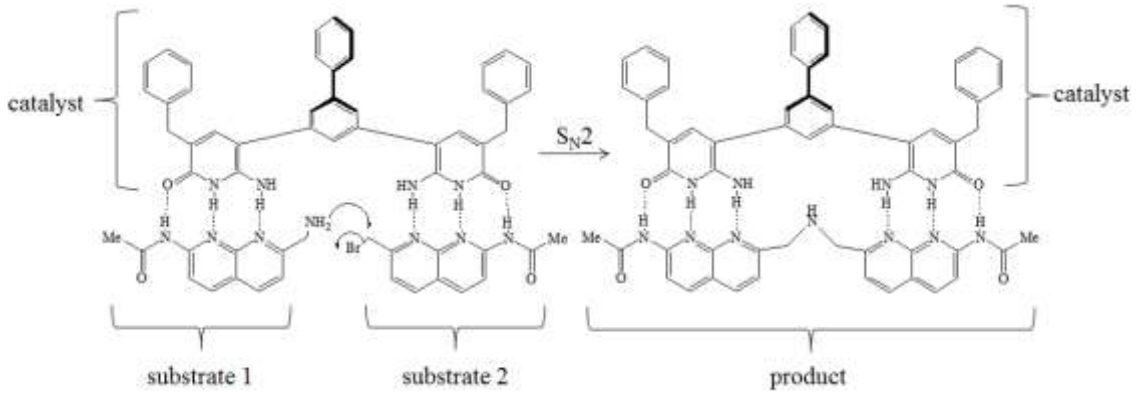

Figure 17 Supramolecular catalysis of S_N2 reaction based on a small molecule catalyst.

To conduct organic syntheses in an innovative way, one can utilize the organic solid state. The solid state provides a rich medium to control both geometry and stereochemistry in solvent-free environment (i.e., green chemistry) and offers a possibility to access molecules that may be inaccessible or difficult to realize from the liquid phase (e.g. ladderanes). However, supramolecular catalysis in the organic solid state was expected to be difficult to achieve due to low diffusion rates of molecules in the crystals. Until very recently, all reported supramolecular catalysts operate in the liquid phase. In 2010, our group reported the first small-molecule supramolecular catalyst, 4,6-diCl-res that catalyzes a [2+2] photodimerization of 4,4'-bpe to give 4,4'-tpcb. To achieve turnover, dry mortar-and-pestle grinding was utilized. Gas-phase DFT calculations performed on 2(4,4'-bpe)·2(4,6-diCl-res) assembly before and after photoreaction, found that binding energy of assembly after the photoreaction is lower. The assembly after photoreaction is destabilized by 1.1 kcal/mol due to weaker CH···N interaction and tendency to assumed a helical twisted conformation in gas phase, which is

not possible in densely packed crystal. Second grind serves to dissociate the more loosely bound product from the catalyst, release strained energy and form a thermodynamically more stable product-catalyst complex.

In a work related to host-guest chemistry, F. Toda describes the solid-state photodimerization of a guest within the host.[91] The host and chalcone as the guest, form a 1:2 host-guest complex (Fig. 18). Upon solid-state irradiation of the complex, a dimer of chalcone is formed in 90% yield. Interestingly, when host was mixed with chalcone in excess (1:4 molar ratio), dimer formed in 87% yield. As pointed out in the report, this shows that host can be used repeatedly, similar to a catalyst. Despite the promise, the lead of this preliminary result was not followed. Later on, F. Toda reported a chiral switching of a host in crystals.[92] Dynamic behavior of crystals was attributed to molecular movements involving rotation around a single C–C bond and changes in hydrogen bonding patterns.

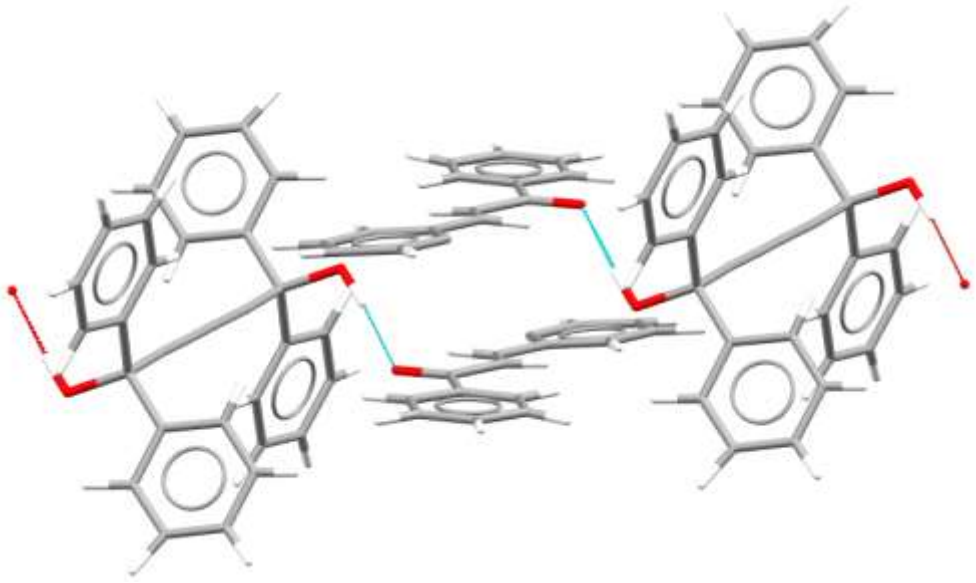

Figure 18 Host-guest complex based on chalcone.

In this chapter, we present an expansion of the concept of supramolecular catalysis in the organic solid state to a new substrate, *trans*-1,2- bis-(2-pyridyl)ethylene (2,2'-bpe) and new catalyst resorcinol (res) that catalyzes quantitative and stereoselective [2+2] photodimerization that yields photoproduct *rctt*-1,2,3,4-tetrakis(2-pyridyl)cyclobutane (2,2'-tpcb). In contrast to catalysis involving 4,4'-bpe and 4,6'-diCl-res, catalytic turnover proceeds spontaneously, without extrinsic energy involved. To investigate the mechanism, detailed gas-phase DFT calculations and X-ray diffraction studies were conducted. We uncovered that rotamerism of 2,2'-bpe substrate and 2,2'-tpcb product have great implications on stabilities of supramolecular assemblies that are basis of crystal structures. We have discovered that photoaddition forces the most stable rotamer prior to reaction to the least stable rotamer upon reaction. To release the accumulated strain, a rotation to assume a more stable rotamer takes place. The process is akin to the operation of a torsional spring as one found in a mousetrap (Fig. 19).

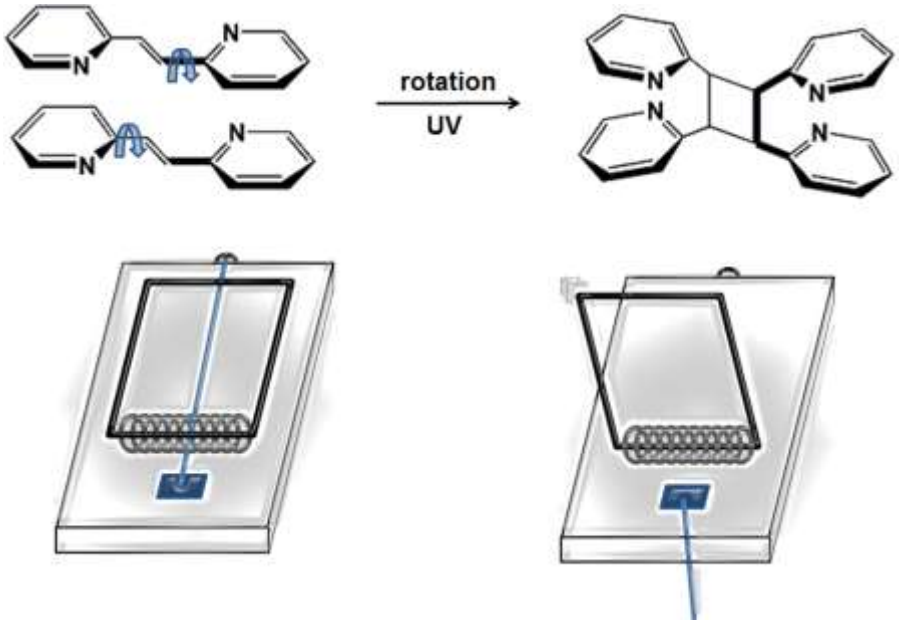

Figure 19 Supramolecular torsional spring. Rotation induced by photoaddition.

3.2 Experimental section

3.2.1 General remarks

All chemicals were purchased from Sigma-Aldrich and used as is. 4,4'-bpe was purchased from Sigma Aldrich and used without further purification. Powder X-ray data were collected on a *Bruker* D-5000 diffractometer equipped with a *Bruker* SOL-X energy-sensitive detector using Cu *K*α radiation (λ=1.54056 Å). ^{1}H NMR spectra were collected using a Bruker 400 MHz spectrometer and DMSO-d_6 as a solvent. All photoreactions were carried out in an ACE photochemical reaction chamber equipped with a broadband, medium pressure UV lamp with quartz mercury arc (Hanovia model PC451.050). Power supply: 230 V, 50 Hz, 450 W.

3.2.2 Catalysis *via* dry grinding

100 mg of 2,2'-bpe was manually ground with res for 20 min using agate mortar and pestle. Percentage and respective mass of res used is summerized in Table 3. The resulting powder was spread between two glass plates and exposed to UV irradiation. The photoreaction was routinely monitored using ^{1}H NMR spectroscopy and X-ray powder diffraction.

Table 3 Catalyst loading and corresponding mass of catalysis.

catalyst loading (%)	mass (res) (mg)
100	60
80	48
70	42
50	30
30	18
20	12
10	6

3.2.3 Synthesis of (res)·(2,2'-tpcb)

(res)·(2,2'-tpcb) was obtained from the photoreaction of 2(res)·(2,2'-bpe). 100 mg of the solid 2(res)·(2,2'-bpe), prepared as reported,[51] was gently ground to give a fine powder and spread between two glass plates and exposed to broad-band UV irradiation. The sample was irradiated until the quantitative conversion to 2,2'-tpcb was confirmed by ^{1}H NMR spectroscopy. Single crystals of (res)·(2,2'-tpcb) were grown by slow evaporation of a chloroform solution of a solid obtained upon photoreaction.

3.2.4 Crystallography

Single-crystal diffraction data were collected on a Nonius Kappa CCD single-crystal X-ray diffractometer at room temperature using $Mo_{K\alpha}$ radiation (λ=0.71073 Å). Data collection, cell refinement, and data reduction were performed using Collect. Structure solution and refinement were accomplished using SHELXS-97 and SHELXL-97, respectively. The structures were solved by direct methods. All nonhydrogen atoms were identified from the difference Fourier map within several refinement steps. All nonhydrogen atoms were refined anisotropically.

3.2.5 Theoretical methods

The initial atomic coordinates were taken from the crystal structure of 2(res)·2(4,4'-bpe) (ABEKUN). All calculations were performed using TURBOMOLE 6.3.1 program suite. All DFT calculations were performed using RI approximation and triple zeta (def-TZVP) basis sets with the corresponding auxiliary basis sets. Dispersion correction form Grimme 2006 (disp) and 2010 (disp3) was used. Structures were optimized without any frequency constraints and characterized as minima on potential energy surface due to the absence of any imaginary frequencies.

3. 3 Results and discussion

3.3.1 Catalysis *via* dry grinding

When powder obtained after dry grinding of substrate 2,2'-bpe and catalyst res, present in catalytic amount of 50%, was exposed to UV radiation, the formation of a

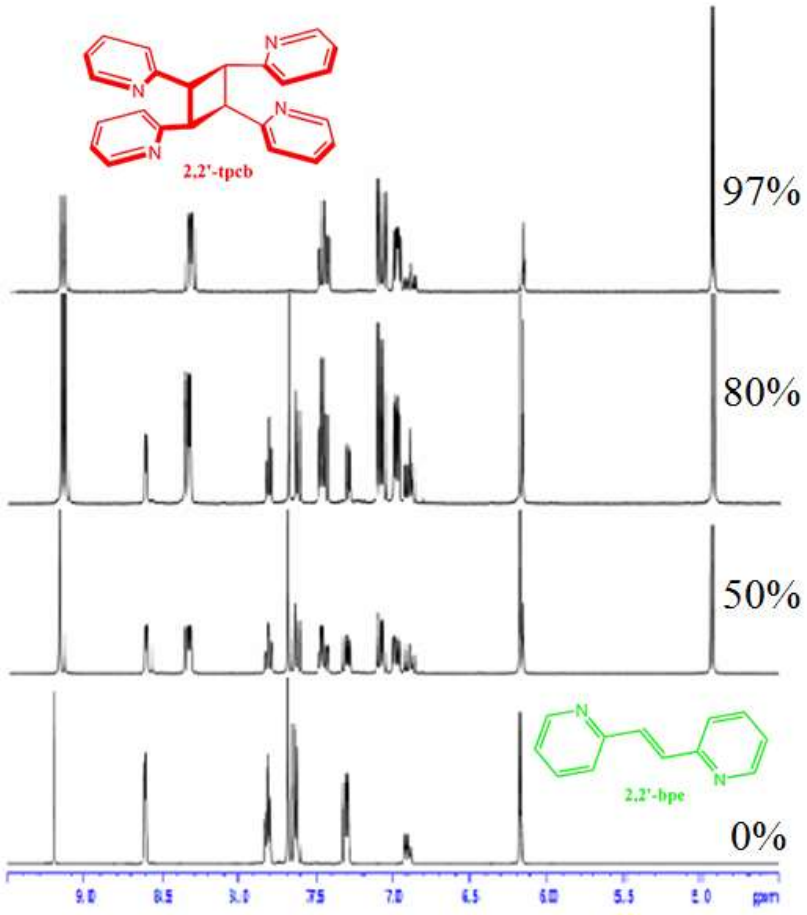

Figure 20 Progress of supramolecular catalysis followed using ^{1}H NMR spectroscopy.

single isomer of 2,2'-tpcb was evident by ^{1}H NMR spectroscopy (Fig. 20). In particular, intensity of the peak at 7.7 ppm, associated with C=C bonds, decreases, and new peak at 4.9 ppm, associated with cyclobutane ring appears. To our surprise, after 50 h of

irradiation, and without a second grind, 2,2’-tpcb formed in 60% yield. After 70 h of irradiation, 2,2’-tpcb formed in 97% yield. Longer exposure to UV light, did not give appreciable increase in yield. To ensure the reproducibility of this result, the experiment was repeated three times and each time, 2,2’-tpcb formed with 97% yield without grinding.

The X-ray powder diffraction (XRPD) pattern of the solid state mixture obtained after the initial grind and prior to UV irradiation, exhibited peaks associated with 2(res)·2(2,2’-bpe) (8.9°) and 2,2’-bpe (12.5°) (Fig. 21). After every 10 h of irradiation, both peaks associated with 2,2’-bpe and 2(res)·2(2,2’-bpe) exhibited decreased intensity, and a set of new peaks (11°), not associated with either, appeared. After 40 h of irradiation, peaks associated with 2,2’-bpe entirely disappeared. The XRPD exhibited set of weak peaks associated with 2(res)·2(2,2’-bpe) and a set peaks associated with a new, unknown phase. Combination of NMR data, that shows 50% conversion of 2,2’-bpe to 2,2’-tpcb after 40 h, and XRPD pattern that does not exhibit peaks associate with free 2,2’-bpe, indicates that only 2,2’-bpe within 2(res)·2(2,2’-bpe) is reactive, which is consistent with previous studies that determined pure crystalline 2,2’-bpe to be photostable. Moreover, the rate of spontaneous formation of 2(res)·2(2,2’-bpe) seems to be at least as high as the rate of photoreaction and release of the photoproduct. Upon prolonged irradiation, peaks associated with 2(res)·2(2,2’-bpe) entirely disappeared, as well. The XRPD pattern, collected after photodimerization was determined to be complete, exhibited a set of peaks that we were not able to assign to any reported crystal structures.

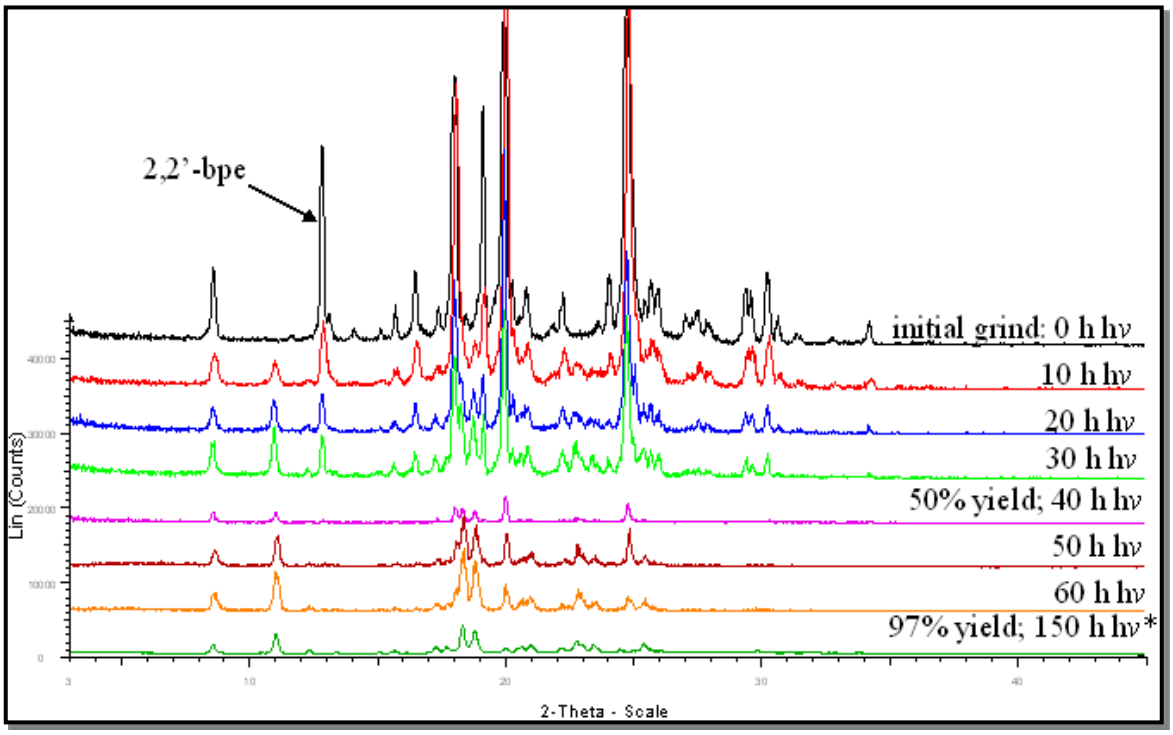

Figure 21 Progress of supramolecular catalysis followed using X-ray powder diffraction.

3.3.2 Crystal structure of (res)·(2,2'-tpcb)

In an attempt to identify new peaks in the XRPD patterns upon irradiation, we tried to obtain the crystal structure of the solid obtained after photoreaction of 2(res)·2(2,2'-bpe). Single crystals of 2(res)·2(2,2'-bpe) were grown as reported and exposed of UV radiation. Since there was no visible indication of a SCSC transformation, the solid obtained after the photodimerization was analyzed using powder X-ray diffraction. Additionally, the solid obtained after the quantitative photoconversion was recrystallized to give single crystals suitable for X-ray analysis. The single crystal structure revealed that a new cocrystal (res)·(2,2'-tpcb) formed; however, the simulated powder pattern of (res)·(2,2'-tpcb) did not correspond to the powder pattern obtained before recrystallization. The crystal structure analysis revealed that 2,2'-tpcb interacts with res via hydrogen bonds to form 1:1 cocrystal. The components crystallize in

monoclinic space group $P2_1/n$, with one molecule of 2,2'-tpcb and one molecule of res in asymmetric unit. Components interact to form infinite 1D chain. that extends along *a*-axis. Two out of four 2-pyridyl groups in 2,2'-tpcb are engaged in OH···N hydrogen bonds, each bond being formed with a different res molecule. The OH···N hydrogen bonds extend 1D chain along *a*-axis. The other two 2-pyridyl groups engage in CH···N interaction between adjacent chains (Fig. 22).

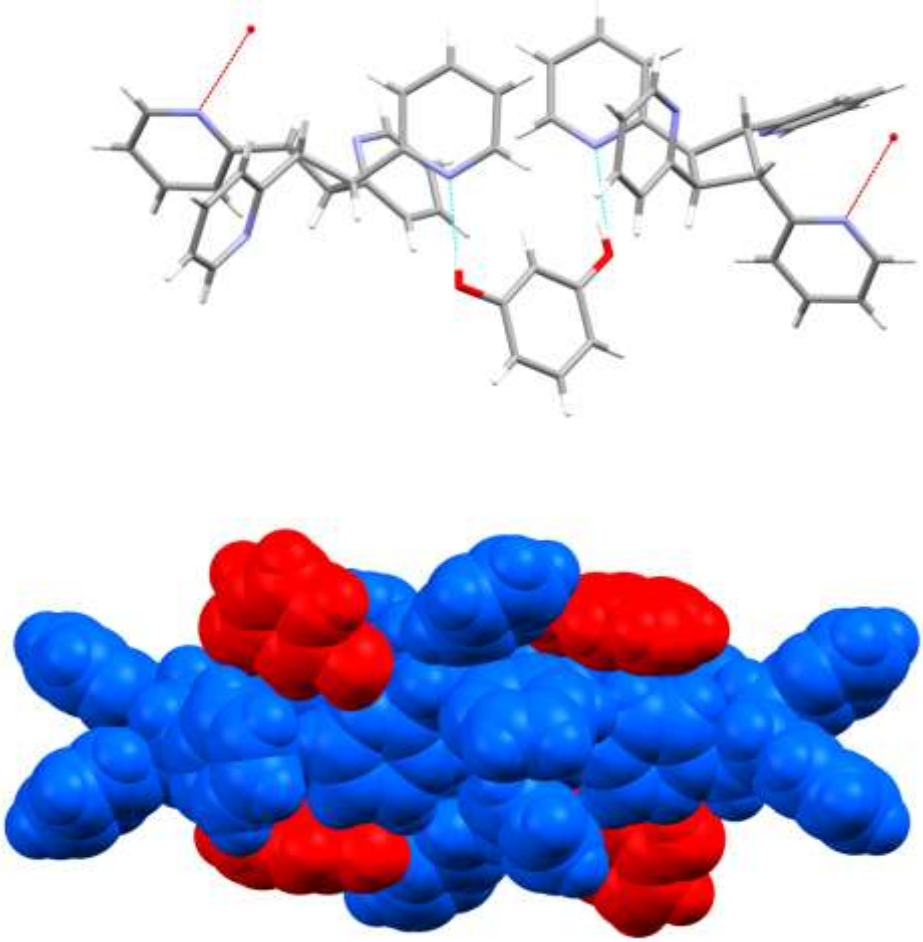

Figure 22 Crystal structure of (res)·(2,2'-tpcb): hydrogen-bonding pattern (top), and space-fill model (bottom).

3.3.3 DFT studies of supramolecular assemblies and rotamers of 2,2'-bpe

Olefin 2,2'-bpe exists as an equilibrium of conformers in solution. The unsymmetrical positioning of the N-atom in the pyridyl ring of 2,2'-bpe in combination with hindered rotation of the pyridyl groups about the single bond to the C=C linkage affords three quasi-planar rotamers of 2,2'-bpe (for the notation of rotamers, see Fig. 23). Rotamerism of 2,2'-bpe has been studied experimentally and using computational methods in solution, as well as in gas phase. The symmetrical rotamer A is the most stable rotamer by ~2 kcal/mol. It is proposed that rotamer A is stabilized by two intramolecular H···N interactions between olefinic H-atoms and N-atoms in pyridyl groups. The other two rotamers are close in energy and there is ambiguity whether rotamer B or C is more stable.

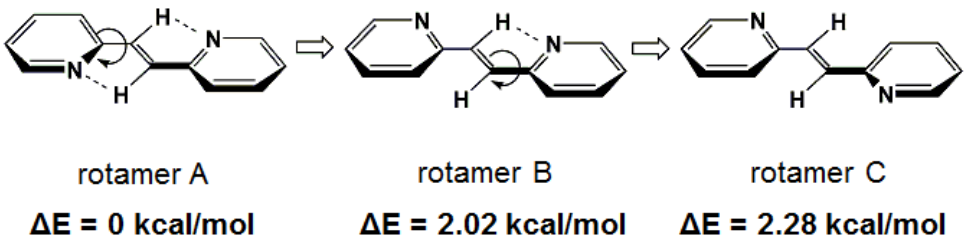

Figure 23 Rotamers of 2,2'-bpe and their relative stabilities.

In the solid state, only rotamer A has been reported as a pure solid. In the cocrystal with res, 2,2'-bpe adopts conformation A and forms a discrete four-membered assembly, namely 2(res)·2(2,2'-bpe(A)). The small-molecule template res enforces 2,2'-bpe into face-to-face double stacks via four O-H···N hydrogen bonds (*d*(O-N) = 2.78 and 2.81 Å). The assembly has a center of inversion. The olefin 2,2'-bpe assumes nearly planar conformation (twist angle 10.77°) and the C=C bonds are separated by 3.88 Å.

Additionally, res is placed side-on in respect to 2,2'-bpe and hydroxyl group interacts with H-atoms of C=C bonds (*d*(O-C) = 3.34 Å).

The DFT optimized structure of 2(res)·2(2,2'-bpe), closely resembles the crystal structure (Fig. 24). The assembly is sustained by four O-H···N hydrogen bonds (*d*(O-N) = 2.72 and 2.79 Å) and has a center of symmetry. The olefin 2,2'-bpe assumes face-to-face geometry to form double stacks where C=C bonds are separated by 3.79 Å and 2,2'-bpe is nearly planar (twist angle 10.69°). When looking perpendicular to the face-to-face stacking direction, 2(2,2'-bpe) 2(res) has a 'Z-shape', unlike 2(4,6-diCl-res)·2(4,4'-bpe) that has an elongated shape. The H-atoms of the C=C bonds are oriented side-on in respect to the resorcinol ring at 2.4 Å separation distances which indicates the secondary side-on interaction. The side-on interaction involves aromatic interactions between

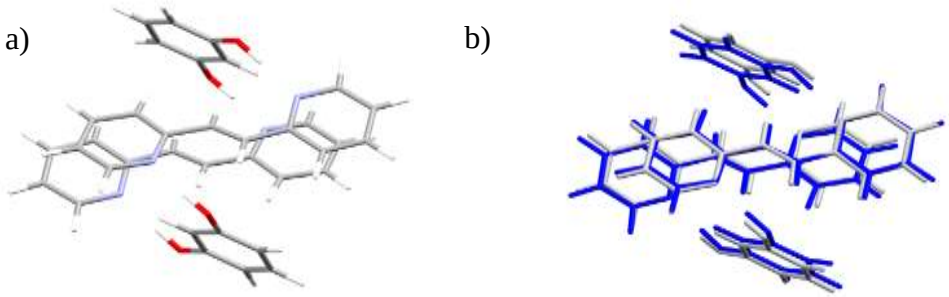

Figure 24 Crystal structure of 2(res)·2(2,2'-bpe): a) optimized structure; and b) overlay of optimized (blue) and crystal structure (grey).

the benzene ring of res and pyridine rings of 2,2'-bpe that are in T-shape (core-to-rim) geometry. Additionally, O-atoms of hydroxyl groups of res and H-atoms of the C=C bonds are in close proximity and may contribute to the secondary interaction.

Binding energies were calculated from the total energies of the individual compounds and the total energy of an assembly as defined in equation (1):

$$B.E.(kcal/mol) = [E_{assembly} - (E_{bpe} + E_{res})]*627.5 \qquad (1)$$

where: B.E.(kcal/mol) is binding energy in kcal/mol; $E_{asγsembly}$ is total calculated energy of assembly; E_{bpe} is total calculated energy of 2,2'-bpe and E_{res} is total calculated energy of res.

Reported calculated pKa values of N-atom in a single 4,4'-bpe and 2,2'-bpe molecule are 5.5±0.3 and 3.7±0.2, respectively. The N-atom in 4,4'-bpe is more basic than in 2,2'-bpe and, thus, it can be expected that 4,4'-bpe would form stronger hydrogen bonds and the binding energy of assemblies based on 4,4'-bpe would be higher. However, our calculations show that the opposite is true. The assembly 2(res)·2(2,2'-bpe(A)) has significantly higher binding energy, 74.54 kcal/mol, which is around 30 kcal/mol higher than reported binding energy for assemblies based on 4,4'-bpe. The relative stabilization can be rationalized taking in account for additional interactions. In particular, the close proximity of res to the C=C bonds indicates the secondary side-on interaction. The side-on interaction involves aromatic T-shape (core-to-rim) interaction between the benzene ring of res and pyridine rings of 2,2'-bpe, and between O-atom of hydroxyl groups of res and H-atoms of the C=C bonds.

To address how a change in conformation may affect the stability of the assemblies and supramolecular interactions, we optimized assemblies based on rotamers B and C, and calculated respective energies (Fig. 25). We found that all three conformers form supramolecular assemblies with res and in all assemblies 2,2'-bpe is close to planar. That assembly 2(res)·2(2,2'-bpe(C))is energetically less favorable by 0.1 kcal/mol, may indicate a slightly weaker secondary interaction compared to the rotamer A. In the assembly based on the rotamer B, two res molecules are forced in close proximity of 3.8 Å. The unfavorable position of res accounts for a repulsive interaction that significantly decreases the stability of the assembly when compared to assemblies based on rotamer A and C.

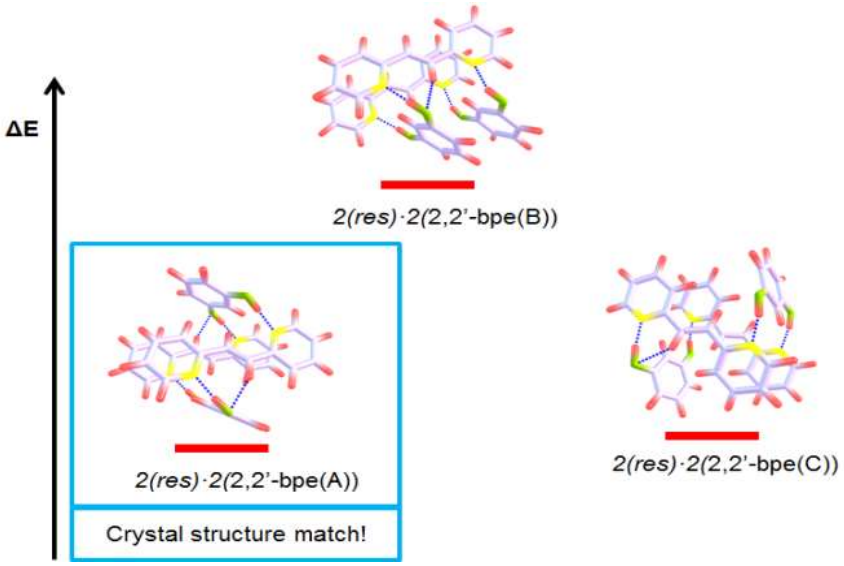

Figure 25 Relative stabilities of assemblies based on three rotamers of 2,2'-bpe.

3.3.4 DFT studies of supramolecular assemblies and rotamers of 2,2'-tpcb

Similar to 2(res)·2(4,4-bpe), 2(res)·2(2,2'-bpe(A)) affords 2,2'-tpcb stereoselectively and in up to 100% yield. The rotamerism in the case of 2,2'-tpcb, or a similar cyclobutane, has not been yet addressed. Moreover, a crystal structure obtained from photoreaction has not been yet reported. Given that olefin 2,2'-bpe adopts conformation A in the cocrystal with res to form 2(res)·2(2,2'-bpe(A)), and the assembly is determined to be the most stable in gas phase, we performed calculations based on the cyclobutane 2,2'-tpcb(I) that is product of dimerization of the rotamer A without rotation around single bonds. The other rotamers of 2,2'-tpcb (II-IV) are shown in Fig. 26.

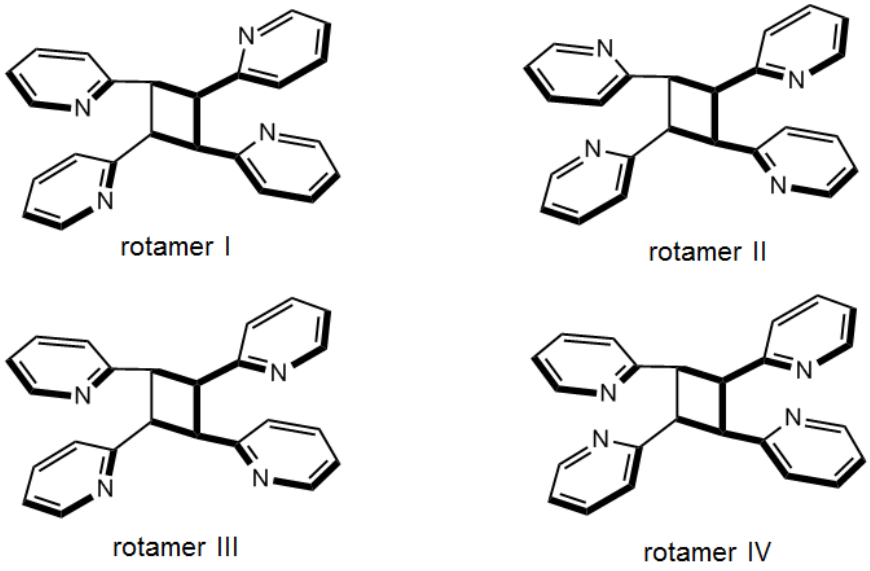

Figure 26 Rotamers of 2,2'-tpcb

The assembly 2(res)·(2,2'-tpcb(I)) is sustained by four hydrogen bonds (*d*(O-N) = 2.79, 2.79, 2.80 and 2.81 Å) (Fig. 27). The cyclobutane ring is slightly puckered (τ = 21.01°) and d(C-C) distances are 1.53, 1.54, 1.60 and 1.60 Å. Two res molecules are in close proximity of cyclobutane ring (2.43 and 2.44 Å), but on the opposite sides, and are in planes parallel to each other. In contrast to assemblies based on 4,4'-tpcb, where N-atoms are further apart than prior to photodimerization, in 2(res)·(2,2'-tpcb(I)) N-atoms are closer than in 2(res)·(2,2'-bpe)

While the energy of assemblies based on 4,4'-tpcb are only ~1 kcal/mol destabilized upon photoreaction, 2(res)·(2,2'-tpcb(I)) is dramatically destabilized by 5.56 kcal/mol (B.E.= 68.98 kcal/mol,). Since the geometry optimization indicates that the lengths of hydrogen bonds have not significantly changed, the strong destabilization has to be explained with other changes introduced upon photoreaction.

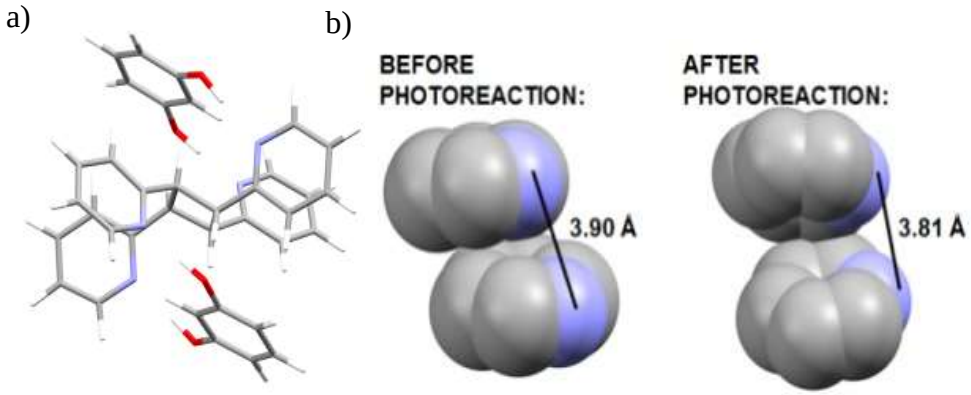

Figure 27 Optimized structure of 2(res)·(2,2'-tpcb(I)): a) full assembly, and b) N-N distance before and after photoreaction.

To address rotamerism of 2,2'-tpcb and elucidate reasons behind peculiar destabilization of assemblies upon photoreaction, we optimized 2,2'-tpcb rotamers both isolated and within discrete assembly when such assembly was possible using the same basis set and method as previously. First, we considered three rotamers that would result in photoreaction of three assemblies, 2(res)·2(2,2'-bpe(A-C)), without rotation around single bonds. Interestingly, the most stable assembly before photoreaction, 2(res)·2(2,2'-bpe(A)), does not yield the most stable rotamer. In fact, rotamer I, is more energetically favorable, than rotamer II by 1.5 kcal/mol. The relative stabilization of rotamer I may be explained by stronger N···H interaction. The same N···H interaction is reported to affect stability of 2,2'-bpe rotamers and it is plausible that plays an important role in stability of 2,2-tpcb rotamers, as well. We also rationalized that a conformation where N-atoms are not atop of each other, and, thus, repulsive N-N interactions are eliminated, would be favorable. Thus, we constructed rotamer IV and optimized using the same basis set and method. We found that rotamer IV is energetically most favorable by more than 6

kcal/mol compared to rotamers I-III. The large stabilization compared to the other rotamersis likely due to the favorable positioning of N-atoms.

Next, we turned to optimization of discrete assemblies based on rotamers II and III (Fig. 28). We found that hydrogen bonding is preserved upon photoreaction in all assemblies. However, the most stable assembly upon photoreaction, 2(res)·(2,2'-tpcb(II)), does not stem from the most stable assembly prior to photoreaction, 2(res)·2(2,2'-bpe(A)). In fact, binding energy 2(res)·(2,2'-tpcb(II)) is 5 kcal/mol more than that of 2(res)·(2,2'-tpcb(I)). The relative stabilization of the assembly is result of more stable rotamer as discussed above.

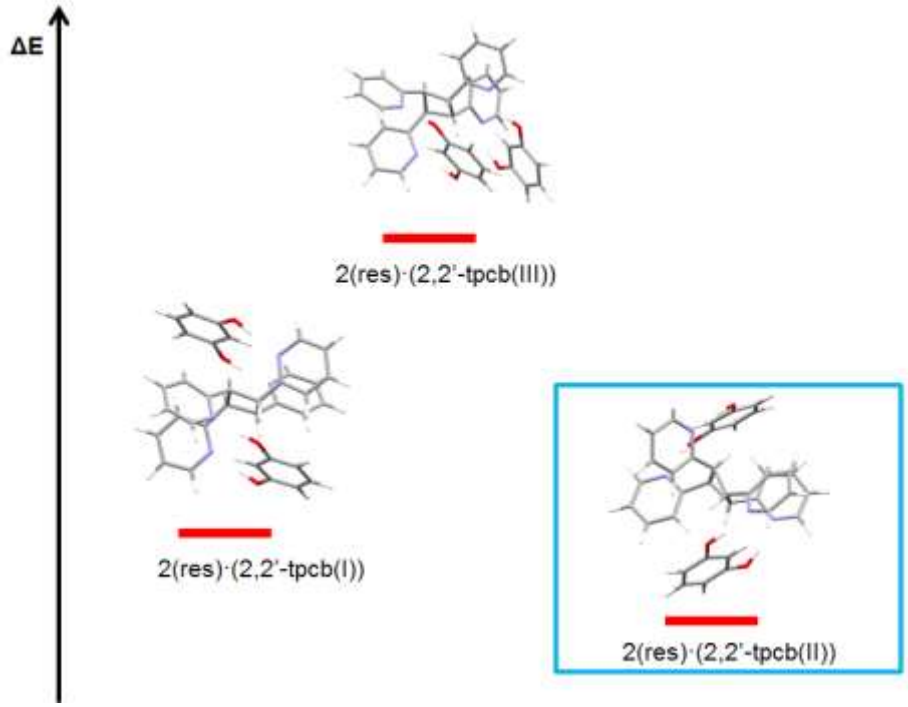

Figure 28 Relative stabilities of assemblies based on three rotamers of 2,2'-tpcb.

The geometry of the most stable rotamer IV is not suitable for formation of hydrogen bonds that would yield discrete assembly resembling those based on rotamers I-

III. However, we expected that due to the large stabilization energy of rotamer IV (more than 6 kcal/mol difference when compared to other rotamers), 2,2'-tpcb in crystalline state will have propensity to assume conformation IV. During the photoreaction of 2(res)·2(2,2'-bpe(A)), pyridyl group will rotate such that in the final photoproduct the most stable conformation IV will be achieved. The rotation will cause hydrogen bonds to break and rearrange (Fig. 29). Overall, the processes will release the accumulated strain through process akin to the operation of a torsional spring in a mousetrap. Effective crystalline molecular machines require molecular components forming an extended, rigid and highly-ordered network (*stators*) that are linked to the dynamic components (*rotors*) by covalent, supramolecular, or mechanical bonds. When considering photodimerization of 2(res)·2(2,2'-bpe), one could envisage olefin and cyclobutane to be a stator part of the assembly, and 2-pyridyl group to have rotatory function of a molecular machine.

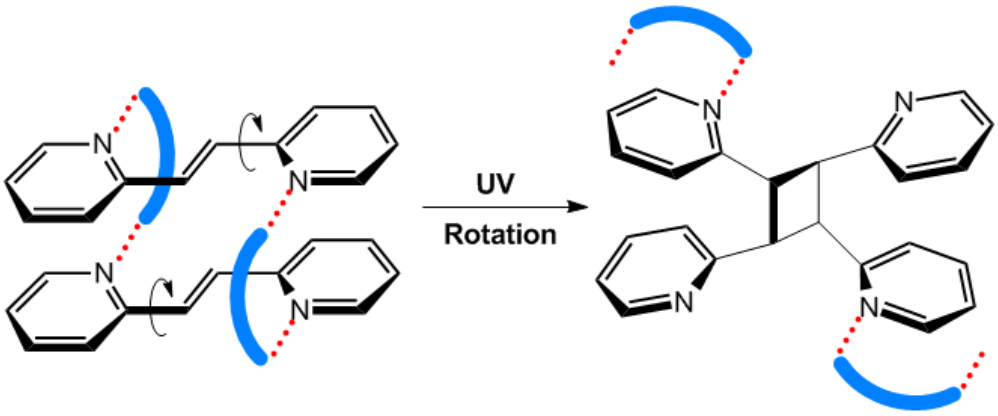

Figure 29 Dynamic behavior upon photoreaction in crystalline state akin to action of a torsional spring.

Such torsional motion upon UV-irradiation could be an effective way for crystal to release accumulated stress. In the context of catalysis, there are several important implications. First, it is likely that upon irradiation crystal undergoes extreme changes on

molecular level. These changes result in macroscopic deformation and cracking of the crystal which can serve as recombination areas. Second, hydrogen bonds upon irradaiton are probably broken or dramatically weaker. Thus, res has strong propensity to reestablish the most stable hydrogen bonding pattern. Considering that binding energies of 2(res)·2(2,2'-bpe) is significantly higher than binding energy of 2(res)·2(2,2'-tpcb), it is likely that res well "grab on" 2,2'-bpe, instead of 2,2'-tpcb, until all 2,2'-bpe is used and catalysis facilitates near to quantitative photodimerization.

3.4 Summary

In this chapter, we report an expansion of supramolecular catalysis to 2,2'-bpe as a substrate and res as a catalyst. It was determined that catalytic turnover proceeds rapidly and spontaneously in solid state. Catalysis is effective using catalyst loading as low as 10% which is comparable to more traditional catalysts, such as palladium based catalyst (typically use 10-15 mol%). This is the first well documented report of molecular mobility in crystals of such a high degree in the context of solid-state synthesis. Detailed mechanistic studies uncovered that subtle interactions and geometrical particularities have great implications on supramolecular assemblies. In particular, to assume the most stable rotamer upon photoreaction, rotation around C-C single bonds takes place. As a result, hydrogen bonding pattern has to change. Overall, this motion is akin to action of a supramolecular torsional spring. It can be expected that results presented here will have impact on area of research focused on design of crystalline molecular machinery and solid-state reactivity of higher level of complexity.

CHAPTER 4 DISCRETE AROMATIC STACKS BASED ON NH···N AND CH···N INTERACTIONS

A portion of this chapter was published as a communication and is adapted with permission from the *Angewandte Chemie International Edition* [Stojakovic, J.; Whitis, A.M.; MacGillivray, L.R., "Discrete Double-to-Quadruple Aromatic Stacks: Stepwise Integration of Face-to-Face Geometries in Cocrystals Based on Indolocarbazole", *Angew. Chem., Int. Ed.* **2013**, *52*, 12127-12130.]

4.1 Introduction

Aromatic stacks of molecules are of great importance both in Nature and industry (Fig. 30). The ability to engineer well-defined stacks is expected to enable expedited development of advanced supramolecular materials with unique properties and, thus, much effort has been placed to develop reliable approaches to stack aromatics based on covalent, metal-ligand, hydrogen-bonding, aromatic-aromatic, and electrostatic forces. However, parallel face-to-face arrangements of aromatics are energetically less favorable

a)

b)

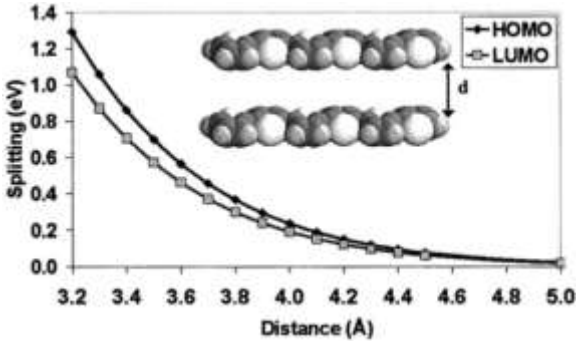

Figure 30 Importance of aromatic stacking in: a) helical structure of biomacromolecules, b) efficiency of organic semiconductor as a function of interatomic distances.

and engineering discrete, moderate-sized aromatic stacks remains a challenge. The issue has been addressed by Fujita *et. al.*, in 2009 "*The ability to engineer discrete, medium-sized stacks of aromatic molecules is limited even though well-defined stacks are essential for examining the parameters governing intermolecular interactions and the transition from molecular to material properties. As such, there has been a continuing interest in controlling both the size and orientation of aromatic stacks.*"[93]

While molecular tweezers have been demonstrated as receptor for aromatics and scaffold for infinitive aromatic stacks, discrete stacks of more than three aromatics mediated by multicomponent self-assembly has, to date, only been achieved with assistance of metal-ligand forces. The ability to stack aromatics in a modular fashion, particularly in the solid state, would grant access to tunable materials with targeted properties

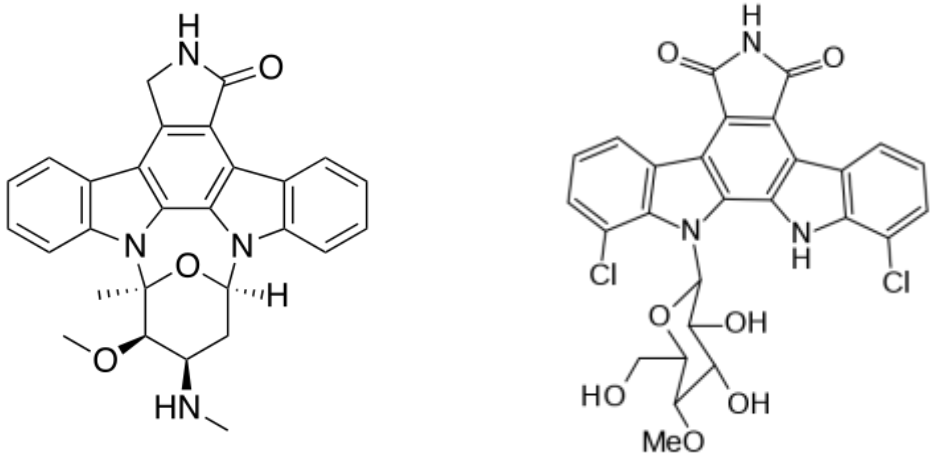

Figure 31 Biologically important indolocarbazoles: a) naturally occurring *Staurosporine*, and b) anticancer agent *Rebeccamycin*.

Indolocarbazoles are class of molecules based on a conjugate aromatic system of two pyrrole and three benzene rings. Variety of natural occurring compounds has indolocarbazole backbone (Fig. 31). The first isolated indolocarbazole, in 1977, was *Staurosporine* that was subsequently determined to have a range of biological activities including anti-fungal and anti-hypertensive properties. In following decades, many other indolocarbazoles were isolated and biological activity of indolocarbazoles was intensely studied.[94] An indolocarbazole, *Rebeccamycin*, is an anticancer agent, and has been studied in clinical trials.[95] The pyrrole rings, which present two rigidly-disposed hydrogen-bond-donor N-H groups, are known to bind strongly to negatively-charged species. Thus, in supramolecular chemistry, indolocarbazoles are employed as potent anion receptors.[96] The N-H groups, however, remain largely unexplored for applications in the solid state. In fact, the N-H groups can, in principle, effectively equip indolocarbazoles as novel molecular receptors in solids.

In this chapter, we will demonstrate that indolo[2,3-*a*]carbazole (IC) can act as a molecular receptor and organize 4,4'-bpe into double, triple, and quadruple stacks within cocrystals of $(IC)_2(4,4'\text{-bpe})_2 \cdot 2(AcN)$, $(IC)_2(4,4'\text{-bpe})_3$ and $(IC)_2(4,4'\text{-bpe})_4$, respectively (Fig. 32). Integration of aromatic stacks into discrete assemblies is achieved using N-H···N hydrogen bonds, and in each case, IC enforces aromatic stacking of 4,4'-bpe exclusively in a face-to-face manner. We will also show that UV irradiation of $(IC)_2(4,4'\text{-bpe})_4$ induces the olefin to undergo a topochemical [2+2] photodimerization to afford 4,4'-tpcb stereoselectively and in maximal theoretical yield based on the enforced quadruple stacking.

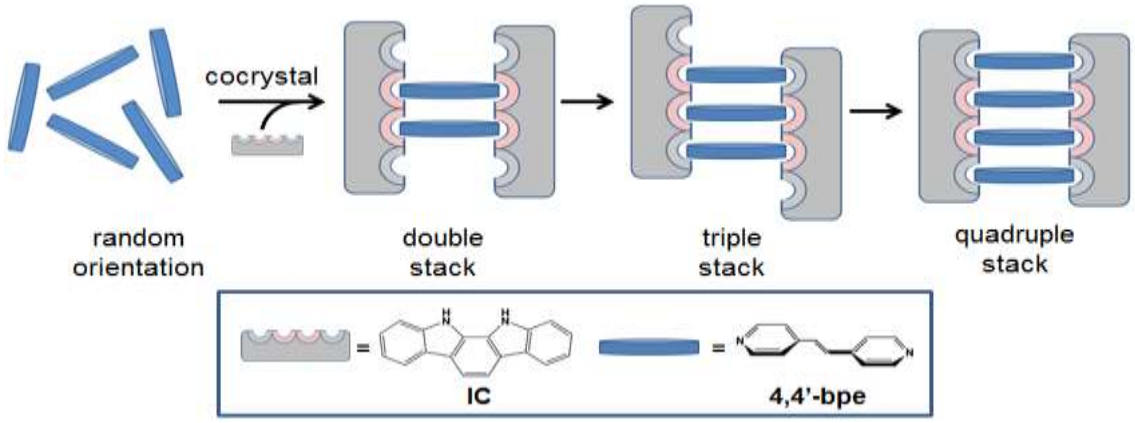

Figure 32 Integration of 4,4’-bpe into double-to-quadruple discrete stacks enforced by IC.

4.2 Experimental Section

4.2.1 General remarks

4,4’-bpe was purchased from Sigma Aldrich and used without further purification. Powder X-ray data were collected on a *Bruker* D-5000 diffractometer equipped with a *Bruker* SOL-X energy-sensitive detector using Cu *K*α radiation (λ=1.54056 Å). ^{1}H NMR spectra were collected using a Bruker 400 MHz spectrometer and DMSO-d6 as a solvent.

4.2.2 Synthesis of IC

IC was prepared using adapted Fischer indole synthesis.[97] Single crystals were grown from hot acetonitrile (AcN) solution.

4.2.3 Synthesis of double stacks, $(IC)_2(4,4'\text{-bpe})_2 \cdot 2(AcN)$

50 mg (0.2 mol, 1 eq.) of IC and 35 mg (0.2 mol, 1 eq.) of 4,4’-bpe were separately dissolved with heating in minimal amount of hot AcN (~1 ml). The solutions were mixed and left to slowly cool to form single crystals in a period of less than 1 h.

4.2.4 Synthesis of triple stacks, $(IC)_2(4,4'\text{-bpe})_3$

50 mg (0.2 mol, 1 eq.) of IC and 70 mg (0.4 mol, 2 eq.) of 4,4'-bpe were separately dissolved with heating in minimal amount of hot AcN (~1 ml). The solutions were mixed and left to slowly cool to form single crystals in a period of less than 1 h.

4.2.5 Synthesis of quadruple stacks, $(IC)_2(4,4'\text{-bpe})_4$

50 mg (0.2 mol, 1 eq.) of IC was dissolved in 10 ml of hot AcN and 70 mg (0.4 mol, 2 eq.) of 4,4'-bpe was dissolved in 10 ml of hot AcN. The solutions were mixed, solvent was left to slowly evaporate, and single crystals formed in a period of 3 days.

4.2.6 Photoreaction

All photoreactions were carried out in an ACE photochemical reaction chamber equipped with a broadband, medium pressure UV lamp with quartz mercury arc (Hanovia model PC451.050). Power supply: 230 V, 50 Hz, 450 W.

In typical experiment, 50 mg of single crystals were powdered by gentle grinding in an agate mortar-and-pestle for 1 min. The resulting powder was spread as a thin layer between two glass plates and exposed to UV irradiation up to 70 h.

4.2.7 Synthesis of photoproduct cocrystal, (IC)(4,4'-tpcb)

50 mg (0.2 mol, 1 eq.) of IC was dissolved in minimal amount of AcN and and 70 mg (0.2 mol, 1 eq.) of 4,4'-tpcb was dissolved in minimal amount of chloroform. The solutions were mixed and left to slowly cool to form single crystals in a period of 1 day.

4.2.8 X-ray crystallography

Single-crystal diffraction data were collected on a Nonius Kappa CCD single-crystal X-ray diffractometer at room temperature using MoKα radiation (λ=0.71073 Å). Data collection, cell refinement, and data reduction were performed using Collect. Structure solution and refinement were accomplished using SHELXS-97 and SHELXL-97 respectively. The structures were solved by direct methods. All nonhydrogen atoms

were identified from the difference Fourier map within several refinement steps. All non-hydrogen atoms were refined anisotropically.

4.3 Results and discussion

4.3.1 Crystal structure of indolo[2,3-*a*]carbazole (IC)

The interest in IC stems from the use of small molecules as templates to direct reactivity in solids. We hypothesized that the N-H groups of IC can form hydrogen bonds with a hydrogen-bond-acceptor such as the bipyridine 4,4'-bpe to enforce a stacking geometry suitable for a photodimerization. To better understand binding motifs of IC in a solid, we first determined the crystal structure of IC. Slow evaporation of an AcN solution of IC yielded colorless plate-like crystals suitable for single-crystal X-ray diffraction. IC crystallizes in the monoclinic space group $P2_1/c$. The asymmetric unit consists of two molecules of IC in a distorted edge-to-face, or T-shaped, arrangement with an angle between planes of 64.2° (Fig. 33). The distances between the pyrrole N-atoms (3.23 and 3.25 Å) are comparable to the N-H groups involved in anion coordination (~ 3.10-3.25 Å), yet less than the hydroxyl O-atoms of resorcinol-based templates (~ 4.8 Å). When viewed along the b-axis, the extended packing is herringbone, similar to high-pressure benzene and naphthalene, where each IC interacts with four neighbors via N-H···π and C-H···π forces.

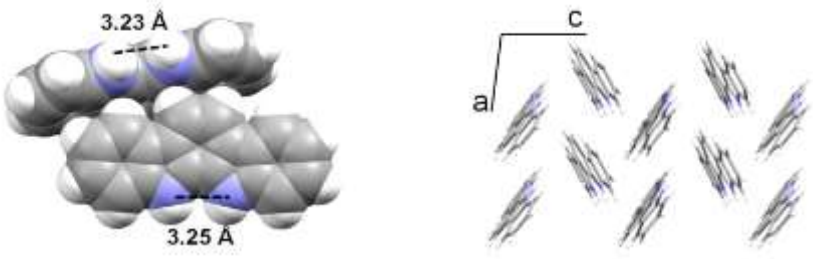

Figure 33 X-ray structure of IC: a) N···N distance and edge-to-face interaction and b) extended packing along b-axis.

4.3.2 Discrete double aromatic stack

IC and 4,4'-bpe were individually dissolved in minimal AcN (1:1 molar ratio). Upon mixing, pale-yellow plate-like crystals grew in less than 1 h. ^{1}H NMR spectroscopy revealed the solid to consist of IC, 4,4'-bpe, and AcN in a 1:1:1 ratio. A crystal structure analysis confirmed IC to interact with 4,4'-bpe in the cocrystal solvate $(IC)_2(4,4'\text{-bpe})_2 \cdot 2(AcN)$ (Fig. 34). The components crystallize in the monoclinic space group $P2_1/n$ with an asymmetric unit that consists of one IC, one 4,4'-bpe, and one AcN. IC and 4,4'-bpe interact *via* a cyclic array of four NH···N bonds (d(N···N) = 2.885(3) and 2.937(3) Å) to give a discrete, four-component assembly. The tilt angle between IC and 4,4'-bpe is 66.3°. Moreover, two molecules of 4,4'-bpe lie stacked in a face-to-face geometry, being offset by *ca* 0.5 Å. The stacked double bonds (C=C) of 4,4'-bpe lie parallel and separated by 3.85 Å. The assemblies pack interdigitated with IC atop 4,4'-bpe. The included AcN interacts with IC *via* C-H···N(AcN) forces. To our knowledge, $(IC)_2(4,4'\text{-bpe})_2 \cdot 2(AcN)$ represents the first example of a cocrystal based on an indolocarbazole.

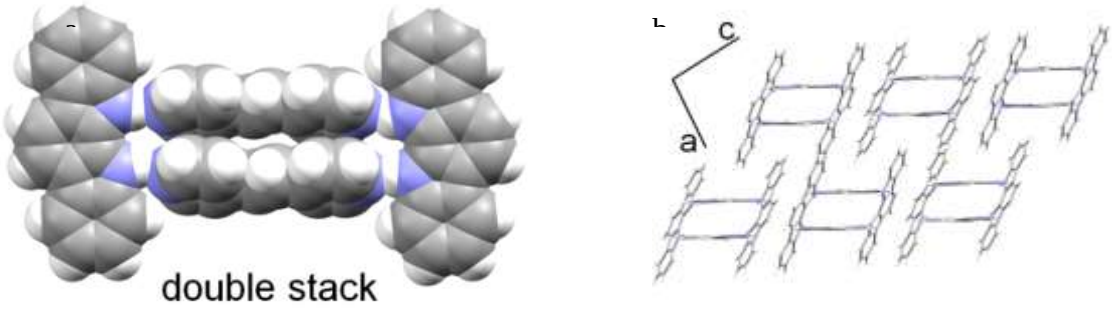

Figure 34 X-ray structure of $(IC)_2(4,4'\text{-bpe})_2 \cdot 2(AcN)$: a) space-filling model and b) extended packing along *b*-axis (solvent omitted for clarity).

4.3.3 Discrete triple aromatic stack

During the course of the experiments, I also obtained crystals of a habit different than $(IC)_2(4,4'\text{-bpe})_2 \cdot 2(AcN)$. More specifically, when cocrystallization was performed in a 1:2 molar ratio of IC to 4,4'-bpe, rapid precipitation from AcN afforded colorless needle-like crystals. ^{1}H NMR spectroscopy revealed the crystals to consist of IC and 4,4'-bpe in a 2:3 ratio.

A crystal structure analysis revealed IC to interact with three molecules of 4,4'-bpe to enforce triple stacking in cocrystals of composition $(IC)_2(4,4'\text{-bpe})_3$ (Fig. 35). The components crystallize in the monoclinic space group $P2_1/c$, with an asymmetric unit of two molecules of IC and two full and two half molecules of 4,4'-bpe. As with $(IC)_2(4,4'\text{-bpe})_2 \cdot 2(AcN)$, the components are sustained by four NH···N hydrogen bonds (d(N···N)= 2.903(3), 2.906(3), 2.988(3) and 2.991(3) Å). In contrast to $(IC)_2(4,4'\text{-bpe})_2 \cdot 2(AcN)$, the IC molecules lie offset such that only the central molecule of 4,4'-bpe (molecule A) is bridged by two NH···N forces. Each remaining N-H group of IC participates in a single NH···N hydrogen bond with 4,4'-bpe (molecules B). The remaining N-atoms of 4,4'-bpe form CH···N forces with IC (d(C···N) = 3.410(5) and 3.473(5) Å). As a consequence of

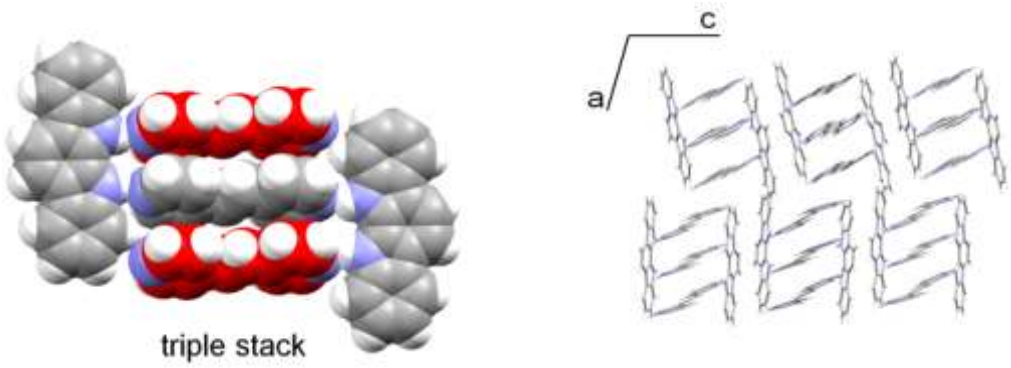

Figure 35 X-ray structure of $(IC)_2(4,4'\text{-bpe})_3$: a) space-filling model and b) extended packing along *b*-axis.

the assembly process, the components form a discrete five-component assembly based on enforced triple stacking. The tilt angles between the planes of IC and 4,4'-bpe are 65.0° (A) and 67.7° (B). The stacking of the three 4,4'-bpe molecules is, thus, manifested in a face-to-face BAB manner. The C=C bonds of the stacked olefins lie parallel with the C-atoms separated by 3.82 and 3.84 Å. The assemblies pack along the *a*-axis with adjacent assemblies interdigitated and offset. This the first report of enforced aromatic stacking of three molecules within a discrete, self-assembled, purely organic structure. Work of Fujita *et. al.* has described double-to-quintuple stacks hosted by metal-organic coordination cages.

4.3.4 Discrete quadruple aromatic stack

Remarkably, when the crystallization conditions to generate triple-stacked $(IC)_2(4,4'\text{-bpe})_3$ were extended to periods of days, slow precipitation from an AcN solution of IC and 4,4'-bpe in 1:2 molar ratio afforded colorless plate-like crystals of composition $(IC)_2(4,4'\text{-bpe})_4$, as determined by ^{1}H NMR spectroscopy.

A crystal structure analysis of $(IC)_2(4,4'\text{-bpe})_4$ revealed discrete six-component assemblies, which crystallize in the monoclinic space group $P2_1/c$, that feature quadruple-stacking of 4,4'-bpe (Fig. 36). In the arrangement, the components, analogous to double-stacked $(IC)_2(4,4'\text{-bpe})_2\cdot 2(AcN)$, are held together by a cyclic array of four NH···N hydrogen bonds (d(N···N) = 2.982(7) and 2.928(6) Å). More specifically, the quadruple stacking is defined by two inner molecules of 4,4'-bpe (A) that participate in the NH···N forces and two outer molecules (B) that form single CH···N forces (d(C···N) = 3.493(9) Å). The C=C bonds of the A molecules lay disordered (occupancies: 0.63/0.37) over two sites. The molecules that define the quadruple stacks, consequently, pack in a face-to-face BAAB manner. The planes between IC and 4,4'-bpe are tilted at 79.4° and 89.1° for the A and B molecules, respectively, which are closer to orthogonality than $(IC)_2(4,4'\text{-bpe})_2\cdot 2(AcN)$ and $(IC)_2(4,4'\text{-bpe})_3$. The C=C bonds between stacked A-A and A-B pairs

are separated by 3.91 Å and 3.94 Å, respectively. Similar to $(IC)_2(4,4'\text{-bpe})_3$, the assemblies lie interdigitated along the *a*-axis.

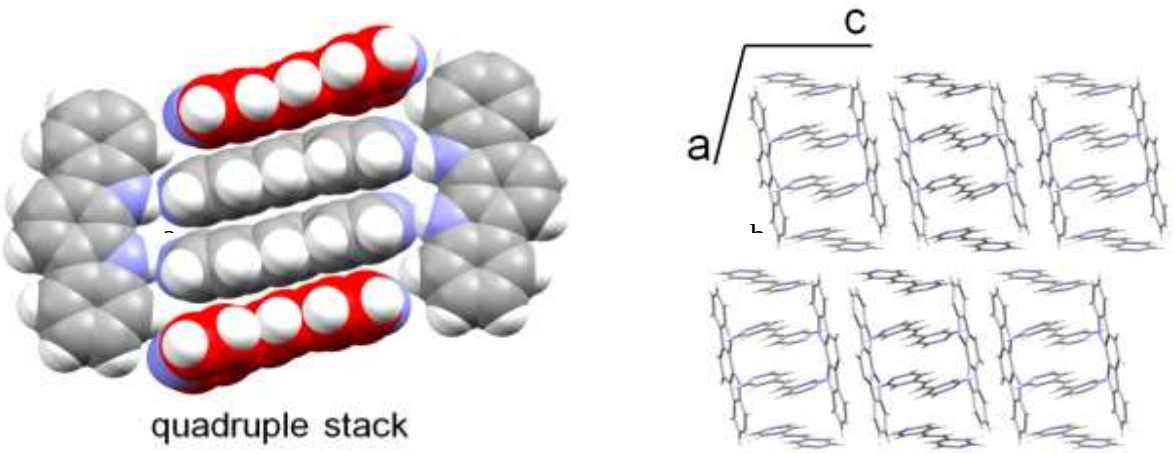

Figure 36 X-ray structure of $(IC)_2(4,4'\text{-bpe})_4$: a) space-filling model and b) extended packing along *b*-axis (disorder omitted for clarity).

4.3.5 Photoreactivity of discrete aromatic stacks

The face-to-face stacking of 4,4'-bpe and proximity of the C=C bonds in each cocrystal prompted us to study a possible [2+2] photodimerization in each solid. Upon prolonged UV irradiation, $(IC)_2(4,4'\text{-bpe})_2 \cdot 2(AcN)$ and $(IC)_2(4,4'\text{-bpe})_3$ were determined to be photostable. However, after 60 h of UV irradiation the olefins of $(IC)_2(4,4'\text{-bpe})_4$ underwent a photodimerization to generate 4,4'-tpcb (Table 4).

Table 4 Summary of photoreactivity experiments.

Cocrystal	Reactivity
$(IC)_2 \cdot (4,4'\text{-bpe})_4$	Photoreactive
$(IC)_2 \cdot (4,4'\text{-bpe})_3$	Photostable
$(IC)_2 \cdot (4,4'\text{-bpe})_2 \cdot 2(AcN)$	Photostable

Based on the ^{1}H NMR analysis, photoreaction proceeded with yield of *ca* 40% yield (Fig. 37). The yield is consistent with the expected maximal theoretical conversion for $(IC)_2(4,4'\text{-bpe})_4$ based on the two disordered A molecules of 4,4'-bpe of the quadruple stack. IC, thus, serves as a template to direct the [2+2] photodimerization in a solid.

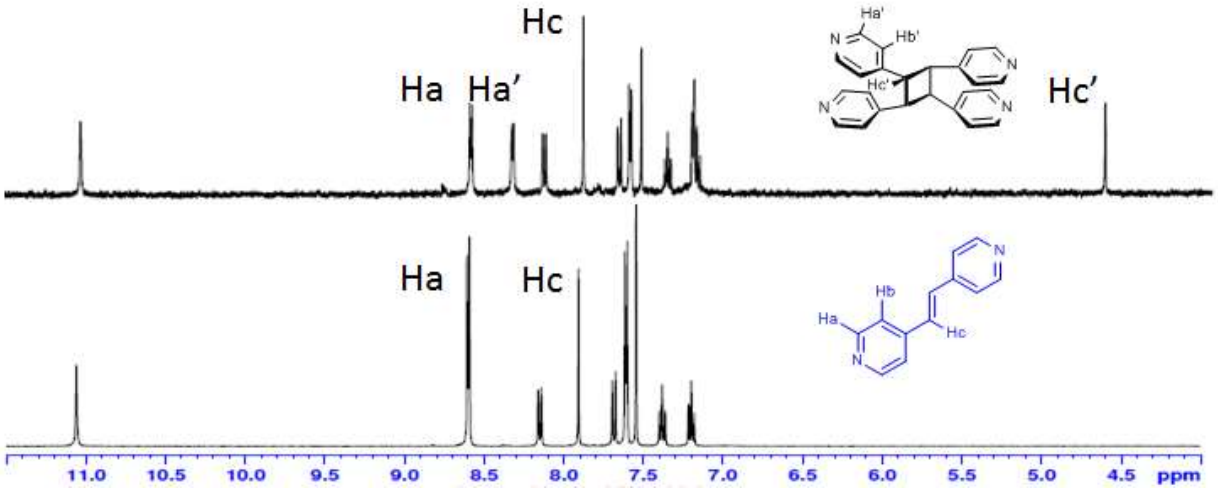

Figure 37 ^{1}H NMR spectra before (bottom) and after (top) UV-irraditaion of of $(IC)_2(4,4'\text{-bpe})_4$.

It is likely that the disordered atoms of the inner olefins of the quadruple stacks are able to undergo movement to form the cyclobutane rings. Given that only the two inner molecules lie in a disordered fashion, the maximum theoretical yield for the solid is expected to be approximately 50%. Thus, the observed yield corresponds to near quantitative photoconversion. To understand the unexpected photostabilities of the double and triple stacks, one has to look beyond the topochemical postulates of Schmidt.[98] In the case of double stacked $(IC)_2(4,4'\text{-bpe})_2 \cdot 2(AcN)$, lack of reactivity may result from included solvent molecules. Additionally, similar to triple stacked $(IC)_2(4,4'\text{-bpe})_3$, insufficient free space in reaction cavity may be cause of photostability. To evaluate the effect of lattice energy, detailed crystal calculations would be needed.

4.3.6 Crystal structure of (IC)(4,4'-tpcb)

Cocrystallization experiments confirm the stereochemistry of 4,4'-tpcb and reveal IC and 4,4'-tpcb, similar to a resorcinol-based template, to interact *via* hydrogen bonds. Thus, when hot AcN and chloroform solutions of IC and 4,4'-tpcb were combined, plate-like, pale-orange single crystals of (IC)(4,4'-tpcb) formed after a period of *ca* 1 day. The components crystallize in the monoclinic space group $P2_1/c$ with full molecule of IC and 4,4'-tpcb in the asymmetric unit. The components, as with the face-to-face stacked cocrystals, interact *via* NH···N hydrogen bonds (d(N···N) = 2.912(2) and 2.880(2) Å) (Fig. 38). In contrast to a resorcinol-based template, the two hydrogen-bond-donor groups of an IC interact with two different molecules of 4,4'-tpcb. The observation can be attributed to the rigidity of the N-H groups, which may also account for the lack of reactivity in the double- and triple-stacked solids $(IC)_2(4,4'\text{-bpe})_2 \cdot 2(AcN)$, $(IC)_2(4,4'\text{-bpe})_3$, respectively

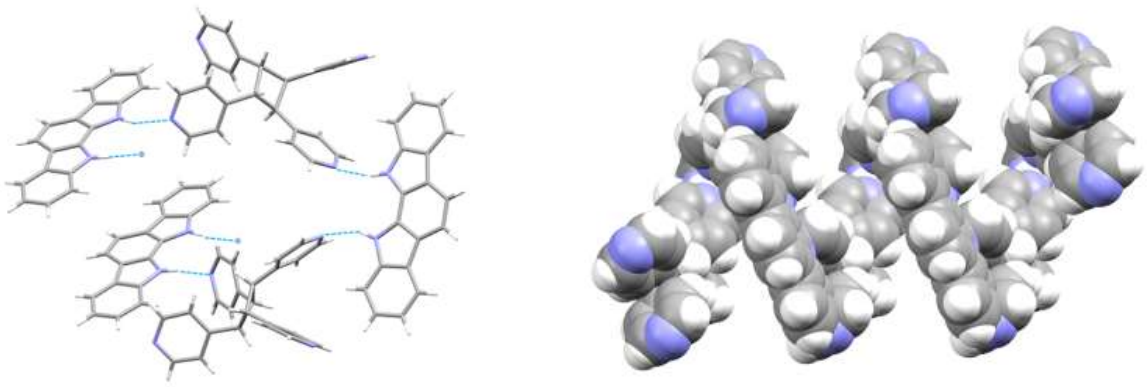

Figure 38 X-ray structure of (IC)(4,4’-tpcb): a) NH···N (---) forces between 4,4’-tpcb and IC and b) space-filling model of 1D wave-like structure.

4.4 Summary

In conclusion, we demonstrated ability of IC to function as a molecular receptor. Moreover, IC was used as a template to assemble discrete double-to-quadruple stacks of aromatics in cocrystals sustained by NH···N hydrogen bonds. This is the first example of cocrystals based on IC. Considering that IC is backbone of many biologically important compounds, this report may stimulate research of indolocarbazole-based APIs cocrystals. While the double and triple aromatic stacks are determined to be photostable, quadruple stacks undergo topochemical [2+2] photodimerization. I also describe the crystal structure based on the photoproduct and IC. Prior to this report, the template approach was used only to assemble up to two molecules in a close proximity within discrete assemblies. IC as a template presents a paradigm shift in what are perceived limits of relatively simple molecular templates. The multiple discrete stacks open the door for many interesting application, including multilayered dimerization, controlled formation of oligomers and multicomponent topochemical cross-reactions. From mechanistic point of view, three prepared cocrystals resulted from relatively mild changes in crystallization conditions. As such, this system may serve as excellent case study for understanding crystallization conditions.

CHAPTER 5. A PRODUCT OF A TEMPLATED SOLID-STATE PHOTODIMERIZATION ACTS AS A TEMPLATE

A portion of this chapter was published as a letter and is adapted with permission from the *Organic Letters* [Bhattacharya, S.; Stojakovic, J.; Saha, B. K.; MacGillivray, L. R. A Product of a Templated Solid-State Photodimerization Acts as a Template: Single-Crystal Reactivity in a Single Polymorph of a Cocrystal.*Org. Lett.* **2013**, *15*, 744-747.] (joint first author)

5.1. Introduction

Products of template-directed reactions that act as templates themselves are the carriers of molecular information and as such, occupy a unique position in chemistry and biology.[99] The transfer of molecular information is of paramount importance, as described by F. Crick: *"The central dogma of molecular biology deals with the detailed residue-by-residue transfer of sequential information."* In Nature, molecules that function as reciprocal templates (e.g. nucleic acids), provide a high-order means to control and direct reactivity in processes such as replication (Fig. 39). Templates that function in a reciprocal sense pass on complementary molecular information in a

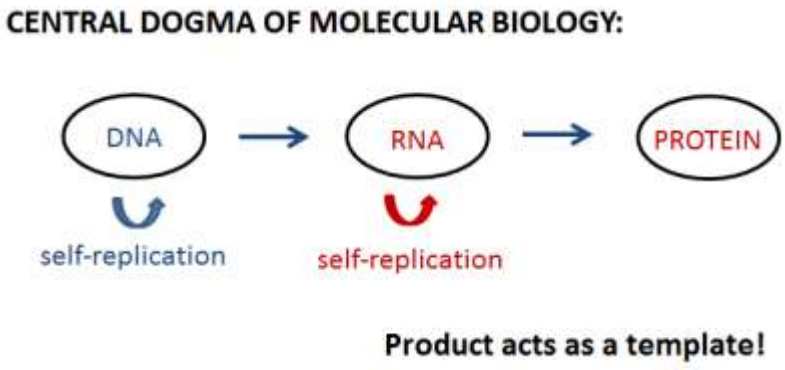

Figure 39 Central dogma of molecular biology.

sequential, independent reaction directed by non-covalent bonds. In this context, the field of supramolecular chemistry aims to mimic a means to direct chemical reactivity encountered in biology.

Small molecules that function akin to reciprocal templates, however, remain rare, which can be attributed to difficulties in controlling subtleties of intermolecular forces encountered in solution. To our knowledge, there exist only two examples of small molecules formed *via* template-directed reactions that have been used in a subsequent reaction as a template. More specifically, Rebek has described a system of receptors based on Kemp's triacid that support rate enhancements of bimolecular reactions[100,101] while Philp has, more recently, reported two mutually-complementary templates that catalyze the formation of each other.[102] Both examples have been reactions performed in solution (*i. e.* liquid phase).

The past decade has witnessed the organic solid state emerge as an attractive medium to perform template-directed reactions using small-molecule templates. The constrained yet flexible environment enables molecules to be assembled into well-defined spatial arrangements that can accommodate movements of atoms in covalent-bond-forming reactions. The [2+2] photodimerization is the most studied reaction to occur in organic solids. The cycloaddition generally requires carbon-carbon double (C=C) bonds to lie parallel and separated less than 4.2 Å to react. Small-molecule bifunctional templates equipped with hydrogen-bond-donor or -acceptor groups have been employed to preorganize C=C bonds in the appropriate position for the cycloaddition to enable the synthesis of molecules difficult to achieve in solution. Despite advances, however, questions regarding whether the resulting photoproducts - that *de facto* are lined with functional groups complementary to the templates - can function as small-molecule templates themselves have been unexplored.

In this chapter, we report the ability of a product of a template-directed [2+2] photodimerization performed in the organic solid state to act as a template. We reveal the

ability of *rctt*-cyclobutanetetracarboxylic acid (cbta) to assemble 4,4'-bpe into 1D hydrogen-bonded chains in cocrystals of composition (cbta)·2(4,4'-bpe). We show the olefin 4,4'-bpe to react to form 4,4'-tpcb stereospecifically and in up to 100% yield.

In the course of the studies to employ cbta as a template, we have also isolated a polymorph of (cbta)·2(4,4'-bpe) that undergoes a rare single-crystal-to-single-crystal (SCSC) reaction[103] that generates 4,4'-tpcb in near quantitative yield. That the reaction occurs in a SCSC manner allows us to unambiguously establish the ability of the cyclobutane ring of cbta to act as a scaffold that directs and accommodates the photoreaction and product, respectively. Small molecule cbta is the first example of a product of a templated solid-state reaction shown to act as a template. In previous work, bipyridines 2,3-bis(4-methylenethiopyridyl)naphthalene (2,3-nap)[104] and 1,8-bis(4-pyridyl)naphthalene (1,8-dpn)[105] have been used to assemble fumaric acid into geometries suitable for photodimerizations in the solid state to form cbta stereospecifically and in up to 100% yield (Fig. 40). In an effort to determine if cbta can act as a template, we turned to cocrystallize cbta with 4,4'-bpe.

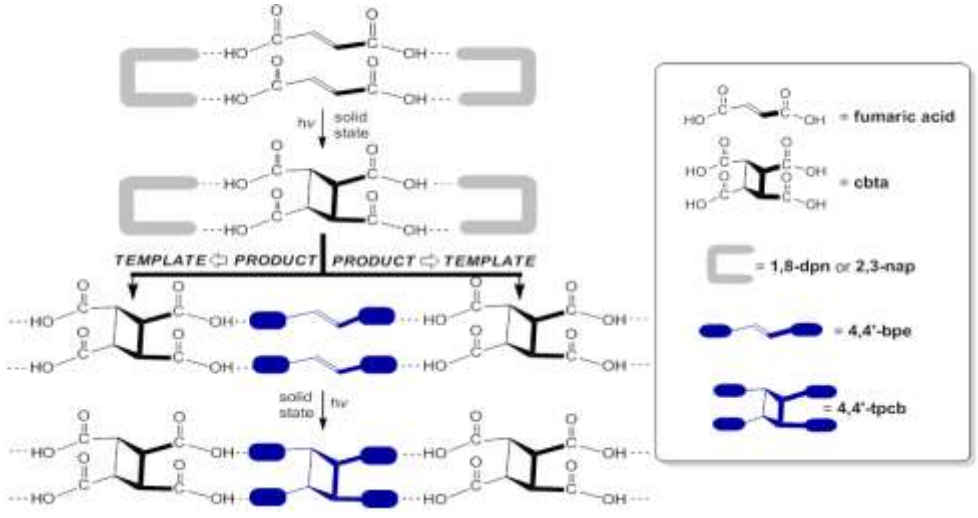

Figure 40 Product of a templated solid-state reaction acts as a template in subsequent reaction.

5.2 Experimental

5.2.1 General remarks

1,2,3,4-Cyclobutanetetracarboxylic acid (cbta) and trans-1,2-bis(4-pyridyl)ethylene) (4,4′-bpe) were purchased from Sigma Aldrich and used without further purification. Powder X-ray data were collected on a *Bruker* D-5000 diffractometer equipped with a *Bruker* SOL-X energy-sensitive detector using Cu *K*α radiation (λ=1.54056 Å). The optical absorption spectra of (cbta)·2(4,4'-bpe), *Form I* and *Form II* were collected using Agilent HP-8453 and included below. All photoreactions were carried out in a photoreactor chamber equipped with a broadband, low pressure UV lamp with a quartz mercury arc (Hanovia lamp, model number PC451.050). ACE glass inc. power supply: 230 V, 50 Hz, 450 W. The lamp was placed in a cooling jacket with running water to maintain temperature in the photoreactor chamber at room-temperature. ^{1}H and ^{13}C NMR spectra were collected using a Bruker 300 MHz spectrometer and DMSO-d_6 as a solvent. ^{1}H spectra were collected in intervals of 10 min.

5.2.2 Synthesis of (cbta)·2(4,4'-bpe), *Form I*

20.0 mg (86.2 mmol, 1 eq.) of cbta and 31.3 mg (172.4 mol, 2 eq.) of 4,4'-bpe were dissolved with heating in a 1:1 volumetric mixture of methanol and dimethyl sulfoxide. The solution was left to slowly cool and within approximately 1 h single crystals were obtained.

5.2.3 Synthesis of (cbta)·2(4,4'-bpe), *Form II*

20.0 mg (86.2 mol, 1 eq.) of cbta and 31.3 mg (172.4 mol, 2 eq.) of 4,4'-bpe were dissolved with heating in dimethyl sulfoxide. The solution was left to slowly cool and within approximately 1 h single crystals were obtained.

5.2.4 Photoreaction – powder

10.0 mg of single crystals of (cbta)·2(4,4'-bpe), *Form I* were powdered by gentle grinding in an agate mortar and pestle for 1 min. Obtained powder was spread in a thin layer between two glass plates (10x10 cm) and exposed to UV irradiation. Same procedure was used for (cbta)·2(4,4'-bpe), *Form II.*

5.2.5 Photoreaction – single crystal

Single crystals of (cbta)·2(4,4'-bpe), *Form II* were placed on a watch glass and exposed to UV radiation for 20 h. Crystals were visually inspected and reaction was followed by ^{1}H NMR spectroscopy in intervals of 5 h. During the course of photoreaction, crystals retained integrity.

The same procedure was repeated for (cbta)·2(4,4'-bpe), *Form I*. However, optical microscopy indicated crystal disintegration following the first interval.

5.2.6 Crystallography

Form I and *Form II* of (cbta)·2(4,4'-bpe): Single-crystal diffraction data were collected on Xcalibur Oxford Diffraction Ltd. with Mo-Kα radiation (λ = 0.71073 Å). Empirical absorption correction using spherical harmonics, implemented in SCALE3 ABSPACK scaling algorithm were applied. Structure solution and refinement were performed with SHELXS-97 and XL respectively using Olex 2-1.1 software package. All nonhydrogen atoms were identified from the difference Fourier map within several refinements. All nonhydrogen atoms were refined anisotropically.

(cbta)·(4,4'-tpcb) (SCSC photoreaction): Single-crystal diffraction data were collected on a Nonius Kappa CCD single-crystal X-ray diffractometer at room temperature using $Mo_{K\alpha}$ radiation (λ=0.71073 Å). Data collection, cell refinement, and data reduction were performed using Collect. Structure solution and refinement were accomplished using SHELXS-97 and SHELXL-97, respectively. The structures were solved by direct methods. All nonhydrogen atoms were identified from the difference

Fourier map within several refinement steps. All nonhydrogen atoms were refined anisotropically.

The structure is solved with high R value of 0.1189. The crystal comes from a single-crystal-to-single-crystal (SCSC) transformation. This transformation yields crystals of poor quality that weakly diffract at higher angles and, thus, higher-angle data is not included in the refinement. However, the collected data were sufficient to establish the atom connectivity and the obtained model can be taken as proof of structure.

5.3 Results and discussion

5.3.1 Crystal structure of (cbta)·2(4,4'-bpe) (*Form I*)

Slow cooling of a solution of cbta and 4,4'-bpe (ratio 1:2) in DMSO-MeOH (v:v 1:1) afforded block-shaped crystals of (cbta)·2(4,4'-bpe), hereafter referred to as *Form I*, after a period of 1 h. The composition of (cbta)·2(4,4'-bpe) (*Form I*) was confirmed using ^{1}H NMR spectroscopy, as well as powder and single-crystal X-ray diffraction.

The components of *Form I* crystallize in the monoclinic space group $P2_1/c$ with a half molecule of cbta and one molecule of 4,4'-bpe in the asymmetric unit (Fig. 41). The components assemble *via* COOH···N(pyridyl) hydrogen bonds (d(O1···N1) = 2.609(2) Å and d(O4···N2) = 2.652(2) Å) to give parallel 1D chains that run along the crystallographic *c*-axis. In the arrangement, cbta assembles 4,4'-bpe as face-to-face stacked pairs with adjacent carbon-carbon double (C=C) bonds parallel and separated by 4.05 Å (Figure 37). The stacked geometry of the olefins conforms to the geometry criteria of Schmidt for a photodimerization in a solid. The 1D chains interact laterally *via* (pyridyl)C-H···O=C(carboxylic acid) forces. Adjacent chains are tilted at an angle of 44.5° while olefins of neighboring chains lie at separation distances of > 4.20 Å. A photodimerization would, thus, be expected to occur within a 1D chain structure.

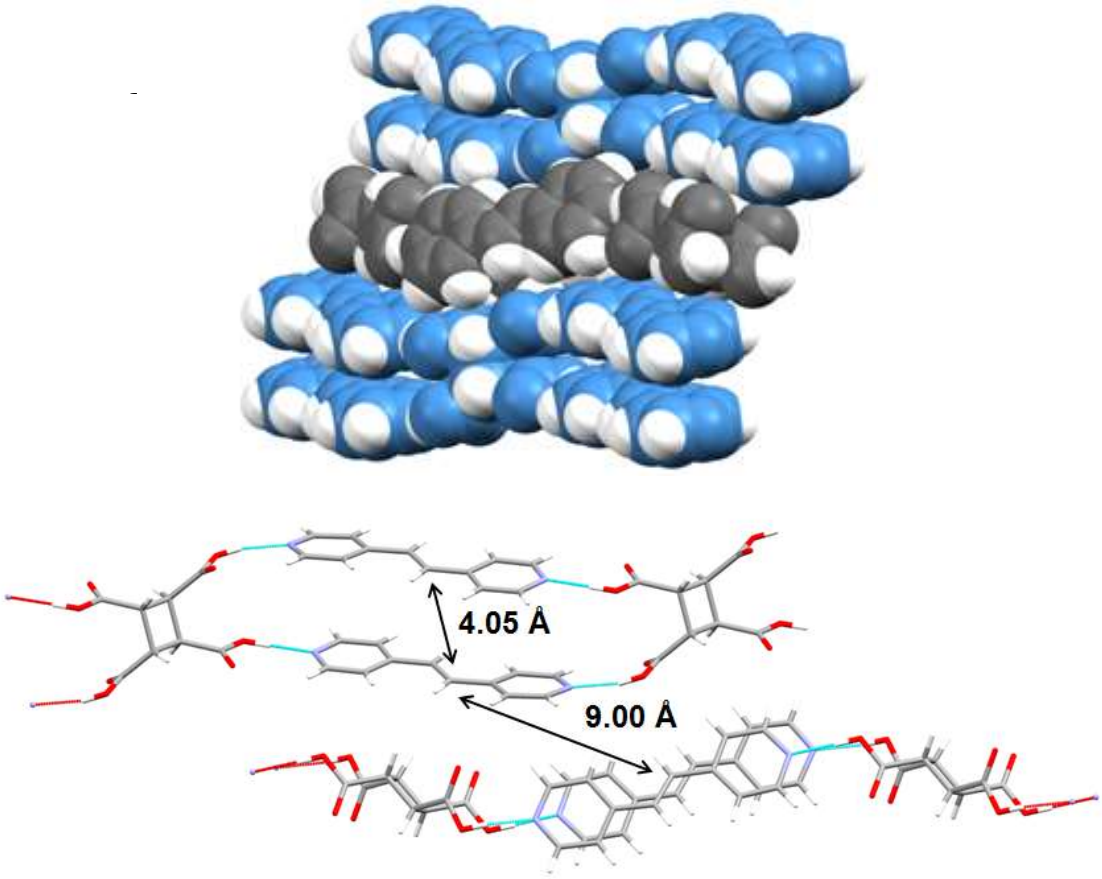

Figure 41 X-ray structure of (cbta)·2(4,4'-bpe) (*Form I*). Top: space-filling view of packed chains highlighting tilts, bottom: double bond distances within chains and between chains.

5.3.2 Crystal structure of (cbta)·2(4,4'-bpe) (*Form II*)

In the course of the work to study cbta as a template, the second polymorph of (cbta)·2(4,4'-bpe) was discovered, hereafter, referred to as *Form II*. Slow cooling of a solution of cbta and 4,4'-bpe (ratio: 1:2) in DMSO alone afforded single plate-like crystals. The composition of (cbta)·2(4,4'-bpe) (*Form II*) was confirmed using ^{1}H NMR spectroscopy, as well as powder and single-crystal X-ray diffraction.

In contrast to *Form I*, the components of *Form II* crystallize in the triclinic space group $P\,\bar{1}$ (Fig. 42). The asymmetric unit consists of two half molecules of cbta and two full molecules of 4,4'-bpe. The C=C bond of one olefin lies disordered over two sites

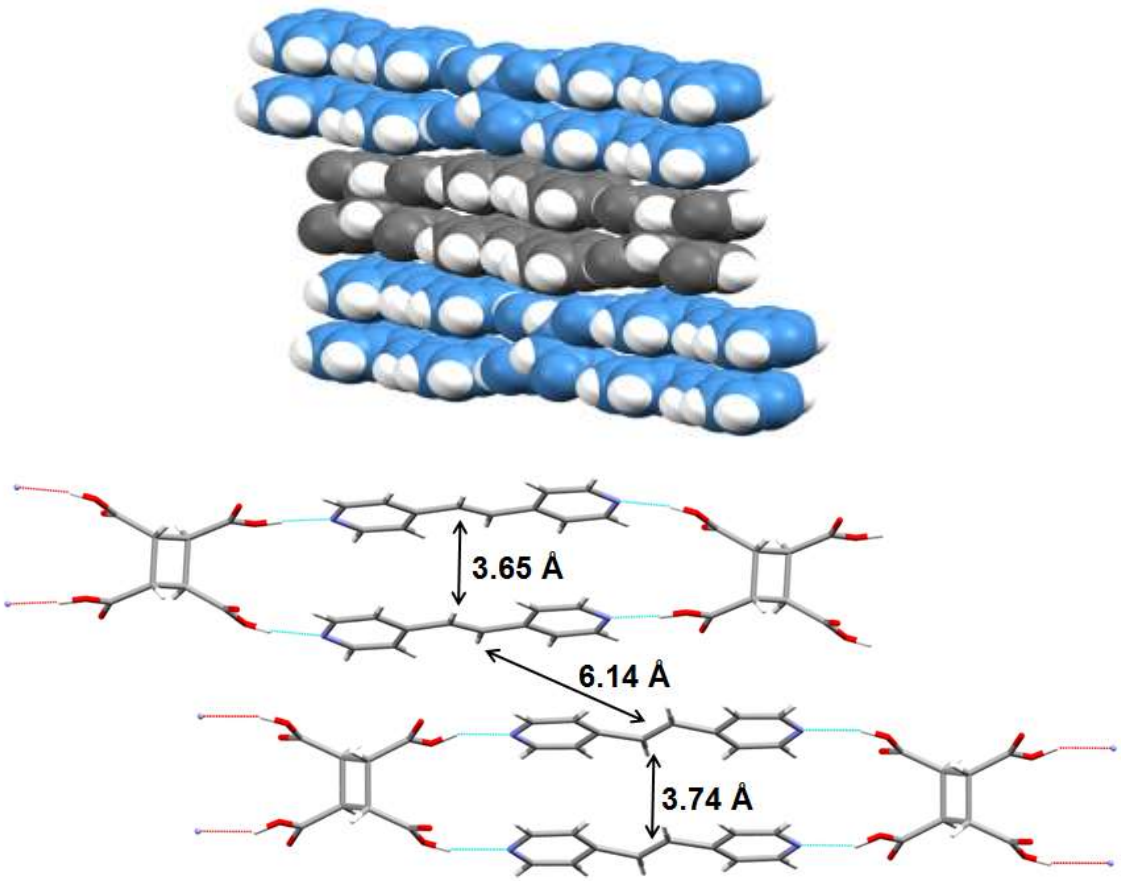

Figure 42 X-ray structure of (cbta)·2(4,4'-bpe) (*Form II*). Top: space-filling view of packed chains highlighting tilts, bottom: double bond distances within chains and between chains.

(occupancies: 0.81/0.19). As with *Form I*, the components are sustained by COOH···N(pyridyl) hydrogen bonds (d(O2···N3) = 2.650(3) Å, d(O4···N4) = 2.567(4) Å, d(O6···N2) = 2.677(5) Å and d(O7···N1) = 2.833(5) Å) that define 1D chains with stacked 4,4'-bpe molecules aligned parallel. Adjacent chains in *Form II* are

crystallographically distinct, with the olefins stacked at 3.65 and 3.74 Å. Whereas neighboring 1D chains run parallel similar to *Form I*, adjacent chains are tilted by only 2.3^{o}. The lack of a significant tilt angle between chains accounts for the major structural difference between the two polymorphs. Olefins of neighboring tapes are separated at a distance > 4.20 Å, meaning that a photoreaction is also be expected to occur within a 1D chain structure.

5.3.3 Photoreactions in two polymorphs of (cbta)·2(4,4'-bpe)

To test the photoreactivity of *Form I*, a powdered crystalline sample (10 mg) was spread between two glass plates and exposed to broadband UV irradiation. 4,4'-bpe was completely converted to 4,4'-tpcb in a period of 2 h, as confirmed by the emergence of a cyclobutane peak (4.62 ppm) in the ^{1}H NMR spectrum (Fig. 43). When single crystals of *Form I* were exposed to the UV-light the samples experienced widespread cracking and disintegrated to a powder during the cycloaddition reaction. Moreover, these experiments establish the ability of the cyclobutane of cbta, which forms in a templated photodimerization, to function as a small-molecule hydrogen-bond-donor template. To test the photoreactivity of *Form II*, a powdered crystalline sample was placed between two glass plates and exposed to broadband UV irradiation. 4,4'-bpe was completely converted to 4,4'-tpcb in a period of only 40 min, as confirmed by ^{1}H NMR spectroscopy. The time required to convert 4,4'-bpe to 4,4'-tpcb in *Form II* was, thus, shorter than in *Form I*.

Single crystals of *Form II*, in contrast to *Form I*, were determined to maintain crystal integrity during the course of the photodimerization, which suggested the reaction to proceed *via* a SCSC transformation. A single-crystal X-ray diffraction study

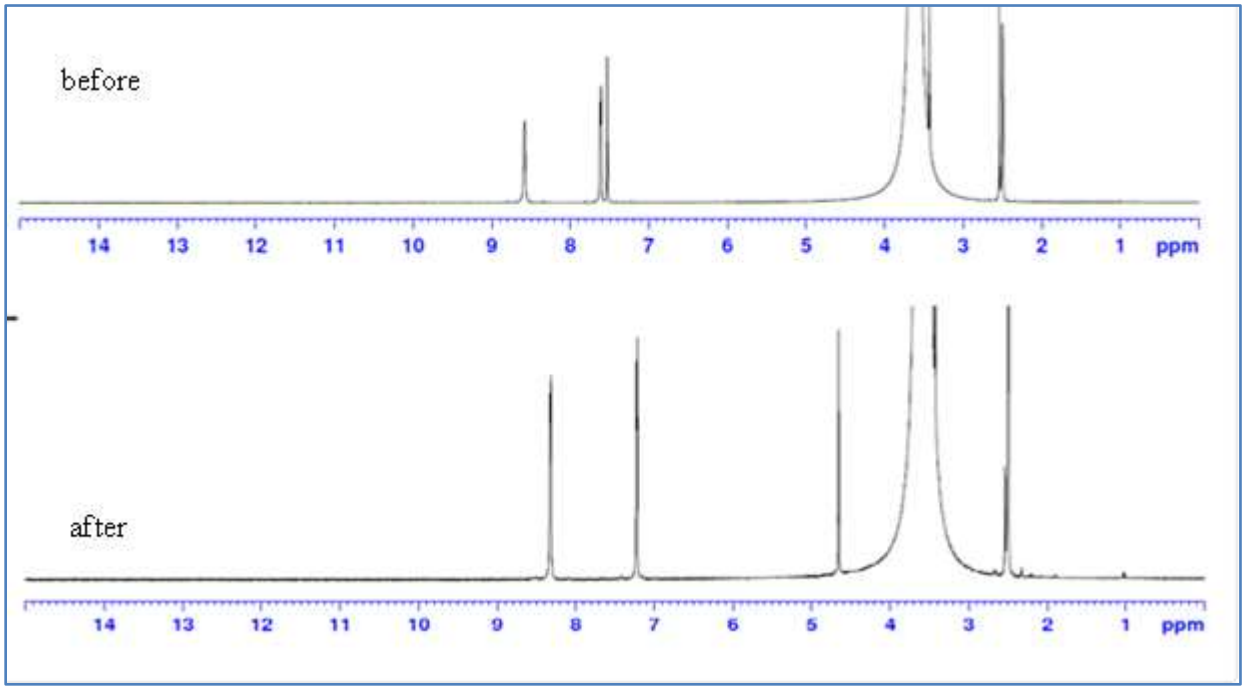

Figure 43 ^{1}H NMR spectra of (cbta)·2(4,4'-bpe), *Form I* before and after photoreaction.

confirmed the reaction to occur in SCSC manner. The asymmetric unit contains one molecule of cbta and one molecule of 4,4'-tpcb, with the components being sustained by COOH···N(pyridyl) hydrogen bonds (*d*(O1···N2) = 2.655(7) Å, *d*(O3···N1) = 2.669(6)Å, *d*(O6···N4) = 2.723(7)Å and *d*(O7···N3) = 2.604(6) Å) (Fig. 44). Moreover, the generation of the cyclobutane ring was not accompanied by significant changes to the structure, with adjacent chains parallel and without a tilt. The SCSC reaction unambiguously establishes the ability of the cyclobutane ring of cbta to enable the tetraacid to act as a template.

Polymorphism of cocrystals in the context of photoreactivity is not well documented. To our knowledge, the only reported examples are polymorphs of 2(res)·2(4,4'-bpe) wherein one polymorph is photoactive and the other is photostable.[106] For (cbta)·2(4,4'-bpe), the differences in both C=C stacking and tilts of

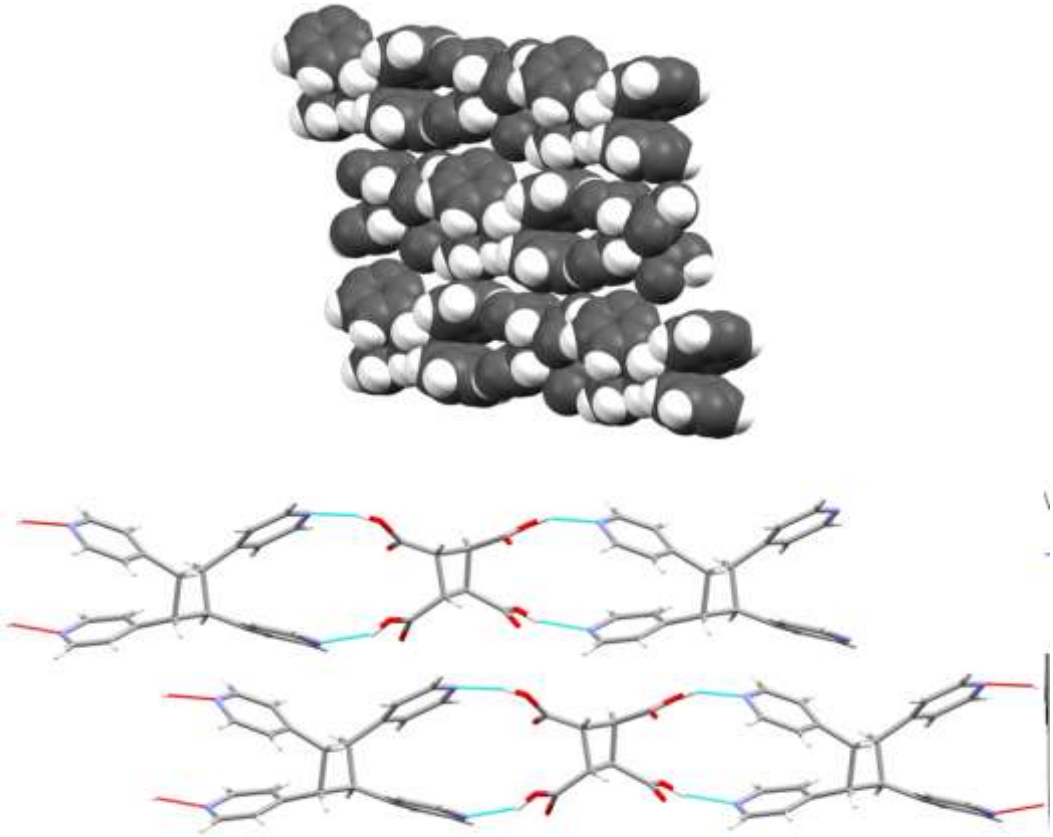

Figure 44 X-ray structure of (cbta)·(4,4’-tpcb) (SCSC). Inset: space-filling view demonstrating the generation of 4,4’-tpcb.

adjacent chains likely contribute to the resulting SCSC behavior, as well as the generally shorter time of the photodimerization, of *Form II* versus *Form I*.

5.4 Summary

In conclusion, we introduced a new concept to solid-state reactivity that a product of a templated reaction can function as a template in subsequent reaction. I demonstrated this concept to be applicable to solid-state [2+2] photodimerization. The product of the first reaction, cbta, is encoded with geometrical information necessary to facilitate photodimerization. In the second reaction, cbta acts as a template to facilitate photodimerization of 4,4’-bpe and, thus, effectively transfers geometrical information in

the organic solid state. In addition, a unique form of polymorphism is described. While both polymorphs are photoreactive, the reaction in one polymorph proceeds in a SCSC reaction. This work provides a base for introducing concept of transfer of molecular information in solid state and basis for reciprocal templates in the organic solid state.

CHAPTER 6. MODULARITY AND HOMOLOGY OF TEMPLATE APPROACH IN SOLID-STATE ORGANIC SYNTHESIS

6.1 Introduction

The ability to effectively direct formation of new covalent bonds is central piece of synthetic chemistry,[107] as well as biology.[108] In Nature, enzymes utilize preorganized structures (*e.g.* steric effects) and directional noncovalent bonds (*e.g.* hydrogen bonds) to control reactions with high degree of selectivity and fidelity. Inspired by action of enzymes, one of the main targets of supramolecular chemistry is to develop enzyme mimics and abiotic templates to perform synthesis in similar fashion.

Although typically utilized medium is liquid phase, covalent bonds can be formed in the solid state, as well. Solid state provides many synthetic advantages, including high degree of stereoselectivity, quantitative yields, minimized reliance on harmful solvents (i.e. green chemistry), and, most importantly, access to molecules that are either difficult or impossible to synthesize in solution. These advantages are result of unique environment that crystals provide for reactions to occur. The reactants are in rigid and confined space that restricts possible reaction pathways, and, at the same time, crystals are sufficiently flexible such that atoms and molecules can move to form covalent bonds.

The main drawback of solid-state synthesis is that the reactivity is dominated by effects of crystal packing which are difficult to predict and control. As a result, the reactions involving members of a homologous series of compounds are hard to achieve. In fact, even a single compound can display different or complete lack of reactivity, as illustrated in the case of different polymorphs of cinnamic acids.[39] To help dissociate effects of crystal packing on reactivity, small molecules can be used as templates to direct the formation of covalent bonds.[52] Akin to the function of enzymes, templates are equipped with specific functional groups that direct substrates into reactive geometries using relatively strong, directional hydrogen bonds. Using the template approach, solid-

state reactivity is largely controlled within local assemblies, instead of long-range uncontrollable crystal packing. However, to fully utilize the template approach, the ability to enforce same reactivity within the homologous members of family has to be clearly established.[109] Moreover, the approach should display modularity, such that systematic changes to templates and substrate result in optimized properties and reactivity.

In this chapter, the homology and modularity of the template approach applied to [2+2] photodimerization of six isomeric bis(pyridyl)-substituted ethylenes (bpes) (Figure 43) will be discussed. The isomeric olefins are namely *trans*-1,2-bis(2-pyridyl)ethylene (2,2'-bpe), *trans*-1,2-bis(3-pyridyl)ethylene (3,3'-bpe), *trans*-1,2-bis(4-pyridyl)ethylene (4,4'-bpe), *trans*-1-(2-pyridyl)-2-(3-pyridyl)ethylene (2,3'-bpe), *trans*-1-(2-pyridyl)-2-(4-pyridyl)ethylene (2,4'-bpe), and *trans*-1-(3-pyridyl)-2-(4-pyridyl)ethylene (3,4'-bpe). The previous work has demonstrated that such olefins can be aligned to form photoreactive four-membered assemblies using resorcinol based templates. Upon irradiation, the olefins

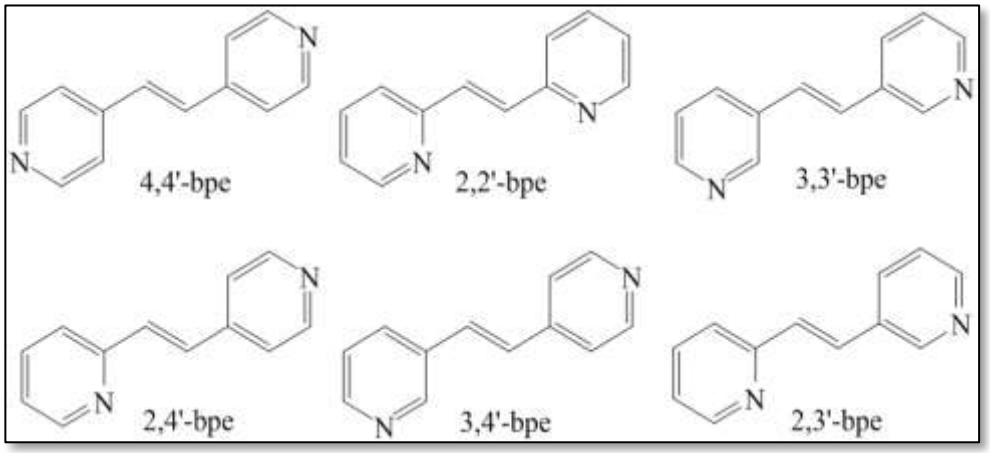

Figure 45 Six isomeric bis(pyridyl)-substituted ethylenes.

undergo a quantitative topochemical photoreaction to yield cyclobutane products, namely, *rctt*-1,2,3,4-tetrakis(2-pyridyl)cyclobutane (2,2'-tpcb), *rctt*-1,2,3,4-tetrakis(3-pyridyl)cyclobutane (3,3'-tpcb), *rctt*-1,2,3,4-tetrakis(4-pyridyl)cyclobutane (4,4'-tpcb), *rctt*-1,2-bis(4-pyridyl)-3,4-bis(2-pyridyl)cyclobutane (2,4'-tpcb), *rctt*-1,2-bis(3-pyridyl)-3,4-bis(4-pyridyl)cyclobutane (3,4'-tpcb) and *rctt*-1,2-bis(2-pyridyl)-3,4-bis(3-pyridyl)cyclobutane (2,3'-tpcb). The unsubstituted res is an efficient template for quantitative photoconversion of 2,2'-bpe and 4,4'-bpe.[51] However, to achieve quantitative conversion of all six isomeric olefins, several halogen-decorated templates had to be screened, namely 4-chlororesorcinol (4-Cl-res), 4,6-dichlororesorcinol (4,6-diCl-res), 4-bromoresorcinol (4-Br-res) and 4,6-dibromoresorcinol (4,6-diBr-res).[110,111] The quantitative conversion of 2,3'-bpe proved to be more difficult and required a synthesis of novel resorcinol-based template. In organic synthesis in liquid-phase, sterically demanding ligands are often used to improve the performance of metal-based catalysts. Inspired by such examples, 4,6-di(1,1-diphenylethyl)resorcinol (4,6-didpe-res), a template with large and bulky groups was synthesized (Fig. 46). The 4,6-didpe-res assembles 2,3'-bpe in discrete four-membered assemblies that upon irradiation give 2,3 tpcb stereoselectively and in quantitative yield. We present here a preparation and crystallographic characterization of assemblies based on 4,6-didpe-res and all bpes, as well as their reactivity upon UV-irradiation. To achieve quantitative and stereoselective [2+2] photodimerization in homologous series of bpes, we also present template screening approach that uses only three commercially available resorcinol-based templates (res, 4-Cl-res and 4,6-diCl-res) (Fig. 46).

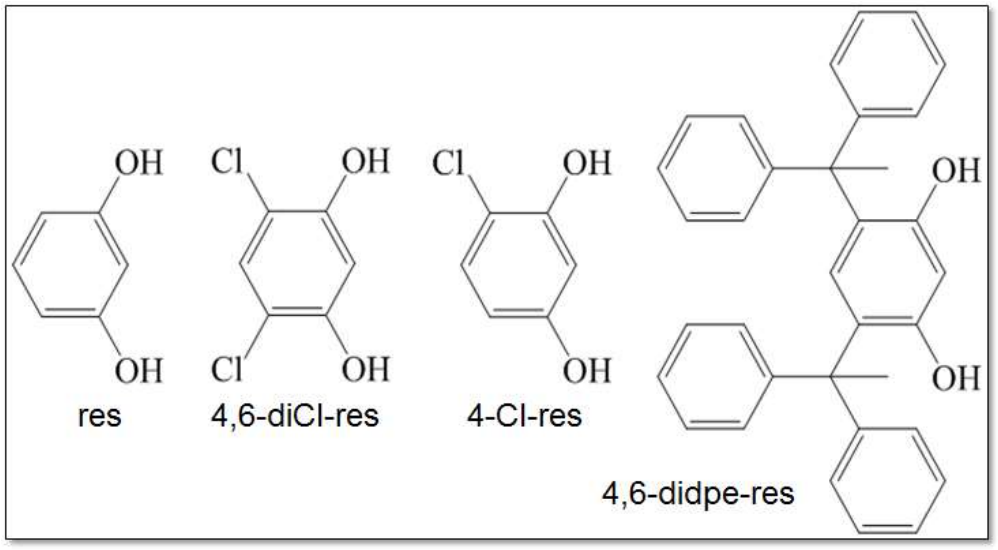

Figure 46 Resorcinol-based templates.

In this chapter, we also performed gas-phase DFT calculations that address unanswered questions associated with the template approach in the solid state. Are discrete hydrogen-bonded assemblies viable architectures outside of crystals or just a result of serendipitous crystal packing? Are hydrogen bonds indeed the main contributing factor to geometry and stability of assemblies? Are assemblies amenable to systematic steric and electronic changes? Although Hammett-like correlation between substituent constants and hydrogen-bonding strength has been already discussed,[112] it is unclear if it will be maintained in a multicomponent and sophisticated four-membered assemblies presented here.

Computational chemistry is garnering popularity as a means to understand subtle effects of intermolecular forces on structures and functions of molecular solids, as well as phenomenologically-related biological systems (i.e. enzymes). The crystal packing problem was originally addressed using computational methods that focus on molecular

shape and electronic potentials (i.e. intramolecular structure) and, more recently, has turned to aspects of long-range molecular and supramolecular organization (i.e. intermolecular forces). It is not clear, however, whether accurate, consistent, and widely-applicable crystal structure prediction is an immediately obtainable goal. Crystal packing of molecules depends primarily on comparatively weak dispersion forces that are difficult to model, and crystallization itself carries inherent randomness that originates from detrimental effects of kinetics governed by subtle changes in crystallization environments (e.g., temperature, pressure). In a related matter, the structure and function of biological macromolecules are typically addressed in more localized manner by placing focus on modeling an active site.

We focus on 5-substituted resorcinol (5-X-res) as a template and 4,4'-bpe as a substrate (Fig. 47). The 5-X-res was chosen for the following reasons: i) 5-X-res templates photodimerizations within discrete hydrogen-bonded structures, ii) 5-X-res can be systemically changed using established procedures of organic synthetic chemistry, and iii) importantly, given that electron-donor and -acceptor groups affect ionizations of phenols, we expected the pendant X- substituents to influence hydrogen bonds between templates and olefin. An electron acceptor would increase the acidity of resorcinol and, thus, strengthen the hydrogen bond, while the opposite effect is expected for an electron donor. Symmetrical nature of substitution in position 5 (*meta*-substitution) ensures only one pathway for electron transfer through aromatic ring. In solid state, the olefin 4,4'-bpe interacts with 5-X-res (where X = H, CN, OCH_3) *via* O-H···N bonds to assume face-to-face π-stacked arrangements within 2(5-X-res)·2(4,4'-bpe) assembly that upon UV-irradiation yield 4,4'-tpcb in quantitative yield. Thus, hydrogen bonding and stability of

all assemblies upon photodimerization are assessed. The combination of gas-phase DFT calculations, corroborated with crystallographic data, demonstrates an accurate modeling of reactive hydrogen-bonded assemblies and a Hammett-like relation between substituents on templates and strength of hydrogen bonding.

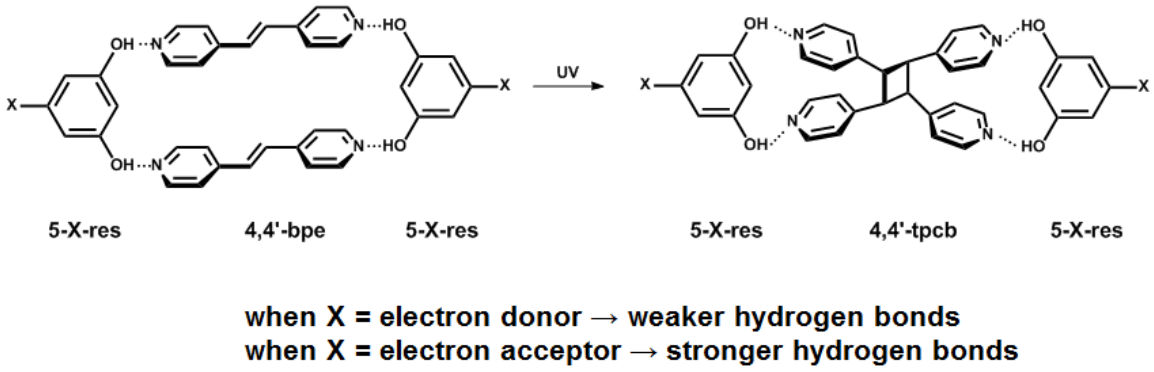

Figure 47 Photodimerization within 2(5-X-res)·2(4,4'-bpe) assemblies.

6.2 Experimental

6.2.1 General remarks

All reagents were purchased from Sigma-Aldrich co. and used as is, unless otherwise stated. ^{1}H NMR spectra were collected using a *Bruker* 400 MHz spectrometer and DMSO-d_6 as a solvent. Powder X-ray data were collected on a *Bruker* D-5000 diffractometer equipped with a *Bruker* SOL-X energy-sensitive detector using Cu K_α radiation (λ=1.54056 Å). All photoreactions were carried out in a photoreactor chamber equipped with a broadband, low pressure UV lamp with the quartz mercury arc, *Hanovia* lamp, model number PC451.050. ACE glass inc. Power supply: 230 V, 50 Hz, 450 W.

6.2.2 Synthesis of 4,6-didpe-res

4,6-didpe-res was synthesized in the reaction of 1,1,-diphenylethanol (30.0 mmol, 5.9 g), with 50% molar excess of resorcinol (10.0 mmol, 1.1 g).[113] The reactants were finely mixed and heated at 100°C in the presence of a sulfuric acid as a catalyst (5.6 mmol, 0.3 mL). The obtained solid was purified by stirring in methanol and rinsing with water. The obtained yield was 3.8 mmol (1.8 g, 35%) for 4,6-diDPE-res.

6.2.3 Synthesis of 3,3’-bpe

3,3'-bpe was synthesized in a palladium-catalyzed consecutive Hiyama-Heck coupling[114] of 3-bromopyridine and triethoxy(vinyl)silane. Triethoxy(vinyl)silane (12.0 mmol, 2.6 mL) was combined with a 0.50 M sodium hydroxide solution (100.0 mL). The mixture was stirred for 5 minutes at room temperature. After stirring, 3-bromopyridine (20.0 mmol, 2.0 mL) and palladium (II) acetate (62.0 μmol, 14.0 mg) were added to the mixture, and the mixture was allowed to reflux with vigorous stirring for 3 hours at 140°C. After cooling to room temperature, the product was extracted using five portions of 50.0 mL ethyl acetate; the organic layers were combined and evaporated using a rotary evaporator. After evaporation, the compound was recrystallized using 20:1 solution of hexanes to ethyl acetate. The obtained yield for the synthesis was 5.4 mmol (97.5 mg, 53%) for 3,3'-bpe.

6.2.4 Synthesis of 3,4’-bpe

3,4-bpe was synthesized in a palladium-catalyzed Heck coupling reaction of 3-bromopyridine and 4-vinylpyridine.[113] The 3-bromopyridine (10.1 mmol, 1.6 g) was added to bis(triphenylphosphine)palladium (II) chloride (235 μmol, 165.0 mg). The mixture was stirred for a few minutes at room temperature, and 4-vinylpyridine (15.7 mmol, 1.6 g) was added, along with 50.0 mL of 0.4 M potassium carbonate solution and 2.1 mmol (0.5 mL) of tributylamine. The mixture was allowed to reflux for 23 hours with vigorous stirring. Upon cooling to room temperature, 3,4'-bpe was extracted using three

30.0 mL portions of chloroform. The organic layers were combined, and the chloroform was evaporated using a rotary evaporator. The product was purified via trituration with n-heptane. The obtained yield was 3.30 mmol (60.4 g, 38%) for 3,4'-bpe.

6.2.5 Synthesis of cocrystals

Cocrystals were formed by dissolving the template and reactant separately in hot solvent. Upon dissolving both components, the solutions were combined and allowed to cool to room temperature. The template and reactant were present in a 1:1 molar ratio with approximately 10% excess of the template. The composition of the obtained solid was determined by ^{1}H NMR spectroscopy and single-crystal X-ray diffraction, when possible.

6.2.6 Computational methods

The initial atomic coordinates were taken from the crystal structure of 2(res)·2(4,4’-bpe) (ABEKUN). All calculations were performed using TURBOMOLE 6.3.1 program suite.[115] All DFT calculations[116] were performed using RI approximation and triple zeta (def-TZVP) basis sets[117] with the corresponding auxiliary basis sets.[118] Dispersion correction form Grimme 2006 (disp) and 2010 (disp3) was used.[119] Structures were optimized without any frequency constraints and characterized as minima on potential energy surface due to the absence of any imaginary frequencies.

6.2.7 Crystallography.

Single-crystal diffraction data were collected on a Nonius Kappa CCD single-crystal X-ray diffractometer at room temperature using $Mo_{K\alpha}$ radiation (λ=0.71073 Å). Data collection, cell refinement, and data reduction were performed using Collect. Structure solution and refinement were accomplished using SHELXS-97 and SHELXL-97, respectively. The structures were solved by direct methods. All nonhydrogen atoms

were identified from the difference Fourier map within several refinement steps. All nonhydrogen atoms were refined anisotropically.

6.3 Results and discussion

6.3.1 Crystal structure and reactivity of cocrystal based on 4,4'-bpe and 4,6-didpe-res

Slow precipitation from acetonitrile solution of 1:1 4,4'-bpe and 4.6-didpe-res afforded colorless prisms after 2 days. The ^{1}H NMR spectroscopy revealed the composition of solid to be 1:1 4,6-didpe-res and 4,4'-bpe. The crystal structure analysis revealed that components crystallize in centrosymmetric triclinic *P-1* space group. The asymmetric unit consists of one 4,6-didpe-res and one 4,4'-bpe molecule (Fig. 48). The structure is based on a discrete four-membered assembly, 2(4,6-didpe-res)·2(4,4'-bpe), that sits around center of inversion. The assembly is sustained by four OH···N hydrogen bonds (2.749(3) and 2.745(3) Å). Within the assembly, two 4,4'-bpe molecules stack along *b*-axis in face-to-face manner and C=C bonds are 5.2 Å apart (centroid to centroid distance) which is outside the range required for [2+2] photodimerization and indicates that solid is photostable. The C=C bonds of 4,4'-bpe molecules lay disordered

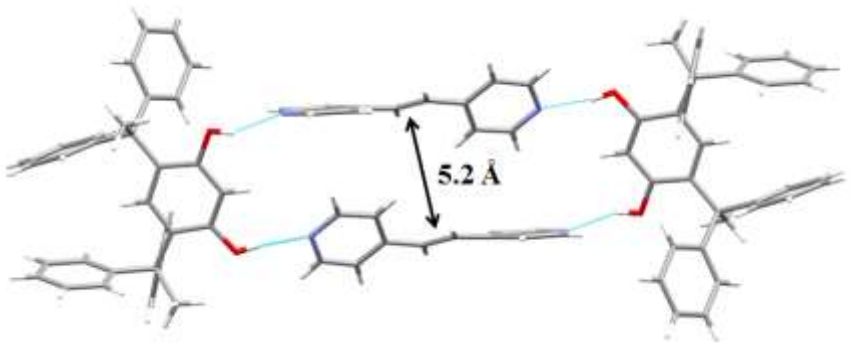

Figure 48 Crystal structure of 2(4,6-didpe-res)·2(4,4'-bpe), the discrete assembly.

(occupancies: 0.87/0.13) over two sites. The olefin 4,4’-bpe is twisted such that two pyridyl groups are tilted, in respect to each other, at the angle of 50.2°. The short-contacts analysis of 4,6-didpe-res indicates the presence of two non-conventional weak intramolecular (methyl)CH···O hydrogen bonds with both C-H-O angles of 123° and distances of 2.778(3) and 3.073(3) Å. The nearest-neighbor assemblies stack along *b*-axis

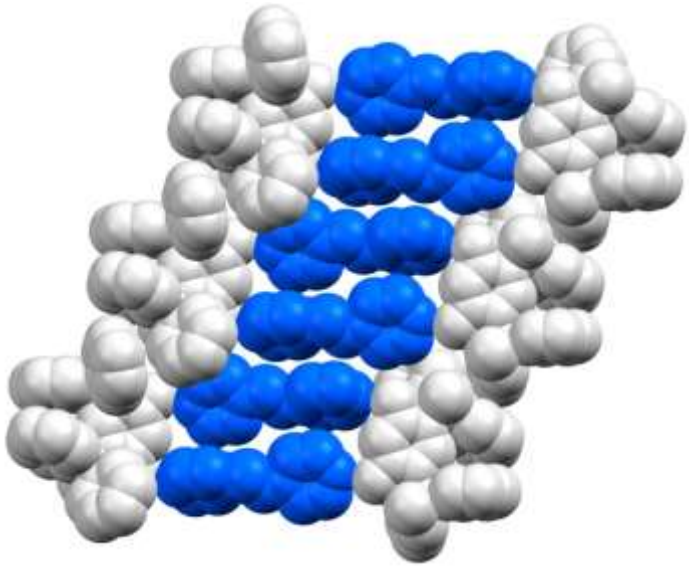

Figure 49 Crystal structure of 2(4,6-didpe-res)·2(4,4’-bpe), extended packing.

with the C=C bonds between assemblies 5.74 Å apart (centroid to centroid distance) (Fig. 49). Thus, the photoreaction between assemblies is not expected to occur. The phenyl groups of nearest 4,6-didpe-res molecules associate via T-shape (‘edge-to-face’) aromatic interaction and distance between planes of phenyl rings is 5.84 Å.

The prolonged UV-irradiation of cocrystals, up to 120 h, did not yield a photoreaction. The demonstrated photostability of 2(4,6-didpe-res)·2(4,4’-bpe) is in agreement with the crystal structure that demonstrated that C=C bonds are too far away to photoreact. In conclusion, the 4,6-didpe-res acts as a template to assemble 4,4’-bpe into

discrete four-membered assemblies. Within assemblies, 4,4’-bpe stacks in face-to-face manner. However, the packing of 4,4’-bpe within 2(4,6-didpe-res)·2(4,4’-bpe) is not close enough to support the [2+2] photodimerization.

6.3.2 Crystal structure and reactivity of cocrystal based on 4,6-didpe-re and 2,2’-bpe

Slow precipitation from acetonitrile solution of 1:1 2,2’-bpe and 4,6-didpe-res afforded colorless thin plates. The ^{1}H NMR spectroscopy revealed the composition of solid to be 1:1.5 4,6’-dpe and 2,2’-bpe. The crystal structure analysis revealed that components crystallize in centrosymmetric monoclinic $P2_1/c$ space group. The asymmetric unit consists of one 4,6-didpe-res molecule, one whole 2,2’-bpe molecule and half molecule of 2,2’-bpe. The structure is based on a discrete four-membered assembly, 2(4,6-didpe-res)·2(2,2’-bpe) and intercalated 2,2’-bpe molecule (Fig. 50). The assembly is sustained by four OH···N hydrogen bonds (2.806(8) and 2.848(8) Å). Within the assembly, two 2,2-bpe molecules stack in face-to-face manner and C=C bonds are 3.9 Å apart (centroid to centroid distance) which is within the range required for [2+2] photodimerization and indicates that solid is photoreactive. The additional 2,2’-bpe

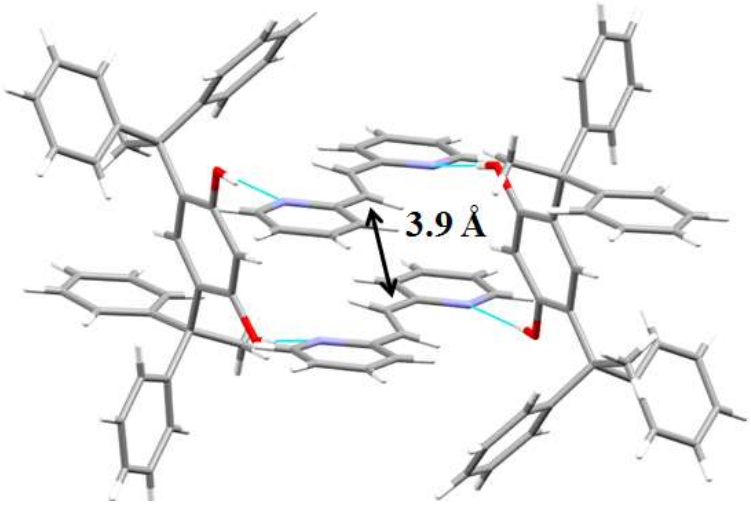

Figure 50 Crystal structure of 2(4,6-didpe-res)·3(2,2’-bpe), discrete assembly.

molecule is embedded in a channel formed by phenyl groups of 4,6-didpe-res. Each 2,2'-bpe is planer. As in the case of 2(4,6-didpe-res)·2(4,4'-bpe), two weak intramolecular (methyl)CH···O hydrogen bonds are present, distances of 2.896(8) and 2.993(8) Å and respective C-H-O angles of 106 and 125°. The nearest-neighbor assemblies stack along

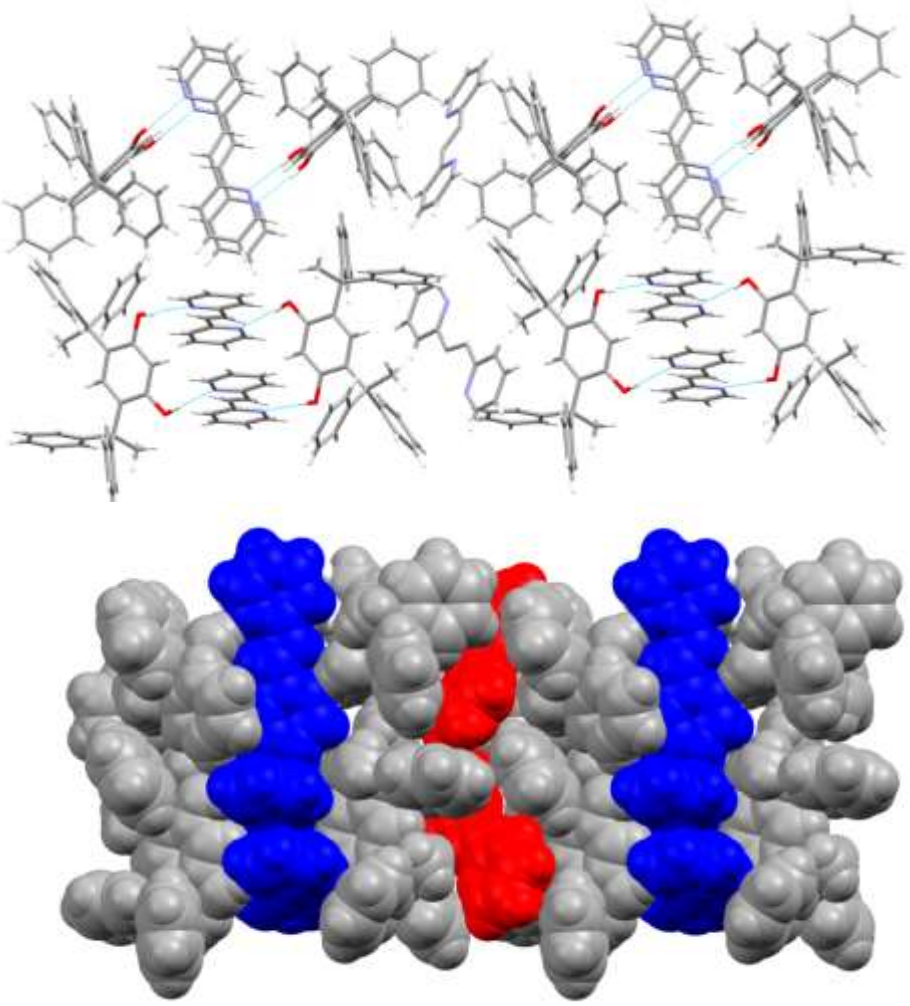

Figure 51 Crystal structure of 2(4,6-didpe-res)·3(2,2'-bpe), extended packing. A space-filling model: grey = 4,6-didpe-res, blue = 2,2'-bpe within assemblies, red = 2,2'-bpe between assemblies.

b-axis both, such that 2,2’-bpe molecules are atop of each other, but the assemblies is rotated at 76.7° and the photoreaction between assemblies is not expected to occur (Fig. 51).

Although 2,2’-bpe molecules within the assemblies are suitably aligned for [2+2] photodimerization, the prolonged UV-irradiation of cocrystals, up to 120 h, did not yield a photoreaction. In other examples that deviate from the postulates of Schmidt, horizontal displacement of C=C bonds, available free space, and lattice energy are some of the factors accounted to have effect on photoreactivity. In the case of the above described cocrystal, 4,6-didpe-res acts as a template that assembles 2,2’-bpe in discrete assemblies, as well as to form aromatic channels that contain additional 2,2’-bpe molecules.

6.3.3 Crystal structure and reactivity of cocrystal based on 4,6-didpe-res and 3,4’-bpe

Slow precipitation from methanol solution of 1:1 3,4’-bpe and 4,6-didpe-res afforded colorless prisms. The ^{1}H NMR spectroscopy reveled the composition of solid to be 1:1 4,6-didpe-res and 3,4’-bpe. The crystal structure analysis revealed that components crystallize in centrosymmetric triclinic *P-1* space group. The asymmetric unit consists of one 4,6-didpe-res and one 3,4’-bpe molecule. The structure is based on a discrete four-membered assembly, 2(4,6-didpe-res)·2(3,4’-bpe) (Fig. 52). The assembly is sustained by four OH···N hydrogen bonds (2.723(3) and 2.720(3) Å). Within the assembly, two 3,4’-bpe molecules stack along b-axis in an off-set face-to-face manner and C=C bonds are 5.9 Å apart (centroid to centroid distance) which is outside the range required for [2+2] photodimerization and indicates that solid is photostable. The C=C bonds of 3,4’-bpe molecules lay disordered (occupancies: 0.59/0.41) over two sites. The olefin 3,4’-bpe is planar. The short-contacts analysis of 4,6’-didpe-res indicates the presence of

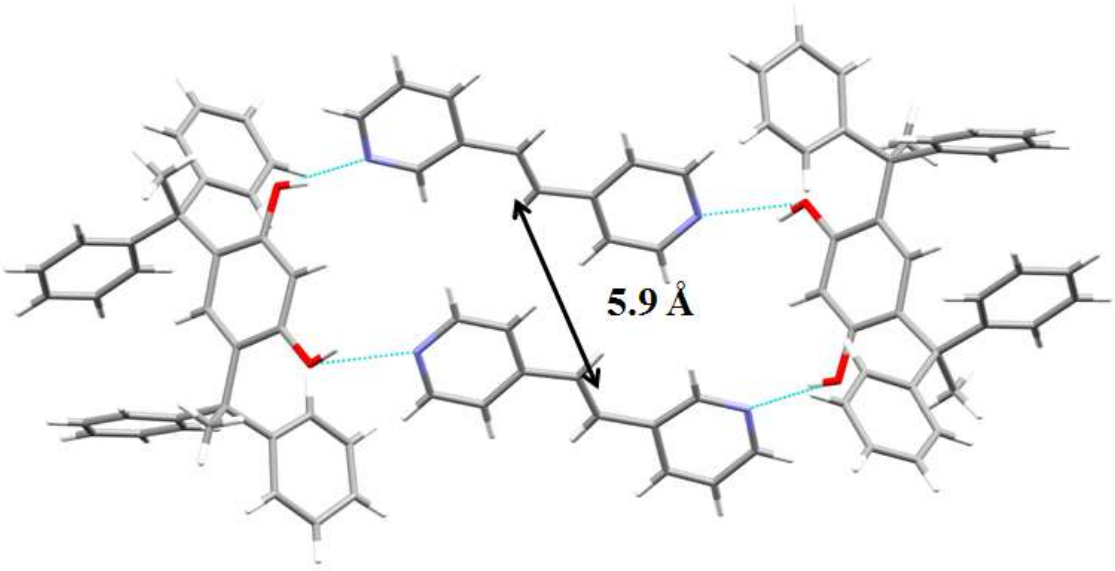

Figure 52 Crystal structure of 2(4,6-didpe-res)·2(3,4'-bpe), discrete assembly.

intramolecular (methyl)CH···O hydrogen bonds with both C-H-O angles of 125 and 123°, and respective distances of 2.948(3) and 2.960(3) Å. The nearest-neighbor assemblies stack along *b*-axis such that there is a face-to-face aromatic interaction between olefin 3,4'-bpe and phenyl rings of adjacent 4,6-didpe-res (centroid to centroid distance of 4.2 Å). Thus, the photoreaction between assemblies is not expected to occur.

The prolonged UV-irradiation of cocrystals, up to 120 h, did not yield a photoreaction. The demonstrated photostability of 2(4,6-didpe-res)·2(3,4'-bpe) is in agreement with the crystal structure that demonstrated that C=C bonds are too far away to photoreact. In conclusion, the 4,6-didpe-res acts as a template to assemble 3,4'-bpe into discrete four-membered assemblies. Within assemblies, 3,4'-bpe stacks in face-to-face manner. However, the olefins of 3,4'-bpe within 2(4,6-didpe-res)·2(3,4'-bpe) are too off-set to support the [2+2] photodimerization.

6.3.4 Crystal structure and reactivity of cocrystal based on 4,6-didpe-res and 2,4-bpe

Slow precipitation from acetonitrile solution of 1:1 2,4'-bpe and 4,6-didpe-res afforded colorless prisms. The ^{1}H NMR spectroscopy reveled the composition of solid to be 1:1.5 4,6-didpe-res and 2,4'-bpe. The crystal structure analysis revealed that components crystallize in centrosymmetric triclinic *P-1* space group (Fig. 53). The asymmetric unit consists of one 4,6-didpe-res molecule and one 2,4'-bpe molecule. Each 4,6-didpe-res

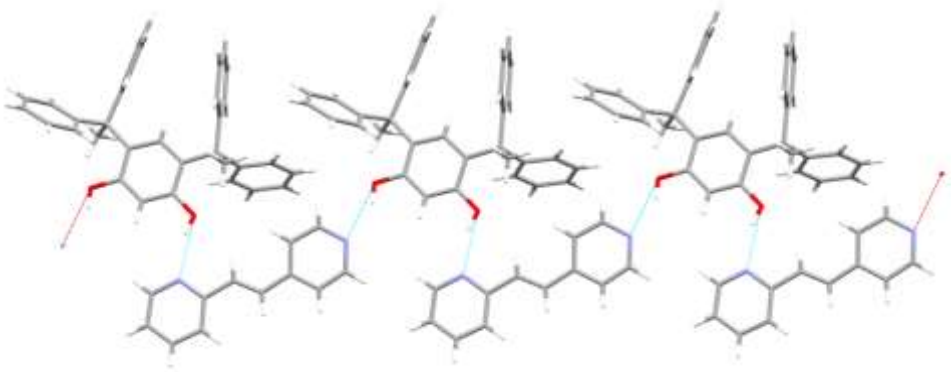

Figure 53 Crystal structure of (4,6-didpe-res)·(2,4'-bpe), hydrogen bonding motif.

interacts with one 2-pyridyl group and one 4-pyridyl group of different 2,4'-bpe molecules via two OH···N hydrogen bonds (2.826(2) and 2.813(2) Å). The structure extends as an infinite 1D chain along *b*-axis. The adjacent chains stack along *a*-axis such that 2,4'-bpe molecules stack in face-to-face manner and head-to-tail orientation (Fig. 54). The distances between the nearest C=C bonds is 5.2 Å (centroid to centroid distance) which is outside of the range required for [2+2] photodimerization and indicates that solid is photostable. As in the other cocrystals based on 4,6-didpe-res, two weak

intramolecular (methyl)CH···O hydrogen bonds are present, distances of 3.002(2) and 2.925(2) Å and respective C-H-O angles of 124 and 126°.

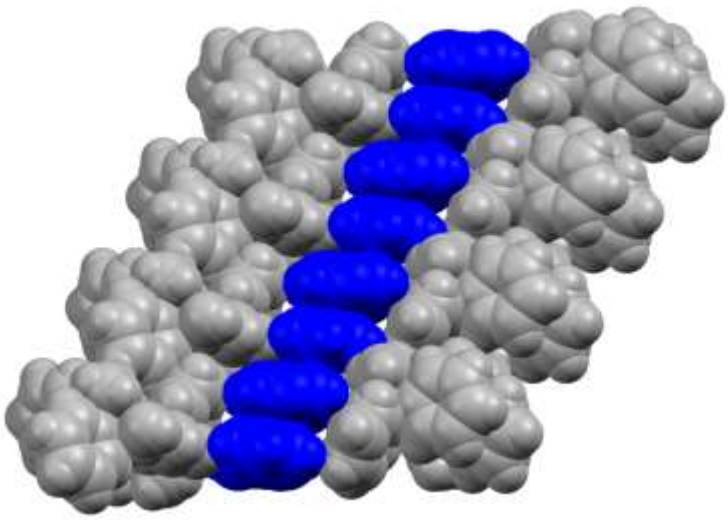

Figure 54 Crystal structure of (4,6-didpe-res)·(2,4'-bpe), hydrogen bonding motif.

Although 2,4'-bpe moleculse within the cocrystal are more than 4.2 Å apart, after 50 h of UV-irradiation of cocrystals, head-to-head photoproduct 2,4'-tpcb was obtained in quantitative yield. The formation of a channel that enables facile sliding motion of planar aromatics was ascribed to unexpected photoreactivity in some cases, and may account for photoreactivity of (4,6-didpe-res)·(2,4'-bpe).

6.3.5 Cocrystals based on 4,6-didpe-res – summary

In summary, 4,6-didpe-res is demonstrated to interact with all six isomeric olefins to form cocrystals. Cocrystals based on 4,4'-bpe, 3,3'-bpe, 3,4'-bpe and 2,3'-bpe are based on discrete hydrogen-bonded assemblies. Cocrystal based on 2,2'-bpe is based on similar discrete assembly, but has additional 2,2'-bpe molecules included in structure. Although, C=C bonds of olefins in cocrystals based on 2,2'-bpe and 2,3'-bpe are within

4.2 Å and parallel, cocrystals 2,3’-bpe and 2,4’-bpe are demonstrated to be photoreactive. The described data are summarized in Table 5.

Table 5 Photoreactivity of cocrystals based on 4,6-didpe-res

cocrystal	structural motif	C=C bonds within 4.2 Å?	C=C bonds parallel?	photo-reactive?
2(4,6-didpe-res)·2(4,4’-bpe)	discrete assembly	no	yes	no
2(4,6-didpe-res)·2(3,3’-bpe)	discrete assembly	no	yes	no
2(4,6-didpe-res)·3(2,2’-bpe)	discrete assembly and additional 2,2’-bpe	yes	yes	no
(4,6-didpe-res)·(2,4’-bpe)	1D chain	no	yes	yes
2(4,6-didpe-res)·2(3,4’-bpe)	discrete assembly	no	yes	no
2(4,6-didpe-res)·2(2,3’-bpe)	discrete assembly	yes	yes	yes

6.3.6 Cocrystals based on 3,3’-bpe and 4,6-diCl-res

Slow precipitation from methanol solution of 3,3’-bpe and 4,6-diCl-res afforded colorless prisms. The ^{1}H NMR spectroscopy reveled the composition of solid to be 1:1 4,6-diCl-res and 3,3’-bpe. The crystal structure analysis revealed that components crystallize in centrosymmetric monoclinic *P* $2_1/n$ space group (Fig. 55). The asymmetric unit consists of one 4,6-diCl-res and one 3,3’-bpe molecule. The structure is based on a discrete four-membered assembly, 2(4,6-diCl-res)·2(3,3’-bpe). The assembly is sustained by four OH···N hydrogen bonds (2.646(3) and 2.760(3) Å). Within the assembly, two 3,3’-bpe molecules stack in face-to-face manner and C=C bonds are 4.1 Å apart (centroid

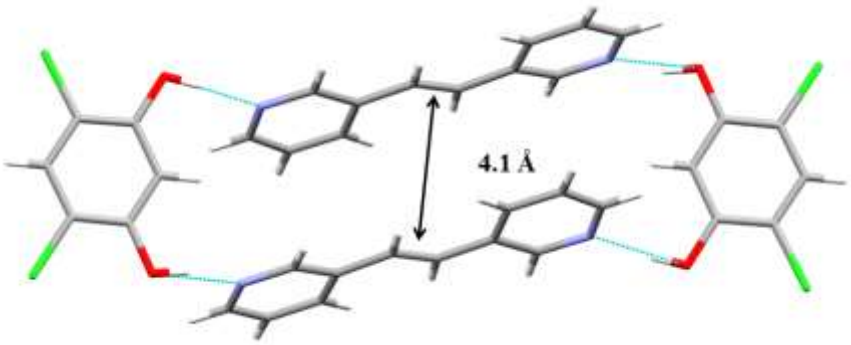

Figure 55 Crystal structure of 2(4,6-diCl-res)·2(3,3'-bpe), discrete assembly.

to centroid distance) which is within the range required for [2+2] photodimerization and indicates that solid is photoreactive. The nearest-neighbor assemblies stack such that 4,6-diCl-res interacts with 3,3'-bpe molecules of adjacent assembly via face-to-face aromatic interactions (ring to ring distance is 4.0 Å). Interestingly, chlorine atoms do not engage in halogen-halogen interactions. Instead (3-pyridyl)CH···Cl interactions are present.

After 60 h of UV-irradiation, the cocrystals yielded 3,3'-tpcb photoproduct stereoselectively and in quantitative yield. The demonstrated photoreactivity of 2(4,6-diCl-res)·2(3,3'-bpe) is in agreement with the crystal structure that demonstrated that C=C bonds are within 4.2 Å. In conclusion, the commercially available 4,6-diCl-res acts as a template to assemble 3,3'-bpe into discrete four-membered assemblies that enable quantitative photodimerization.

6.3.7 Cocrystals based on 3,4'-bpe and 4-Cl-res

Slow precipitation from acetonitrile solution afforded colorless prisms. The ^{1}H NMR spectroscopy revealed the composition of solid to be 1:1 4-Cl-res and 3,4'-bpe. The crystal structure analysis revealed that components crystallize in centrosymmetric orthorhombic *P bca* space group (Fig. 56). The asymmetric unit consists of one 4-Cl-res and one 3,4'-bpe molecule. The structure is based on a discrete four-membered assembly,

2(4-Cl-res)·2(3,4’-bpe). The assembly is sustained by four OH···N hydrogen bonds (2.682(3) and 2.753(3) Å). Within the assembly, two 3,4’-bpe molecules stack in face-to-face manner and C=C bonds are 3.4 Å apart (centroid to centroid distance) which is within the range required for [2+2] photodimerization. However, the C=C bonds are not parallel, instead they are crisscrossed which indicates that solid is photostable. The assemblies stack along *b*-axis such that 3,4’-bpe of nearest neighbor assemblies are 6.2 Å apart and photoreaction is not expected to occur between assemblies.

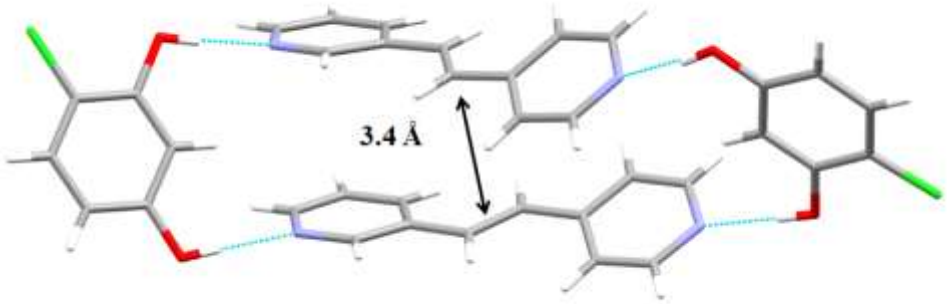

Figure 56 Crystal structure of 2(4,6-diCl-res)·2(3,4’-bpe), discrete assembly.

After 60 h of UV-irradiation, the cocrystals yielded 3,4’-tpcb head-to-head photoproduct stereoselectively and in quantitative yield. The demonstrated photoreaction may be attributed to pedal-like motion observed in photoreactive crystals that do not have C=C bonds parallel. In conclusion, the commercially available 4-Cl-res acts as a template to assemble 3,4’-bpe into discrete four-membered assemblies that enable quantitative photodimerization.

6.3.8 Cocrystals and photodimerization based on resorcinols - summary

The crystal structures and reactivity data presented here demonstrate that stereoselective and quantitative [2+2] photodimerization of entire homologous family of bpes in solid state can be achieved. We used only three commercially available templates, namely res, 4-Cl-res and 4,6-diCl-res to direct the C=C bonds in suitable geometry. While photodimerizations of 4,4'-bpe, 2,2'-bpe and 2,4'-bpe using res or chlorinated resorcinols were already reported, we expanded the use of chlorinated resorcinols to bpes with 3-pyridyl moieties, namely 3,3'-bpe, 3,4'-bpe and 2,3'-bpe. The data are summarized in Table 6. The results in italic have been previously reported. Mixture refers to the solid obtained after photoreaction to be a mixture of head-to-head and head-to-tail products. For example, upon UV-irradiation of 2(4-Cl-res)·2(2,3'-bpe), head-to-head product was obtained in 97% yield and head-to-tail product was obtained in 3% yield.

Table 6 The templated photodimerization of six isomeric bpes. previously reported data is italicized.

	Templates and achieved yields (%)		
Substrate	res	4-Cl-res	4,6-diCl-res
4,4'-bpe	*100*[51]	100	*100*[66]
2,2'-bpe	*100*[51]	94	70
3,3'-bpe	*0*[113]	100	100
2,4-bpe	*100 (mix)*	*100*[51]	100
3,4-bpe	*0*[113]	100	100
2,3-bpe	*0*[113]	100 (97:3)	100 (mix)

6.3.9 Optimized structures involving 4,4’-bpe

The olefin 4,4’-bpe adopts a quasi-planar conformation in solution. In solids, 4,4’-bpe exhibits different twist angles of the two pyridyl rings that range from planarity to nearly perpendicular. In the crystal structure of 2(res)·2(4,4’-bpe), res enforces 4,4’-bpe into face-to-face double stacks via four O-H···N hydrogen bonds (*d*(O-N) = 2.74 and 2.75 Å) within a discrete assembly that has a center of inversion. The olefin 4,4’-bpe assumes nearly planar conformation (twist angle 6.93°) and the C=C bonds are separated by 3.65 Å.

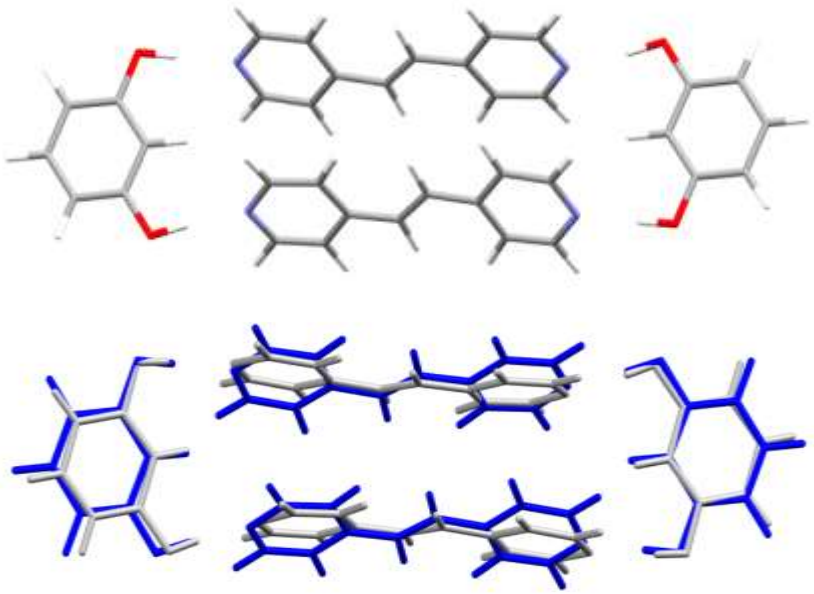

Figure 57 The optimized structure of 2(res)·2(4,4’-bpe) (top) and overlay of optimized and crystal structure of 2(res)·2(4,4’-bpe) (bottom).

The optimized structure of 2(res)·2(4,4’-bpe), obtained using RIBP+disp/def-TZVP basis set, compares well to the reported crystal structures (Fig. 57). The assembly

is sustained by four O-H···N hydrogen bonds (*d*(O-N) = 2.79 and 2.80 Å) and, as the crystal structure, has a center of inversion. The olefin 4,4'-bpe is forced into face-to-face geometry and assumes nearly planar conformation (twist angle 6.53°). The C=C bonds are separated by 3.58 Å. The results of the DFT calculations demonstrate that the gas-phase DFT calculations can accurately model the assembly that is found to be a building block of a solid. Moreover, the calculations confirm that the described assembly is a viable construct in gas, as well as in the solid phase.

6.3.10 Substituent effects in 2(5-X-res)·2(4,4'-bpe)

Substituent constants related to the Hammett correlation are typically used to characterize the ability of a substituent to perturb the local electron environment of benzoic acids: positive value reflects electron-withdrawing effect (more acidic behavior), whereas negative values reflect electron-donating effect (more basic behavior). We hypothesized electron-withdrawing substituents to result in weakening of O-H bond in res and, thus, strengthen O-H···N hydrogen bond between *n,n'*-bpe and res and vice versa for electron-donating substituent.

Using the same basis set and method, we calculated the binding energies for a total of 14 neutral substituents. The calculated binding energies and respective universal substituent constant values in *meta* position, σ^0, are listed in Table 6. For 2(5-X-res)·2(4,4'-bpe), the binding energies varied between 43.82 (2(5-$N(CH_3)_2$-res)·2(4,4'-bpe)) and 51.69 kcal/mol (2(5-NO_2-res)·2(4,4'-bpe)). The extremes correspond to the most electron-donating (*e.g.*, -$N(CH_3)_2$) and the most electron-withdrawing substituents (*e.g.*, -NO_2), respectively. When plotted against σ^0, the binding energies linearly correlate to σ^0 values (R^2 = 0.96). The results confirm our hypothesis that electronic properties of substituents affect the hydrogen bonding and, thus, binding energies of the reactive supramolecular assemblies. The substituent effect is proportional to the σ^0 values and the linearity of the plot indicates a Hammett-like correlation.

Table 7 Substituent effect on binding energies of 2(5-X-res)·2(4,4'-bpe) and 2(5-X-res)·(4,4'-tpcb).

		B.E. (kcal/mol)	
Substituent	σ^0	4,4'-bpe	4,4'-tpcb
$N(CH_3)_2$	-0.1	-43.82	-43.55
CH_3	-0.06	-44.83	-44.55
H	0	-45.23	-44.92
Ph	0.05	-46.31	-44.95
OCH_3	0.1	-45.19	-45.69
CCH	0.2	-47.26	-46.70
F	0.34	-47.89	-47.23
Cl	0.37	-48.40	-47.27
CCH_3O	0.38	-48.20	-47.72
Br	0.39	-48.62	-47.86
CHO	0.41	-49.16	-48.20
CF_3	0.46	-50.25	-49.15
CN	0.62	-51.08	-50.02
NO_2	0.71	-51.69	-50.69

6.3.11 Optimized structures involving 4,4'-tpcb

It has been shown that upon UV irradiation, 2(5-R-res)·2(4,4'-bpe) (where R= H and CN) undergo a single-crystal-to-single-crystal photodimerization to afford 2(5-R-res)·(4,4'-tpcb) (where R= H and CN) stereoselectively and in up to 100% yield.[65] The formation of the cyclobutane ring requires movement of C-atoms of C=C bonds closer to each other which leads to loss of conjugation and planarity. To quantify the perturbations exhibited upon photoreaction, we optimized hydrogen-bonded discrete assemblies based on 4,4'-tpcb and 2,2'-tpcb using RIBP+disp/def-TZVP basis set, as in the assemblies prior to photodimerization. In general, reactions in solids involve minimal atomic movement and, thus, we expected the hydrogen bonds to be preserved, as experimentally

demonstrated in formation of three-membered discrete assemblies 2(res)·(4,4'-tpcb) and 2(5-CN-res)·(4,4'-tpcb).

Compared to 4,4'-bpe, 4,4'-tpcb has been studied appreciably less. In fact, other than reports of 4,4'-tpcb as the product of photodimerization in solution, there are no theoretical studies, either in solution or in solid state, reported prior to 2000, likely due to difficult synthesis. The crystal structure of 2(res)·(4,4'-tpcb) is obtained in solid-state photodimerization of 2(res)·2(4,4'-bpe). The structure is based on the discrete assembly that has a center of symmetry and is sustained by four O-H···N hydrogen bonds (*d*(O-N) = 2.72 and 2,79 Å). The cyclobutane ring is planar with d(C-C) 1.539 and 1.602 Å. While C-atoms in the center of assembly move closer upon photoreaction by almost 2 Å, the opposite is true for N-atoms of 4-pyridyl rings. In 2(res)·(4,4'-tpcb), the N-atoms are 4.83 Å apart compared to 3.80 Å in 2(res)·2(4,4'-bpe).

Similarly to the crystal structure of 2(res)·2(4,4'-bpe), the optimized assembly 2(res)·(4,4'-tpcb) is sustained by four O-H···N hydrogen bond s(*d*(O-N) = 2.76, 2.76, 2.76 and 2.8 Å) (Fig. 58). The optimized structure is not symmetrical with all four bonds of the cyclobutane ring being different (d(C-C) = 1.55, 1.55, 1.60 and 1.60 Å). Moreover the cyclobutane ring is puckered ($\tau = 21.01°$), while the cyclobutane ring in the crystal structure is planar. Two res molecules are twisted with respect to each other (32.85°), while in the crystal structure two res molecules lay in the same plane. We first reported the helical twist in gas phase in a similar, DFT optimized, assembly, 2(4,6-diCl-res)·(4,4'-tpcb). In the crystal structures of both 2(res)·(4,4'-tpcb) and 2(4,6-diCl-res)·(4,4'-tpcb), puckering and helical twist do not occur and are likely hindered by effects of crystal packing.

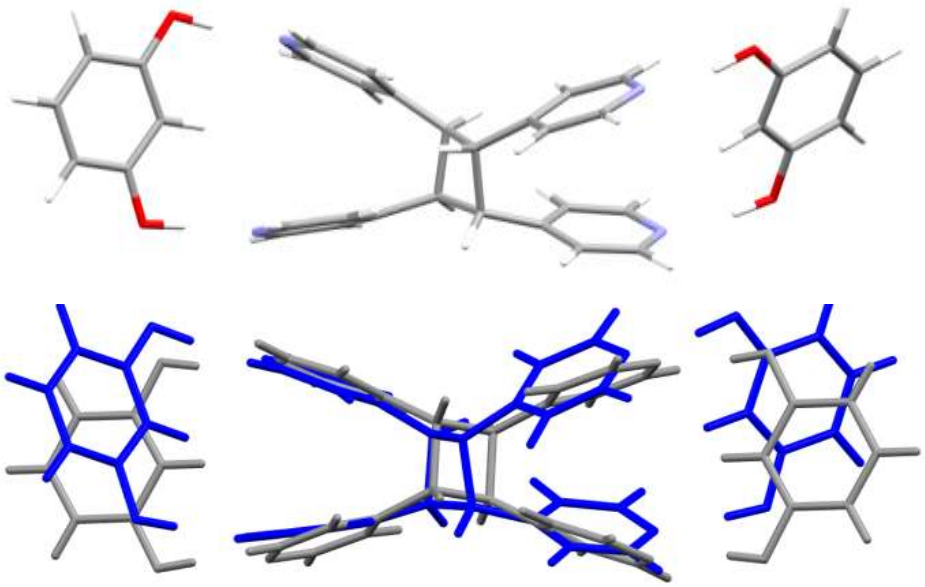

Figure 58 The optimized structure of 2(res)·(4,4'-tpcb) (top) and overlay of optimized and crystal structure of 2(res)·(4,4'-tpcb) (bottom).

6.3.12 Substituent effects in 2(5-X-res)·(4,4'-tpcb)

As prior to photodimerization, we expected the Hammett-like correlation in assemblies after the photodimerization. The calculated binding energies and respective universal substituent constant values in *meta* position, σ^0, are listed in Table 6. For 4,4'-tpcb, the binding energies varied between 43.55 (2(5-N(CH_3)$_2$-res)·(4,4'-tpcb)) and 50.69 kcal/mol (2(5-NO_2-res)·(4,4'-tpcb)). The extremes correlate with the most negative and the most positive σ^0 values. As in the case of assemblies based on 4,4'-bpe the trend is linear, which is in line with Hammett-like correlation. Compared to the olefins, the binding energies of 2(5-X-res)·2(4,4'-tpcb) are smaller by ~1 kcal/mol. The lower binding energy may be surprising considering higher basicity upon photoreaction. However, geometrical changes induced by photodimerization contribute to relative destabilization of assemblies. For example, CH···N interactions are weaker.

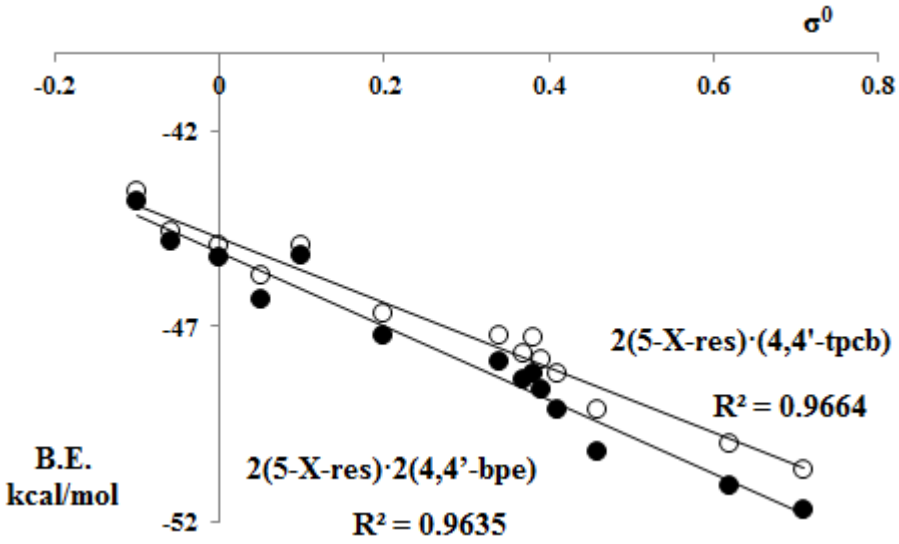

Figure 59 Binding energies plotted against σ^0 values. Full circles, data for 2(5-X-res)·2(4,4'-bpe) , empty circles, data for 2(5-X-res)·(4,4'-tpcb).

6.4 Summary

In this chapter we attempted to achieve solid-state photodimerization of six isomeric olefins using a single bulky template 4,6-didpe-res. Although all six olefins formed cocrystals with 4,6-didpe-res, only two, namely 2,3'-bpe and 2,4'-bpe, afforded photoproduct. Thus, we turned to template screening approach. Using only three commercially available templates, we were able to achieve quantitative photodimerization of olefins that were not effectively templated with 4,6-didpe-res. In conclusion, using the template screening approach that is similar to catalyst screening when optimizing a typical liquid-phase synthesis, we were able to achieve homology in the organic solid-state synthesis.

To explore the modularity of the template approach and substituent effect on the stability of the reactive assemblies, we conducted detailed gas-phase DFT calculations.

The calculations confirmed that four-membered hydrogen-bonded assemblies are viable molecular complexes in gas-phase. This confirms the hypothesis that geometry of assemblies is result of directionality of hydrogen bonds and not only a serendipitous effect of crystal packing. To assess electronic effects of substituents on stability and hydrogen bonds of assemblies, 14 different substituents have been placed on the template. We found a Hammett-like correlation between binding energies of assemblies and substituent constants.

While present in liquid-phase synthesis, homology and modularity of solid-state reactivity is, in general, still lacking. As a result, solid-state is often overlooked as a medium to conduct synthesis, in spite of many advantages when compared to liquid-phase synthesis. The work presented in this chapter demonstrates that homology and modularity can be achieved in solid state. We expect that these results, in addition to solid-state chemists, will appeal to general audience of synthetic chemists.

CHAPTER 7. PRINCIPLES OF SUPRAMOLECULAR CHEMISTRY, SOLID-STATE REACTIVITY, AND MECHANOCHEMISTRY IN UNDERGRADUATE LABORATORIES FOR GREEN SYNTHESES

7.1 Introduction

Supramolecular chemistry, solid-state reactions and mechanochemistry are areas of research that are experiencing an expedited growth. In part, the increased interest stems due to realization that these principles can be greatly useful in the context of Green Chemistry. A more sustainable and holistic approach to chemical synthesis is sought after not only in industry, but in academia, as well. We are increasingly taunted with awareness of how unsustainable is our dependence on fossil-derived organic solvents that are almost unavoidable in liquid-phase synthesis. Organic solvents are recognized and labeled as carcinogens, reproductive hazards and neurotoxins. Such solvents are also known to have a direct negative environmental impact. Therefore, there has been a great legislative push to reduce industrial usage of solvents. For example, a CFC solvent market is about half as large as it was 10 years ago.[120] Along with substituting hazardous solvent with more innocuous solvents, there is an alternative route of the 'solvent-free' synthesis. Solid-state reactions and mechanochemistry have a long and rich history, but have usually been a secondary approach. Historically, the solid state has been dismissed as "a graveyard of chemical reactivity".[121] This ancient and incorrect notion still lingers on, although many recent examples demonstrated the solid state as a rich medium for the organic synthesis, When starting a synthesis, the majority of chemist will ponder which solvent should be used instead of questioning whether solvent is necessary. Indeed, the biggest obstacle to installing a wider use of solvent-free syntheses is changing "the synthesis mind-set".[122]

We incorporate the basic concepts of green chemistry into the undergraduate curriculum at the University of Iowa. We emphasize the practical learning in an effort to

create a different synthesis mind-set. In the undergraduate course *Organic Chemistry Laboratory,* the "Green Chemistry Experiment"[123] has been practiced for last decade. In the laboratory, students are introduced to principles of supramolecular chemistry which are employed to control reactivity in the organic solid state using the template approach. The photochemical reaction occurs upon UV irradiation using either a photochemical reactor or sunlight. The reaction proceeds stereoselectively, in quantitative yield, has a high atom economy, and the pure product is isolated by a simple non-chromatographic method. In this chapter, incorporation of a mechanochemical approach in the form of mortar-and-pestle grinding into the "Green Chemistry Experiment" will be presented. Grinding further reduces the use of environmental pollutants such as organic solvents and increases the overall yield of the experiment.

Prior to the "Green Chemistry Experiment", students prepare their own starting material. To achieve this, the older version of the "Wittig Experiment", in which students used to prepare stilbene, is changed such that the final product is 4,4'-bpe. Although, the Wittig reaction itself is not conducted using principles of green chemistry, the product 4,4'-bpe is used as the starting material later in semester. This is in contrast to previous version of the experiment, where obtained product stilbene was disposed as chemical waste. In addition, in house preparation of the starting material is more economical and lowers the overall cost of the course.

The "Green Chemistry Experiment" is followed by a dry lab involving computational chemistry. Using computational methods students study both covalent bonds and supramolecular interactions. In particular, students evaluate strength of hydrogen bonds that are found as the supramolecular synthons responsible for self-assembly that facilitates photodimerization in "Green Chemistry Experiment."

Over the last five years, the "Template-Directed [2+2] Photodimerization in the Solid State Mediated by Argentophilic Forces" experiment[124] has been a part of the *Inorganic Chemistry Laboratory* course. Undergraduate Chemistry majors are introduced

to the template approach to control reactivity in the solid state. In this context, the students are using argentophilic forces to align organic molecules and conduct a steroselective and quantitative organic synthesis. The photochemical reaction proceeds *via* SCSC transformation. Since upon SCSC reactions the integrity of single crystals is preserved, the photoproduct is analyzed using single crystal X-ray diffraction in a time suitable for an undergraduate course. Last part of the experiment is crystal structure solution and refinement. The data set is collected from the best student crystal and distributed to students. Under the guidance of instructors, each student solves, refines and analyzes the crystal structure before and after photoreaction. After completing the experiment, students have hands-on experience with essential but rarely taught techniques of the solid-state analysis: powder X-ray diffraction, single-crystal X-ray crystallography and crystal structure solution and refinement. The details of the adaptation for the undergraduate course and experiences of teaching the course will be presented.

Table 8 New experiments in the undergraduate curriculum at the University of Iowa.

Experiment	**Course**	**Course code**	**Students per semester**	**Semesters taught**
Green Chemistry	Organic Laboratory	4:2210	150-200	9
Wittig Experiment	Organic Laboratory	4:2210	150-200	9
Molecular Modeling	Organic Laboratory	4:2210	150-200	9
Solid-state and X-ray Experiment	Inorganic Laboratory	4:153	20-26	4

7.2 The Wittig reaction: Preparation of trans-4,4'-bpe

7.2.1 Background of the Wittig experiment

The Wittig reaction provides an invaluable method for the conversion of an aldehyde or ketone to an olefin. The reaction involves the nucleophilic addition of a phosphorous stabilized anion (the ylide) to the carbonyl compound with subsequent elimination providing an alkene. Triphenylphosphine oxide, which contains a strong P=O bond, is produced as a side product in the Wittig reaction. The Wittig reactions is regularly taught both as a part of *Organic Chemistry* course and *Organic Chemistry Laboratory* course. Previous years, the reaction was taught in the lab as a means to prepare *trans*-stilbene, the product that was discarded upon completion of the lab. Considering that later in the semester, students use a relatively expensive diazastilbene, *trans*-4,4'-bpe, we modified the Wittig reaction to synthesize *trans*-4,4'-bpe. The synthesis of *trans*-4,4'-bpe via Wittig reaction is not reported and isolation of only trans-isomer proved to be complicated. However, the procedure has been optimized such that over last four years, although in relatively low yields, each class of students was able to produce enough of *trans*-4,4'-bpe to supply the cohort when conducting the "Green Chemistry Experiment".

7.2.2 Overview of the Wittig experiment

As the first step, triphenyl(4-pyridylmethyl)phosphonium chloride salt is formed in reaction of 4-pyridylmethyl chloride and triphenylphosphine. The salt is left to dry until the next lab period. Upon addition of strong base to the suspension of salt, a reactive ylide is formed *in situ*. Because the ylide is very reactive it is generated in the presence of the 4-pyridine carboxyaldehyde. The ylide reacts with of 4-pyridine carboxyaldehyde to produce a mixture of *cis*- and *trans*- isomers of 4,4'-bpe. Upon protonation and subsequent neutralization, only *trans*-4,4'-bpe precipitates under the reactions conditions.

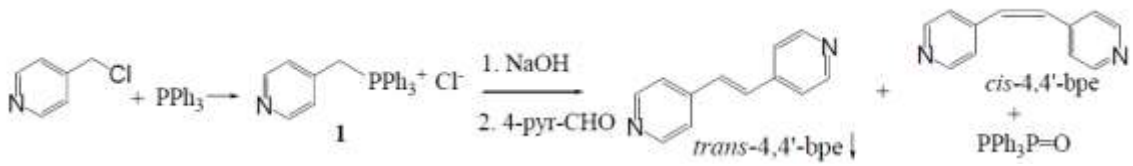

Figure 60 Synthesis of trans-4,4'-bpe. The Witting reaction

7.2.3 Experimental procedure

2.25 g of 4-pyridylmethyl chloride and 3.6 g of triphenylphosphine and 15 ml of DMF are heated 80 °C for 45 minutes. Upon cooling on ice for 20 min, precipitate, triphenyl(4-pyridylmethyl)phosphonium chloride, forms. The salt is isolated using vacuum filtration and left to dry until next lab period. The ^{1}H NMR spectra and the melting point are obtained.

4.0 g of the triphenyl(4-pyridinylmethyl)phosphonium chloride are suspended in 10 ml of dichloromethane. Add 1.2 mL of 4-pyridine carboxyaldehyde while vigorously stirring the suspension. Add a strong basic solution prepared by dissolving 25 g of NaOH in 40 ml of cold distilled water. Stir for 30 minutes. Add 100 ml of distilled water and 15 ml of dichloromethane. Extract organic layer twice using 10 mL of dichloromethane. Add 30 ml of 10% HCl to organic layer to protonate product and transfer it to water layer. Separate water layer and neutralize using NaOH solution. Around pH 7, your product will start to precipitate from solution. Filter off the final product. Obtain the melting point and ^{1}H NMR spectra.

7.2.4 Hazards

Basic organic chemistry laboratory safety procedures should be observed when carrying out the experiment. Protective glass, goggles and lab coat should be worn at all times. The strong base (NaOH) and strong acid (HCl) present a hazard for chemical

burns. The organic solvents should be manipulated only in the well ventilated hoods as their fumes present health hazard. There is a potential for explosion and braking of the glass separatory funnel during extraction. The extraction should be conducted within the hood, behind the glass shield and the content should be vent after each inversion.

7.2.5 Results and discussion.

The formation of salt at the end of the first lab period was in general facile and high-yielding. In the instances where students did not observe formation of the solid after 30 min, students were advised to induce crystallization either by scratching the flask with glass rod or seeding the solution with a small amount of product obtained by their lab partner. The formation of ylide and trans-4,4'-bpe is accompanied by dramatic color changes ranging from clear, to dark orange-brown to final pale yellow to orange. The color changes are a good indication that students have actually added all required reagents in appropriate amounts. The series of extractions was more challenging to students because the exact order has to be followed and the correct layers have to be carried on to the next cycle of extraction. As a precaution, the students are advised not to irrecoverably discard any layers until the experiment is completed to minimize the loss of the product due to confusion about which layer to keep. Finally, the neutralization has to be done slowly and carefully to maximize the yield because "overshooting" the pH can decrease the yield significantly. The ^{1}H NMR spectra indicates the product of high purity (over 95% pure for most of the students) and it is relatively easily interpreted by students as it exhibits only three peaks: doublet at 8.6 ppm associated with pyridyl proton that is in alpha position in respect to nitrogen atom; doublet at 7.65 ppm associated with pyridyl proton that is in beta position in respect to nitrogen atom and singlet at 7.55 ppm associated with proton of the C=C bond. The spectra are collected using DMSO as a solvent. Melting point of *trans*-4,4'-bpe is 150-153°C. Students are asked to find this information searching the literature and compared to the value that they obtained. The

dryness of the compound has effect of the value obtained for melting point. Given the appropriate time to dry the product, students were able to measure melting point in the range 149-155°C.

7.3 Green chemistry experiment: A template-directed [2+2] photodimerization conducted in the solid state

A misconception often encountered in organic chemistry is that all organic reactions that produce covalent bonds (e.g. C-C single bonds) must occur in solution (i.e. liquid phase). However, organic reactions can readily occur without solvent. From an environmental perspective, such solvent-free reactions are desirable since they eliminate the use of organic solvents (e.g. chloroform). Organic solvents are typically toxic and can pollute the environment (e.g. damage to ozone layer). The area of organic chemistry that is concerned with the reduction of organic solvents in chemical synthesis and, more generally, the reduction of environmental pollutants in synthetic chemistry is known as green chemistry.

Mechanochemistry refers to methods that use the mechanical energy to achieve chemical reactions. The oldest example of mechanochemical reaction is making fire. The pieces of wood are rubbed against each other to create friction and heat. The heat initiates the combustion of wood. As mechanochemistry can often be conducted without use of solvent, in recent years it is becoming more popular in context of green chemistry.

7.3.1 Background of the green experiment

In the Green Experiment, students conduct an organic reaction in crystalline state that is a solvent-free medium. In particular, the C=C bonds of 4,4’-bpe undergo photoreaction to afford a cyclobutane photoproduct that is difficult to obtain from solution. As a pure solid, 4,4’-bpe is photostable because the C=C bonds are too far away to react in solid state. Thus, a template molecule, res, is used to assemble two reactant molecules, 4,4'-bpe using hydrogen bonds, in a process known as a cocrystallization. The

students use 4,4’-bpe that they prepared earlier in the semester. The solid-state reaction occurs by irradiating the crystals with ultraviolet (UV) radiation in a photochemical reactor or using natural sunlight. The details of earlier version of the experiment have been published. Herein, I report in details only the recent improvement of the experiment that relates to incorporation of mechanochemistry as a means to conduct cocrystallization. Mechanochemical cocrystallization is more efficient, requires lesser amount of starting materials and further minimizes use of organic solvents.

7.3.2 Overview of the green experiment

First part of the experiment is mechanochemical preparation of the cocrystals. The prepared solid is characterized, using melting point determination, ^{1}H NMR spectroscopy and TLC analysis. Next, the sample is prepared for photoreaction, both by UV-irradiation in chemical photoreactor and using natural sunlight. As a control experiment, pure 4,4’-bpe is exposed to UV-irradiation, as well. The solids are irradiated until next lab period when students characterize the photoproduct and determine that pure 4,4’-bpe did not yield photoproduct.

7.3.3 Experimental procedure

180 mg of the 4,4’-bpe prepared in the Wittig lab and 120 mg of res are placed in a clean and dry mortar and pestle (1:1 molar ratio). Two solids are ground together for a period of 25-30 minutes. Particular attention should be placed on mixing solids thoroughly. The resulting fine powder should be collected and photoplates should be prepared. Small amount of powder should be preserved for melting point determination, ^{1}H NMR spectra collection and TLC analysis.

7.3.4 Hazards

Hazards associated with dry mortar-and-pestle grinding are minimal. However, as the health hazards of prepared cocrystals are not fully studied, the grinding should be conducted in the well-ventilated hood to avoid inhalation of fine powder.

7.3.5 Results and discussion

The cocrystallization via manual grinding offers a quantitative cocrystallization which is significant improvement compared to earlier version of experiment. As a result, students use less of the starting materials. Small amount of cocrystals (up to 10%) is lost during the transfer of the solid from mortar to the photoplates. In general, students are not used to working with powders and this experiment requires them to develop dexterity when dealing with solid samples. However, the fact that no solvent is necessary and that photoreaction can be conducted using free and renewable solar energy receives overall positive perception from students.

7.4 Molecular modeling

Owing to the development and exponential increase in computer speed, the use of computers is playing more significant roles in chemistry. Conducting syntheses in the lab can be laborious. On the other hand, performing experiments on a computer is a simple and fast alternative. Computational power has increased enough that we can quickly and reliably model structures, reactions, and properties of increasingly complex molecules. Without entering the lab, we can evaluate the stability of a molecular target, study electronic structure, probe effects of different substituents, and predict spectroscopic and other properties.

7.4.1 Background of molecular modeling experiment

Goal of this experiment is to use computational chemistry to probe electronic effects on both covalent and non-covalent bonds. Bond order, aromaticity, and

substituents have strong effects on bond strengths, energies, and reactivities of molecules and molecular complexes. Students review principles of resonance, which are extremely useful when rationalizing the chemical behavior of many compounds, aromaticity and Hückel rule, and factors that affect molecular stretching and their appearance in IR spectra. In next period, students focus on supramolecular interactions and molecular complexes. For the purpose of this experiment, a molecular complex is an assembly of two or more neutral molecules held together by non-covalent interactions (e.g. hydrogen bonds). In particular, strength of hydrogen bond is evaluated upon variations in electronic and steric effects.

7.4.2 Overview of molecular modeling experiment

As the first part of the experiment, students predict the vibrational spectral frequencies for six cyclic ketones using molecular orbital (MO) methods, and trends in the bond length and C=O stretching frequencies are compared to expectations based on resonance theory and aromaticity models.

As the second part of the experiment, stabilities of three hydrogen-bonded molecular complexes, and strengths and lengths of hydrogen bonds are predicted. Trends are rationalized based on substituent effects.

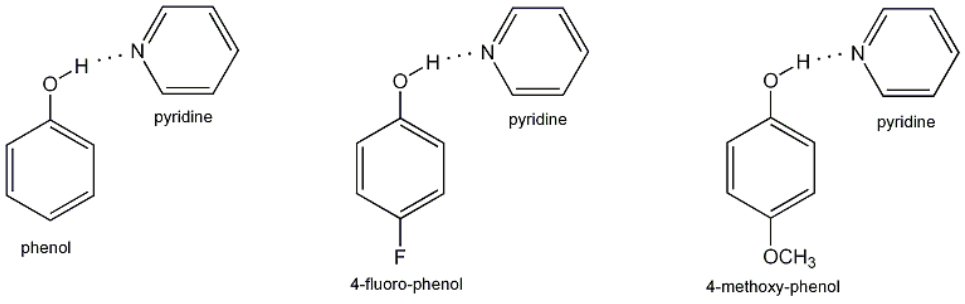

Figure 61 Hydrogen-bonded assemblies studied in molecular modeling experiment.

7.4.3 Experimental details

For the calculations, students use a computer program known as *Spartan'10* (Wavefunction Inc.) on PCs located in the Department of Chemistry.

7.4.4 Hazards

There are no chemical hazards associated with this experiment

7.4.5 Results and discussion

At the end of the lab period students obtain all data required to fill in three Tables that are provided in the manual. Based on the results and understanding of chemical principles discussed at the beginning of the experiment, students are required to draw the correct resonance forms (neutral and charge separated) for all cyclic ketones. Based on the number of π-electrons that are present in each ring, students distinguish aromatic compounds. Based on the trend in the C=O stretching frequencies, students can conclude that conjugation with double bods lowers stretching frequencies. In terms of ring size, incorporation of C=O group in smaller rings, increase the stretching frequency. On the other hand, the presence of aromaticity lowers the stretching frequency. Students are asked to compare their data to reported stretching frequencies:
cyclopropanone:1813 cm^{-1} cyclopentanone:1700 cm^{-1} cycloheptanone:1700 cm^{-1}
cyclopropenone:1840 cm^{-1} cylcopentadienone:1870 cm^{-1} cycloheptatrienone: 1651 cm^{-1}

In terms of hydrogen bonding, students can clearly establish Hammett-like correlation between binding energies of molecular complexes and electronic properties of substituents. The shorter O···N distance indicates stronger hydrogen bond, while opposite is true for O-H distances. These trends are compared to reported literature values:

phenol: 3386 cm^{-1} 4-F-phenol: 3367 cm^{-1} 4-OCH_3-phenol:3401 cm^{-1}

At the end of the experiment, students should have a practical skill to conduct calculations and modeling using *Spartan* software. The experiment should further strengthen their understanding of basic chemical principles, such as resonance,

aromaticity and hydrogen bond strength. Moreover, the experiment should highlight the use of safe and inexpensive calculations to guide the organic synthesis in the laboratory.

7. 5 Template-directed [2+2] photodimerization in the solid state mediated by argentophilic forces

As in the Green Chemistry experiment, students conduct an organic reaction in the crystalline state. However, in this specific experiment, the reaction occurs in a metal-organic crystal. To direct photoreaction of a substrate, students will use inorganic, metal template, a disilver(I) dication. The template consists of two Ag^{I} cations bonded through metallophilic forces. Group 11 elements (*e.g.*, Cu, Ag, Au) contain fully occupied *d* shells (md^{10}) and a partially occupied *s* shell (ns^{1}). To form a chemical bond, these atoms share electrons. In case of bulk metals, the "excessive" ns^{1} electron is shared with a neighboring atom in a solid to adopt a closed-shell configuration. On the other hand, when Group 11 elements as ions participate in the formation of a bond, the oxidized atoms are left in an energetically very stable closed-shell state (*i.e.*, +I oxidation state). Although the md^{10} species are expected to repel each other, the atoms attract each other by dispersion forces. The strength of the dimetal interaction generally increases with atomic weight. Metallophilic forces are weaker than ionic forces and covalent interactions, but stronger than van der Waals interactions. When metallophilic interactions involve Ag^{I}, they are referred to as argentophilic forces (lat. argentum = silver).

During the experiment, students also observe a rare SCSC transformation. Normally, when atoms react in a solid, there is a build-up of stress and strain such that the single crystal cracks and shatters. The stress and strain is a result of movement of the atoms to form the new covalent bonds. SCSC reactions are quite rare and it is thought that the crystals that undergo these transformations can form the basis of device applications. Since the single-crystal structure remains intact, X-ray crystallography can

be used to effectively monitor the movement of the atoms following the chemical reaction.

Last part of the experiment is intended to introduce students to the main aspects of chemical crystallography; namely, structure solution, refinement, and data analysis. In the manual, guidelines for structure solution and refinement of the $[Ag_2(\mathbf{4sbz})_4][CO_2CF_3]_2$ using the programs *SHELX* and *Mercury* are provided. The structural information obtained over the course of the experiment provide students with a means to understand how modern crystallographic software and hardware can be utilized to develop an understanding of [2+2] photodimerization reactions in the solid state. Although manual does not provide a capacious introduction to fundamentals of crystallography (*e.g.* X-ray scattering, crystal symmetry, space group theory, data-collection theory, Fourier synthesis), it successfully guides student to independent use of all programs to complete assigned tasks.

7.5.1 Experiment overview

As a first part of the experiment, students use a modified Wittig reaction, namely the Horner-Wadsworth-Emmons (HWE) reaction, to prepare organic ligand 4-Stilbazole (4sbz). The ligand 4-sbz will be used to form photoreactive inorganic complex with silver(I). Upon UV-irradiation, the complex undergoes photodimerization to yield cyclobutane photoproduct in quantitative yield. The photoreaction proceeds in SCSC manner. To characterize the crystals before and after photoreaction, students will use X-ray crystallography. The tour of X-ray facility at the Department of Chemistry is organized for students, as well as meeting with the crystallographer. The process of crystal selection, crystal mounting and data collection is described to students in details and aided with visual demonstrations. The data set collected from the best students' crystal is provided to students and last two days of experiment are focused on instructing students how to solve, refine and analyze crystal structures independently.

7.5.2 Experimental details

Part A. Synthesis of 4sbz. Prepare a suspension of *t*-BuOK in tetrahydrofuran (THF) by adding 1.12 g (10 mmol) of *powdered* *t*-BuOK to 10 mL of tetrahydrofuran (THF) in an Erlenmeyer flask (50 mL). Use a spatula or mortar and pestle to convert the *t*-BuOK into a fine powder if the solid is present as small 'clumps'. Dissolve 2.34 g (10.25 mmol) of 4-(diethoxy-phosphorylmethylene)benzene in THF (1 mL). Prepare a second solution by dissolving 4-pyridinecarbaldehyde (1.07 g, 10 mmol) in 1 mL of THF. Then, first add the solution of 4-(diethoxyphosphorylmethylene)benzene in THF to the vigorously stirred *t*-BuOK/THF suspension and subsequently add the solution of 4-pyridinecarbaldehyde in THF to the mixture. Securely clamp the flask, plug the neck with a rubber stopper, and continue to stir the resulting solution for 1 h at room temperature. Monitor the contents of the flask over time and record the consistency of the flask content in 5 min intervals. Assemble a Hirsh funnel, a heavy-walled side-arm filtering flask, a rubber adaptor, and filter paper for a vacuum filtration. Once the reaction is complete, pour the reaction mixture on ice (250 mL) placed into a 400 mL beaker. A white precipitate of 4sbz will form immediately. Add 50 mL of water to the 4sbz/water mixture. Stir the content of the beaker under gentle heating (30–40 °C) using a stir/hot plate until the ice is dissolved (about 15 min). Filter the 4sbz, place the solid on a petri dish, and dry the solid in an oven at 90 °C for 15 min. Measure the mass and calculate the percent yield of 4sbz for your report.

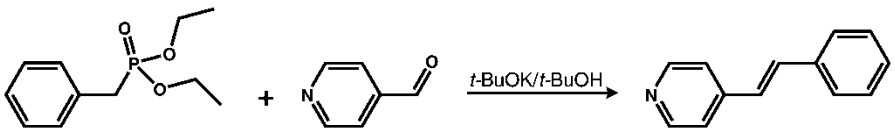

Figure 62 Synthesis of 4sbz in HWE reaction.

Part B. Preparation of Single Crystals and Bulk Powder of $[Ag_2(4sbz)_4](CF_3CO_2)_2$. Using two 20 mL vials, prepare separate acetonitrile solutions of $AgCF_3CO_2$ and 4sbz. Dissolve 0.061 g (0.28 mmol) of $AgCF_3CO_2$ in 1 mL of acetonitrile. Shake the content of the vial until the solid dissolves. Suspend 100 mg (0.55 mmol) of 4sbz in 1 mL of acetonitrile in the other vial. Heat the suspension gently until the solid entirely dissolves, and you obtain a clear and brown solution. Add the $AgCF_3CO_2$ solution slowly to the 4sbz solution. Cap the vial, wrap the vial with aluminum foil and label your sample. Place the vial in your drawer. Single crystals of $[Ag_2(4sbz)_4](CF_3CO_2)_2$ suitable for X-ray diffraction are expected to grow by the next lab period.

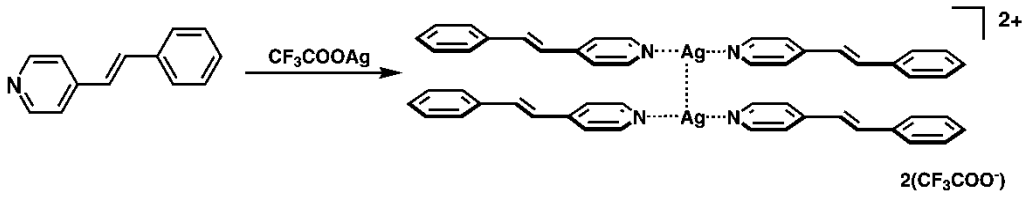

Figure 63 Reaction of $AgCF_3CO_2$ and 4sbz to form $[Ag_2(4sbz)_4](CF_3CO_2)_2$.

To prepare a powder of $[Ag_2(4sbz)_4](CF_3CO_2)_2$, prepare $AgCF_3CO_2$ and 4sbz solutions as described above. Dissolve 0.122 g (0.56 mmol) of $AgCF_3CO_2$ in 1 mL of acetonitrile using a 20 mL vial. Shake the content of the vial until the solid dissolves. Suspend 200 mg (1.10 mmol) of 4sbz in 1 mL of acetonitrile in the other vial, and heat the suspension gently until the solid entirely dissolves. Add the $AgCF_3CO_2$ solution quickly to the 4sbz solution. Cap the vial and label it before you place the vial in an ice bath. Small crystals of $[Ag_2(4sbz)_4](CF_3CO_2)_2$ will precipitate from the brown solution after 15 min. Wrap the vial with aluminum foil and place it in your drawer.

Part C. Isolation of Single Crystals and Powder of $[Ag_2(4sbz)_4](CF_3CO_2)_2$. Isolate both the single crystals and crystalline powder that have been prepared on Part B via vacuum filtration using a Hirsh funnel, a heavy-walled side-arm filtering flask, a rubber adaptor, and filter paper. Record the mass and calculate the percent yield of your single crystals and powder samples. The single crystals should be saved to be used in Parts E and F.

Part D. Characterization of the Powder. Convert the bulk powder sample to a fine powder using mortar and pestle. Place approximately 5 mg of the fine bulk $[Ag_2(4sbz)_4](CF_3CO_2)_2$ powder in an NMR tube and add 600 μL of DMSO-d_6. Analyze your samples using ^{1}H NMR spectroscopy. The spectrum is to be analyzed and described in your report.

Place approximately 70 mg of the bulk $[Ag_2(4sbz)_4](CF_3CO_2)_2$ powder in a sample vial. Your sample will be collected by your TA for characterization by powder X-ray diffraction. Save the remainder of the powder for Part F.

Part E. Selection of Single Crystals for X-ray Crystallography and Photoreaction. Your single crystals of $[Ag_2(4sbz)_4](CF_3CO_2)_2$ will be studied using X-ray diffraction. The X-ray experiment will provide an atomic-level understanding of the structure of $[Ag_2(4sbz)_4](CF_3CO_2)_2$ before the photoreaction so that you can determine the geometry of the metal and organic components in the solid. This portion of the laboratory will be performed in both your wet lab and the X-ray lab.

To prepare your single crystals for mounting and data collection, each person from each group should spend no more than five minutes to view his or her sample of single crystals under a microscope. Each person should select one single crystal that looks the best for X-ray diffraction and also collect a batch of five single crystals on a watch glass to be used for the photoreaction. An appropriate crystal will have dimensions of approximately 0.5 mm and will be transparent and of uniform shape.

Once your group has selected a final crystal, your TA will escort your group to the X-ray laboratory to learn how to mount a single crystal on the X-ray diffractometer and collect data. The best single crystal from all groups will then ultimately be selected by our X-ray manager for data collection.

Part F. Photoreactions of Single Crystals and Powder.

Preparation of Sample A: Place your five remaining single crystals of $[Ag_2(4sbz)_4](CF_3CO_2)_2$ on a watch glass. Spread the single crystals so that the crystals are not touching each other. Label your sample.

Preparation of Sample B: Grind gently 70 mg of the bulk $[Ag_2(4sbz)_4](CF_3CO_2)_2$ using mortar and pestle until the material turns into a fine powder. Place the powder between two pre-cut transparency films provided by your TA. Spread the solid evenly between the transparencies. Stick the transparency films together using masking tape (one on each side) (Fig 64). Label your sample.

Submit Samples A and B to your TA to be placed in the UV reactor. The samples will be exposed to broadband UV irradiation for approximately 20 h.

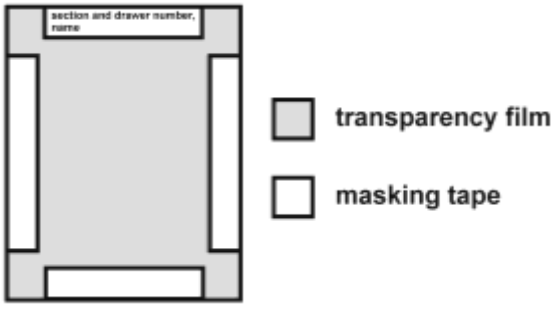

Figure 64 Schematic of a transparency prior to photoreaction.

Part G. Isolation of Photoreacted Solids and Characterization of Powder. Collect the single crystals and fine powder that were exposed to the UV radiation. The crystals and powder should be placed in separate vials.

Place approximately 5 mg of the reacted fine powder in an NMR tube and add 600 μL of DMSO-d_6. Analyze your sample using ^{1}H NMR spectroscopy. The spectrum is to be analyzed and described in your report. The remaining powder will be collected by your TA for characterization by powder X-ray diffraction.

Part H. Selection of Photoreacted Single Crystals for X-ray Crystallography. Your reacted single crystals will be studied using X-ray diffraction. The X-ray experiment will provide an atomic-level understanding of the structure of the solid following the exposure to the UV irradiation.

As in Part E, each person from each group should view his or her sample of single crystals under a microscope and identify the best crystal. Make an accurate sketch of the crystal in your notebook. Also make an observation of the general state of the reacted crystals (e.g. transparent? cracked?). Each group should then select their best overall single crystal.

Mounting of the single crystal and data collection will again take place in the X-ray laboratory. The best crystal from all groups will be selected by our X-ray manager for data collection.

Part I. Tutorial on Single-Crystal X-ray Diffraction. A tutorial on the basics of single-crystal X-ray diffraction and structure solution will be given. The information that you learn in this portion of the experiment will be applied to solving and analyzing the structures before and after the photoreaction.

Structure Solution, Refinement, and Analysis of $[Ag_2(4sbz)_4](CF_3CO_2)_2$ and Photoreaction Product. Following the tutorial (Part I), the experiment continues in the computer laboratory.

Step 1 – Create Project Folder and Download Data Files

Go to *My Computer*, open your personal drive (H:) and create a new folder named *exp5-structures*. Then open a web browser to access the ICON course website. Under the *Content* tab you will find all the data files. Download the data files to *exp5-structures*. Go to your personal drive and open the *exp5-structures* folder (H:\exp5-structures). Extract the two zipped folders: *before* and *after*.

Step 2 – Define Project Folder

After starting *WinGX* from the *Windows Start* menu, the taskbar will appear on your screen (Fig. 1, left). You need to define the folder wherein your crystallographic data is stored (*i.e. ins* and *hkl* files). For this purpose, select "*Project"→"Start/Select new*

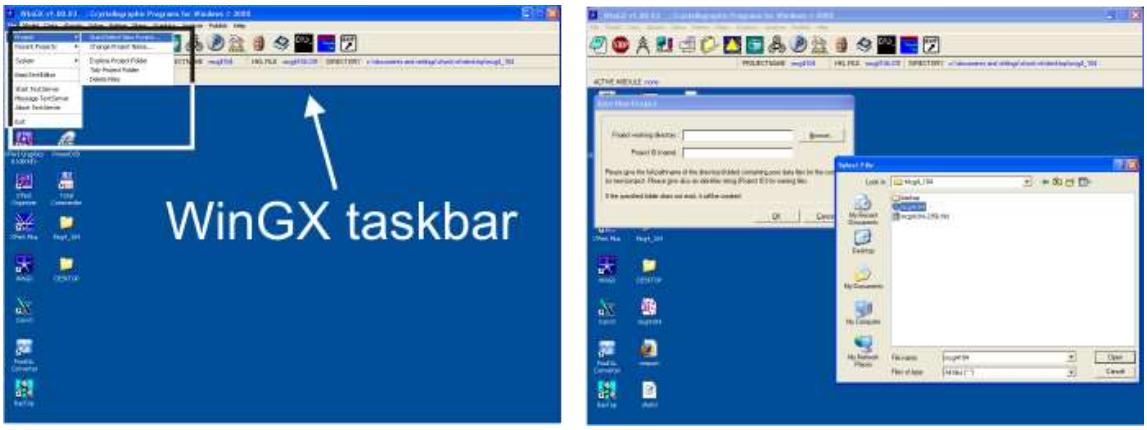

Figure 65 Starting a new project in *WinGX*.

project" from the *File* menu bar. The *"Start New Project"* window will appear. Browse for the folder *before* and select the *before.ins* file (Fig. 63).

The *ins* file can be accessed any time by clicking the "*Open INS file"* option in the *Refine* menu (Fig. 3, right). The results of your structural analyses will be stored in this folder. The *ins* file contains the following information :

a) the name of the dataset (followed by 'TITL')

b) information about the X-ray wavelength and cell unit cell parameters (followed by ‘CELL’ and ‘ZERR’)
c) description of the crystal symmetry (followed by ‘SYMM’),
d) information about the content of the unit cell (followed by ‘SFAC’ and ‘UNIT’)
e) information about the format of the *hkl* file (followed by ‘HKLF 4’)
f) information about crystal size and data-collection temperature.

Structure solution cannot be initiated if the *ins* file lacks any of the information listed above.

Step 3 – Structure solution

The structure solution process begins by selecting *SHELXS-97* in the *Solve* menu (Fig. 65, left), upon which the *“SHELXS-97 Control Panel”* pops up on your screen (Fig. 5, right). Under *Global Parameters* change the theta range by changing *Sigma threshold* to 0 and *2-theta maximum* to 50. You will use direct methods to solve your crystal structure. Therefore, select the *Direct* tab from the control panel and click OK to start the structure solution procedure.

Upon initiation of the structure-solution procedure, an output file will appear on your screen. This output file ends with an entry that indicates that 35 areas of high electron density were found in the asymmetric unit. The 35 electron density areas, or peaks (*i.e.* Q-peaks), most likely represent atoms (Fig. 66, left). Upon structure solution, *WinGX* will start *SXGraph* - the *SHELX* graphical editor. *SXGraph* will graphically depict the positions of all Q-peaks in the asymmetric unit (Fig. 66, right). Verify that the following options are enabled in the right-hand panel: *Display Q-peaks*, *Label Q-peaks*, and *Show Q-peak bonds*. If *SXGraph* does not pop up, click the sextant icon in the *WinGX* task bar or go to the “*Model*” menu in *WinGX* and select “*SXGraph*”.

Notice that most Q-peaks resemble atomic positions equivalent to those in one half of the expected structure of your silver complex (Fig. 66, right). One Q-peak was also automatically assigned as the Ag atom owing to the high electron density (comparable to other peaks) associated with the peak. Since the graphical representation is a reasonable match of your complex, you can consider the structure as having been 'solved' by *SHELXS-97*.

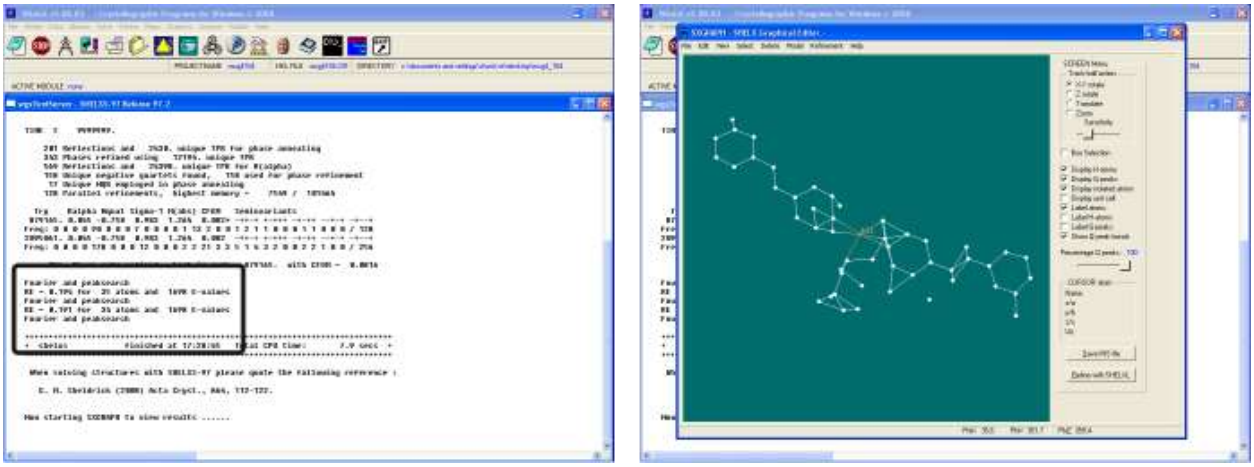

Figure 66 Crystal structure solution in *WinGX*.

Step 4 – Structure Refinement

The next step is structure refinement. During the process, you will assign atom types to the Q-peaks. Note that some Q-peaks do not represent actual atoms. Such Q-peaks are often referred to as "wild" Q-peaks.

The results of the structure solution procedure are stored in the *res* file (*i.e. before.res*). The res file can be accessed any time by clicking the "*Open RES file"* option in the *Refine* menu). The first part of the *res* file contains a copy of the content of the *ins* file. The second part of the res file contains a list of both atom positions and Q-peaks. The Ag atom and the Q peaks in your *res* file will be listed in alphabetical order (*i.e.*

Ag1, Q1, Q2,…Q49) together with the element code numbers (*i.e.* 1,…,6). The element code for all Q-peaks is set to be 1 by default. The code number is followed by the *x*, *y* and *z* coordinate of the atom position or the electron-density peak, and then by the occupational parameter (*i.e.* 11.00000). An occupational parameter of 11.00000 corresponds to a 100% (*i.e.* 1.00000) probability of finding an atom at the given coordinates. To keep the occupancy parameter constant in upcoming refinement cycles, a value of 10 is added to the given numerical value of the occupancy parameter (*e.g.* 10 + 1.00000 = 11.00000). Note that the occupation parameter does not have to be 100%. Sometimes atoms move around the empty spaces in crystals, or they occupy fixed positions in only a small portion of all available empty spaces in a crystal. In that case, their movement or the random occupation of crystal voids can be described with occupation parameters than are less than 1 (*e.g.* 0.76 = 76%).

Note that the structure solution provided one half of the expected structure of the Ag^{I} complex. This indicates the presence of a symmetry element in our complex. For your crystal, the dinuclear complex sits around a center of inversion. The coordinates of the other half will be calculated based on the determined coordinates and on symmetry operators characteristic for the space group of your crystal.

Before crystal structure refinement begins, you must first eliminate those Q-peaks that do not represent real atoms and then assign the correct atom type to the remaining peaks.

Click the "*label Q-peaks*" option in the right-hand menu of *SXGraph*. A close look at the initially solved structure in the *SXGraph* interface will allow you to recognize the Q-peaks that either have no chemical meaning or correspond to hydrogen atoms. These Q-peaks should be deleted. To select them, use the left mouse button. In the example below (Fig. 67, right) the meaningless Q-peaks are selected and colored yellow. Once selected, these Q-peaks can be deleted by activating the "*Selected atoms*" option in the "*Delete*" menu.

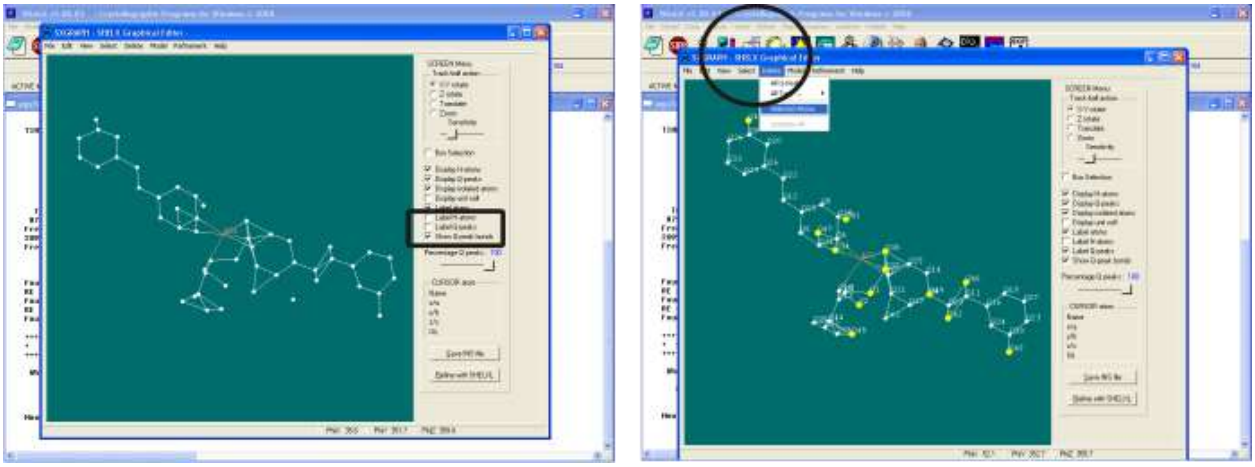

Figure 67 Process of structure refinment in *WinGX*.

After the Q-peaks are deleted, you will obtain a clear three-dimensional model that represents all non-hydrogen atoms of one half of the Ag^{I} complex. Now, you have to assign the atom type. Find the Q-peaks that correspond to N-atoms and select them (using the left mouse button, they should turn yellow upon selection). To assign these Q-peaks as N-atoms, select both Q-peaks and click the right mouse button. The *"Change Group Properties"* dialog box will pop up. An atom type will be assigned by selecting *"Nitrogen"* in the "*Atomic Scattering Factor*" pop-down menu. The newly assigned nitrogen atoms should be given suitable names (*e.g.* N1, N2).

Assign all the other Q-peaks to appropriate atom types (*i.e.* C, O, F) in the same manner as the N-atoms. A group of selected Q-peaks can be assigned to only one atom type, and only 20 atoms can be renamed at a time Rename the carbon atoms to C1 – C28 starting from the atoms closest to the nitrogen atoms. The C-atom belonging to the COO-group of CF_3COO- should be renamed to C27, whereas the CF_3 carbon atom should be renamed to C28. The O-atom closest to the Ag atom should be renamed to O1, the more distant one to O2. Once all Q-peaks are assigned to an atom type, you are ready to initiate

the structure refinement. To do so you, you need to overwrite the initial *ins* file by selecting the "*Save INS File*" option in the right-hand menu in *SXGraph*

You are now ready to initiate the structure refinement. Either click "*Refine with SHELXL*" in the right-hand menu in *SXGraph* or click the *"Run SHELXL"* option in form the *"Refinement"* menu in *SXGraph*. After four refinement cycles, *SXGraph* will provide a summary (*i.e.* SHELX Refinement Summary) of the refinement procedure. A warning will appear (in yellow): "** *Cell content from UNIT instruction and atom list do not agree* **".

This warning informs you that your structural model lacks H-atoms. You will see that most of the Q-peaks appear either where the H-atoms are supposed to be located or other locations that are in close proximity to the non-H-atoms.

Before inserting the H-atoms, you will need to perform refinements that treat your non-H-atoms as anisotropic. Select all atoms in the *SXGraph* window by either clicking each atoms or by going to the "*Select*" menu and clicking the "*All Atoms*" option. Once all atoms are selected, click the right button on your mouse to open the "*Change Group Property*" menu. Select "*Set Uij's anisotropic*". Create a new *ins* file by clicking "*Save INS file*" in the right-hand menu of SXGraph. Initiate another four refinement cycles by selecting the "*Refinement*" option in "*Run SHELXL*".

After the refinement cycles are finalized, you will see that the positions of the Q-peaks do not overlap with any atoms, nor they are positioned in very close proximity to any atoms. In fact, the Q-peaks are now positioned where H-atoms are. You are now ready to generate H-atoms at suitable C-atoms. An inspection of your structural model will indicate that C-atoms C1, C2, C4-C7 and C9-C13 are both sp^2 hybridized and connected to only two other C-atoms. These atoms, thus, need to be "equipped" with a single H-atom. Before adding the H-atoms, remove the newly generated Q-atoms by going to the "*Delete*" menu and selecting "*Q-peaks*".

To add the H-atoms, select the sp^2 hybridized C-atoms, go to the "*Model*" menu in *SXGraph*, and select the "*Aromatic C-H*" option from the "*Add Hydrogens*" submenu. The "*Add Aromatic C-H*" window will pop up. Close the submenu by clicking "*OK*" button. Notice that the sp^2 hybridized atoms will be marked green. Create a new *ins* file and further refine the structure. The "*SHELX Refinement Summary*" window should reveal an *R* parameter close to 0.0444.

Step 5 – Final Refinement and Generation of CIF File

To complete the structure determination of your Ag^I complex, repeat the refinement procedure by clicking "*Refine with SHELXL*" until the *"mean shift/esd*", the "*maximum shift/esd*", "*max. shift*" and "*max dU*" parameters drops down to a value of 0.000. The crystal structure is now solved and refined.

Generation of CIF file: The last step in the structure-determination process is to create an output file suitable for data analysis and publication. Go to the "*Model*" menu in *SXGraph* and select the "*Cell Content*" option. First click the "*Update UNIT card*" and then the "*Apply changes*" button. Then go to the "*Refinement*" menu and select the "*ListFiles*" option. Check the "*Write ACTA CIF file*" option on the right-hand menu, and click again "*Apply changes*". Go to the "*View*" menu and select "*Screen menu*". Create a new *ins* file and refine your structure a last time. The last refinement will result with a Crystallographic Information File, or CIF file. You will use the CIF file to analyze the structural details using the program Mercury.

The Crystallographic Information File (CIF)

The CIF is a standard archive file used for publication purposes (*e.g.* submission of crystallographic data to a journal, preparation of tables), as well as for transfer of crystallographic data among scientists. The CIF is also the file of choice for deposition of crystallographic data in the Cambridge Structural Database – a database of more than 500.000 crystal structures that contain a carbon-carbon bond. Besides the structural data, a CIF also contains experimental details, comments on the structure refinement,

description of physical properties of the investigated crystal, the authors contact information, and more.

In order to accurately describe structural changes in single crystals of **$[Ag_2(4sbz)_4][CO_2CF_3]_2$** during the [2+2] photodimerization in the solid state, you will need to measure changes in the Ag···Ag, Ag-N, and Ag-O distances, separations between the –C=C– groups of neighboring 4sbz molecules, as well as C-C distances in the cyclobutane ring. For this purpose, you will use *Mercury* – a program for structure visualization and the exploration of structural features of crystal structures. *Mercury* is developed by the Cambridge Crystallographic Data Centre, and can be obtained free of charge at:

http://www.ccdc.cam.ac.uk/free_services/mercury/downloads/

After starting *Mercury* from the *Windows Start* menu, the Mercury main window will appear on your screen. Now, you need to locate the CIF file (*i.e. before*.cif) in the folder wherein your have solved the crystal structure of your compound. To do so, select "*Open"* from the *File* menu bar. Browse for the folder *exp5-structures* on your personal drive (H:) and select the *before.cif* file.

Once you selected the file and clicked the "*OK*" button, your crystal structure will appear on the screen. You will notice that only one half of the silver complex is shown on your screen. To visualize the entire complex, check the "*Short contact*" box in the lower left "*Display*" options of the *Mercury* main window. *Mercury* will show you all atoms that exhibit a close contact (*i.e.* shorter than the sum of van der Waals radii). Check the "*Label atoms*" option in the "*Options*" box to visualize their labels (this should help you to locate the other half of the silver complex). Select the Ag-atom (labeled as Ag1) that exhibits a close contact to the Ag1 atom initially visualized within the first half of the silver complex. This action will enable the visualization the entire silver complex.

In order to measure distances between two atoms, you need to select the "*Measure Distance*" option from the "*Picking Mode*" menu. From now on, *Mercury* will

measure the distance between any pair of atoms that you select. Measure the following distances: Ag···Ag separation, -C=C- separation, Ag-N1 distance, Ag-N2 distance, Ag-O1 distance. The "*Measure distance*" option can be disabled by selecting the "*Select Atoms*" option from the "*Picking Mode*" menu. All measured distances can be deleted from your screen by clicking the "Clear Measurements" option located next to the "*Picking Mode*" menu.

The silver complex can be visualized in other display styles, such as "*Spacefill*" or "*Ellipsoid*". The "*Ellipsoid*" option is usefull for structure-validation purposes to identify atoms with ellipsoids of undesired sizes and shapes.

To create a figure of the complex for publication purposes (or for your report), you need to select the "*Save as*" option in the "*File*" menu. You need to chose a file format (*i.e. .bmp, .jpg, .png* and *.tif*; recommended: *.tif*) from the "*File Format*" menu, as well as the location of the folder where the figure should be placed once the file format in the "*File Format*" menu was selected by clicking "*OK*" (Fig. 68), right).

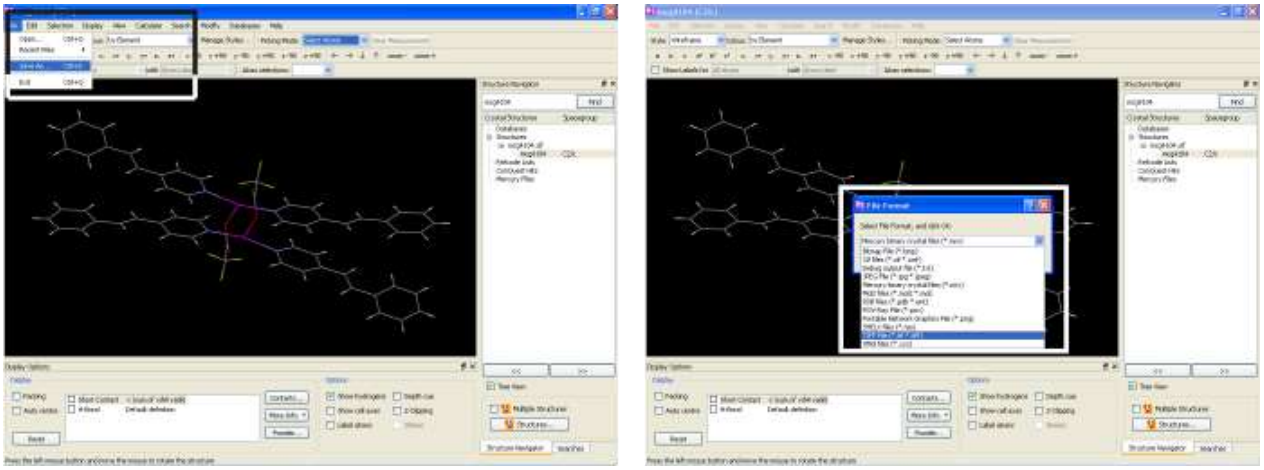

Figure 68 Structure analysis using *Mercury*.

7.5.3 Hazards

Basic organic chemistry laboratory safety procedures should be observed when carrying out the experiment. Protective glass, goggles and lab coat should be worn at all times. The strong base (*t*-BuOK) presents a hazard for chemical burns. The organic solvents should be manipulated only in the well ventilated hoods as their fumes present health hazard. The reaction following the addition of *t*-BuOK/THF is strongly exothermic, thus, there is a potential for explosion and braking of the glass. During the visit to X-ray facility, the students should be warned about hazards of X-ray to pregnant women.

7.5.4 Results and discussion

The HWE synthesis of 4-sbz has proved to be highly robust and effective. Students regularly obtain more than 1 g of 4-sbz. The purity of formed 4-sbz is confirmed using ^{1}H NMR spectroscopy. The formation of single crystals of $[Ag_2(4sbz)_4](CF_3CO_2)_2$ sometimes requires more than a day. This should be kept in mind when planning the experiment and at least two days should be allowed to pass following Part C. The competitive selection of the suitable single crystal seems to stimulate interest and enthusiasm among students. The photoreaction is followed using X-ray diffraction as well as ^{1}H NMR spectroscopy. The formation of photoproduct is clearly indicated in ^{1}H NMR data by disappearance of peaks associated with protons on C=C double bonds at 7.6 ppm and appearance of peak at 4.6 ppm associated with formation of cyclobutane product. In the computer lab, within one lab period all students are able to master structure solution and refinement of provided crystal structure, under the guidance of the instructor. Ability to use 3D visualization programs seems to greatly benefit the students' comprehension of spatial organization of studied structures.

CHAPTER 8. CONCLUSIONS AND FUTURE WORK

In this thesis a novel technique to conduct mechanochemistry was described. The method is based on the use of a vortex mixer and enables automated grinding and simultaneous irradiation of a solid sample. Such set up was not commercially available. The vortex grinding method can replace manual mortar-and-pestle grinding, or ball-milling, and it is transparent to UV-light. We demonstrated successful development and application of a vortex method to a solvent-free cocrystallization and supramolecular catalysis in the organic solid state. We also demonstrate that the vortex method can be generalized to the solid-state synthesis of a metal–organic framework (MOF). The vortex grinding is a simple, readily accessible, and automated method to achieve the mechanochemical preparation of supramolecular materials. The relatively low cost of the constituent components means that the method is generally two orders of magnitude less expensive than those present in commercial ball mills. Moreover, the simultaneous combination of grinding and UV irradiation had a favorable effect on rate of supramolecular catalysis. We also expanded the scope of the method by incorporation of small amount of liquid, akin to liquid assisted grinding. Such set-up afforded rapidly and in one step [2.2]paracyclophane. We will next focus on applying the method to solid-state materials based on additional functional groups and of increasingly complex structures.

In chapter 3, we expanded the scope of the supramolecular catalysis of [2+2] photodimerization to 2,2’-bpe as a substrate, res as a catalyst that yields 2,2’-tpcb as a product. In contrast to previously reported system, the catalytic turnover in this system proceeds without input of external energy. The mechanism of catalysis was studied in details using X-ray diffraction and DFT calculations. We uncovered that rotamerism in 2,2’-bpe and 2,2’-tpcb leads to molecular motion akin action of supramolecular torsional spring that may propel molecular displacement necessary for catalysis.

In chapter 4, we report the first cocrystal based on biologically important IC. Moreover, we demonstrated that IC can serve as a molecular receptor in solid state to assemble aromatics in discrete double, triple and quadruple stacks. Such sequential stacking of aromatics in organic solid state has not been yet reported. We also determined that quadruple stack can facilitate topochemical [2+2] photodimerization to afford cyclobutane product in maximal theoretical yield. In future, the scope of indolocarbazoles as templates to direct solid-state reactivity of higher-order assemblies and structures will be investigated.

Next, we report the ability of a product of a template-directed [2+2] photodimerization performed in the organic solid state to act as a template. We uncovered the ability of cbta to assemble 4,4'-bpe into 1D hydrogen-bonded chains in cocrystals of composition (cbta)·2(4,40-bpe). Olefin 4,4'-bpe reacts to form 4,4'-tpcb stereoselectively and in up to 100% yield. We have also isolated a polymorph of (cbta) ·2(4,4'-bpe) that undergoes a rare SCSC reaction that generates 4,4'-tpcb·in near-quantitative yield. The SCSC reactivity allowed us to unambiguously establish the ability of the cyclobutane ring of cbta to act as a scaffold that directs and accommodates the photoreaction and product, respectively. The photoproduct cbta is the first example of a product of a template solid-state reaction shown to act as a template.

Homology, modularity and generality in solid-state organic synthesis are still not firmly established, due to dependence on crystal packing. In this thesis, we presented an important contribution to these topics. The reactivity achieved using the template approach is largely independent of the crystalline environment of the assemblies. Importantly, when difficulties still arise due to the effects of molecular close packing, template screening can be exploited. As a result, we achieved quantitative and stereoselective [2+2] photodimerization of a homologous series of olefins. We also demonstrated that gas-phase DFT calculations can be used to achieve accurate modeling of assemblies that bear reactivity of solids. Considering the rapid development of solid-

state analysis of techniques (e.g., diffractometers) and quantum-mechanical algorithms, we can expect significant progress in the design and prediction of complex multicomponent molecular solids.

In the last chapter, incorporation of concepts of supramolecular chemistry, solid-state reactivity and mechanochemistry in undergraduate curriculum is described. To be fully exploited, it is necessary that chemists at early stage of education are introduced to these concepts in theory, as well as in hand-down approach. We hope that our efforts will foster more interest in supramolecular solid-state chemistry.

REFERENCES

[1] Lehn, J. M. Supramolecular chemistry - molecules, supermolecules, and molecular functional units (Nobel lecture). *Angew. Chem.* **1988**, *100*, 91.

[2] Lehn, J. M. *Proc. Natl. Acad. Sci. U. S. A.* **2002**, *99*, 4763.

[3] Van Der Waals, J.D. The equation of state for gases and liquids *Nobel Lectures in Physics*: **1910**, 254.

[4] Fischer, E. Einfluss der Configuration auf die Wirkung der Enzyme, *Chem. Ber*. **1894**, *27(3)*, 2985.

[5] Wolf, K. L.; Frahm, H.; Harms, H. *Z. physik. Chem.***1937**, *B36*, 237.

[6] Watson, J. D. *The double helix: a personal account of the discovery of the structure of DNA*. **1968**, London: Weidenfeld & Nicolson.

[7] Pedersen, C. J. *J. Amer. Chem. Soc.* **1967**, *89*, 7017.

[8] Fyfe, M. C. T.; Stoddart, J. F. *Acc. Chem. Res.* **1997**, *30*, 393.

[9] Benenson, Y.; Paz-Elizur, T.; Adar, R.; Keinan, E.; Livneh, Z.; Shapiro, E. *Nature* **2001**, *414*, 430.

[10] Lehn, J. M. *Angew. Chem., Int. Ed.* **2013**, *52*, 2836.

[11] Lehn, J. M. *Top. Curr. Chem.***2012**, *322*, 1..

[12] Cheng, P.; Pham, J. D.; Nowick, J. S. *J. Am. Chem. Soc.* **2013**, *135*, 5477.

[13] Daniel, M.; Astruc, *Chem. Rev.* **2004**, *104*, 293.

[14] Davis, J. T. *Angew. Chem., Int. Ed.* **2004**, *43*, 668.

[15] Guo, D.; Liu, Y. *Acc. Chem. Res.***2014**, Ahead of Print.

[16] Desiraju,G. R. *Crystal Engineering. The Design of Organic Solids*, **1989**, Elsevier, Amsterdam

[17] Dunitz, J. D. *Pure Appl. Chem.* **1991**, *63*, 177.

[18] Pepinsky, R., *Phys. Rev.* **1955**, *100*, 971.

[19] Schmidt, G. M. J., *Pure Appl. Chem.* **1971**, *27*, 647.

[20] Bond, A. D. *CrystEngComm* **2007**, *9*, 833.

[21] Dunitz, J. D, *CrystEngComm* **2003**, *5*, 506.

[22] Corey, E. J. *Pure Appl. Chem.* **1967**, *14*, 19.

[23] Desiraju, G. R. *Angew. Chem. Int. Ed.* **1995**, *34*, 2311.

[24] Etter, M. C. *Acc. Chem. Res.* **1990,** *23*, 120.

[25] Burrows, A. D. *Struct. Bonding* **2004**, *108*, 55.

[26] Dunitz, J. D.; Gavezzotti, A. *Acc. Chem. Res.* **1999**, *32*, 677.

[27] Dunitz, J. D.; Schweizer, W. B. *CrystEngComm* **2007**, *9*, 266.

[28] Desiraju, G. R. *CrystEngComm* **2002**, *4*, 499.

[29] Price, S. L. *Chem. Soc. Rev.* **2014**, *43*, 2098.

[30] Lehmann, C. W. *Angew. Chem., Int. Ed.* **2011**, *50*, 5616.

[31] Chezeau, J. M.; Strange, J. H. *Phys. Rep*. **1979**, *53*, 1.

[32] Vogelsberg, C. S.; Garcia-Garibay, M. A. *Chem. Soc. Rev.***2012**, *41*, 1892.

[33] Conyard, J.; Addison, K.; Heisler, I. A.; Cnossen, A.; Browne, W. R.; Feringa, B. L.; Meech, S. R. *Nat. Chem.* **2012**, *4*, 547.

[34] Arcos-Ramos, R.; Rodriguez-Molina, B.; Romero, M.; Mendez-Stivalet, J. M.; Ochoa, M. E.; Ramirez-Montes, P. I.; Santillan, R.; Garcia-Garibay, M. A.; Farfan, N. *J. Org. Chem.***2012**, *77*, 6887.

[35] Biradha, K.; Santra, R. *Chem. Soc. Rev.* **2013**, *42*, 950.

[36] Paul, I. C.; Curtin, D. Y. *Accounts Chem. Res.* **1973**, *6*, 217.

[37] Stoermer, R.; Laage, E. *Ber. Dtsch. Chem. Ges. B* **1921**, *54B*, 77.

[38] Bernstein, H. I.; Quimby, W. C*J. Am. Chem. Soc*.**1943**, *65*, 1845.

[39] Cohen, M. D.; Schmidt, G. M. J. *J. Chem. Soc.* **1964**, 2000.

[40] Schmidt, G. M. J. *Pure Appl. Chem.* **1971**, *27*, 647.

[41] Schmidt, G. M. J. *J. Chem. Soc.* **1964**, 2014.

[42] Gnanaguru, K.; Ramasubbu, N.; Venkatesan, K.; Ramamurthy, V. *J. Org. Chem.,* **1985**, *50*, 2337.

[43] Kearsley, S. K. *The Prediction of Chemical Reactivity within Organic Crystals Using Geometric Criteria, in Organic Solid State Chemistry,* ed. G. R. Desiraju, Elsevier, New York, **1987**.

[44] Cohen, M. D. *Angew. Chem., Int. Ed. Engl.*, **1975**, *14*, 386;

[45] Gavezzotti, A. *J. Am. Chem. Soc.*, **1983**, *105*, 5220.

[46] Green, B.S.; Schmidt, G. M. J. *Tetrahedron Lett*., **1970,** 11, 4249

[47] Elgavi, A.; Green, B. S.; Schmidt, G. M. J.*J. Am. Chem. Soc.*, **1973**, *95*, 2058.

[48] Cheng, X.-M.; Huang, Z.-T.; Zheng, Q.-Y. *Tetrahedron*, **2011**, *67*, 9093.

[49]Xu, R. ; Schweizer, B.; Frauenrath, H. *J. Am. Chem. Soc.*, **2008**, *130*, 11437.

[50] Sharma, C. V. K.; Panneerselvam, K.; Shimoni, L.; Katz, H.; Carrell,

H. L.; Desiraju, G. R. *Chem. Mater.*, **1994**, *6*, 1282.

[51] MacGillivray, L. R.; Reid, J. L.; Ripmeester, J. A. *J. Am. Chem. Soc.* **2000**, *122*, 7817.

[52] MacGillivray, L. R.; Papaefstathiou, G. S.; Friscic, T.; Hamilton, T. D.; Bucar, D.; Chu, Q.; Varshney, D. B.; Georgiev, I. G. *Acc. Chem. Res.***2008**, *41*, 280.

[53] Aoyama, Y.; Endo, K.; Anzai, T.; Yamaguchi, Y.; Sawaki, T.; Kobayashi, K.; Kanehisa, N.; Hashimoto, H.; Kai, Y.; Masuda, Y. *J. Am. Chem. Soc.* 1996, *118*, 5562.

[54] Ito, Y.; Borecka, B.; Trotter, J.; Scheffer, J. R. *Tetrahedron Lett.*1995, *36*, 6083.

[55] Feldman, K. S.; Campbell, R. F. *J. Org. Chem.* 1995, *60*, 1924.

[56] Papaefstathiou, G. S.; Kipp, A. J.; MacGillivray, L. R. *Chem. Commun.* 2001, 2462.

[57] Friscic, T.; MacGillivray, L. R. *Chem. Commun.* 2005, 5748.

[58] Gao, X.; Friscic, T.; MacGillivray, L. R *Angew. Chem., Int. Ed.* 2004, *43*, 232.

[59] Praetorius, P.; F. Korn, *Ber. Dtsch. Chem. Ges.*, **1910**, *43*, 2744.

[60] Lewis, F. D.; Quillen, S. L.; Hale, P. D.; Oxman, J. D. *J. Am.Chem. Soc.*, **1988**, *110*, 1261.

[61] Papaefstathiou, G. S.; Zhong, Z.; Geng, L.; MacGillivray, L. R. *J. Am. Chem. Soc.* **2004**, *126*, 9158.

[62] Chu, Q.; Swenson, D. C.; MacGillivray, L. R. *Angew. Chem., Int. Ed.* 2005, *44*, 3569

[63] Hamilton, T.D.; Papaefstathiou, G.S.; Friscic, T.; Bucar, D.-K.; MacGillivray, L.R. *J. Am. Chem. Soc.*, **2008**, *130*, 14366.

[64] Hamilton,T.D.; Bucar, D.-K.; Baltrusaitis, J.; Flanagan, D.R.; Li, Y.; Ghorai, S.; Tivanski, A.V.; MacGillivray, L.R. *J. Am. Chem. Soc.***2011**, *133*, 3365.

[65] Karunatilaka, C.; Bucar, D.-K.; Ditzler, L.R.; Friscic, T.; MacGillivray, L.R.; Tivanski, A.V. *Angew. Chem., Int. Ed.* **2011**, *50*, 8642.

[66] Sokolov, A. N.; Bucar, D.; Baltrusaitis, J.; Gu, S. X.; MacGillivray, L. R. *Angew. Chem., Int. Ed.* **2010**, *49*, 4273.

[67] James, S. L.; Adams, C. J.; Bolm, C.; Braga, D.; Collier, P.; Friščić, T.; Grepioni, F.; Harris, K.D.M.; Hyett, G.; Jones, W.; Krebs, A.; Mack, J.; Maini, L.; Orpen, A. G.; Parkin, I. P.; Shearhouse, W.C.; Steed, J. W.; Waddell, D.C. *Chem. Soc. Rev.* **2012**, *41*, 413.

[68] Kaupp, G. *CrystEngComm* **2009**, *11*, 388.

[69] Takacs, L. *J. Mineral Met. Mater. Soc.*, **2000**, *52*, 12.

[70] Balaz, P. *Mechanochemistry in Nanoscience and Minerals Engineering*, **2008**, Springer-Verlag, Berlin Heidelberg,

[71] Tanaka, K.; Toda, F. *Chem. Rev.*, **2000**, *100*, 1025.

[72] Friscic, T. *Chem. Soc. Rev.* **2012**, *41*, 3493.

[73] Shmaefsky, B. R. *Biotechnology 101*, **2006,** Greenwood Press, Westpost,

[74] Calandra, G. B.; Whitt, R. S. *J. Clin. Microbio*.,**1980**, *12*, 84.

[75] Colosi, J. C.; Schaal, B. A.; *Nucleic Acid Research*, **1993**, *21*, 1051.

[76] Hanton, S. D.; Parees, D. M. *J. Am. Soc. Mass Spectrom.*, **2005**, *16*, 90.;

[77] Hanton, S. D.; Stets, J. R. *J. Am. Soc. Mass Spectrom.*, **2009**, *20*, 1115.

[78] Friscic, T.; MacGillivray, L. R. *Chem. Commun.* **2003**, 1306-1307.

[79] Friscic, T.; Jones, W. *Cryst. Growth Des.* **2009**, *9*, 1621.

[80] Deguchi, S.; Mukai, S. *Chem. Lett.* **2006**, *35*, 396.

[81] Khawam, A.; Flanagan, D. R. *J. Pharm. Sci.*, **2006**, *95*, 472.

[82] Khawam, A., Flanagan, D. R. *J. Phys. Chem. B*, **2006**, 110, 17315.

[83]Finney, E. E. Finke, R. G. *Chem. Mater.*, **2009**, 21, 4692.

[84] McBride, J. M.; Segmuller, B. E.; Hollingsworth, M. D.; Mills, D. E.; Weber, B. A. *Science*, **1986**, *234*, 830.

[85] *Metal–Organic Frameworks*, ed. MacGillivray, L. R. **2010**. Wiley, New Jersey,

[86] Pichon, A.; Lazuen-Garay, A.; James, S. L. *CrystEngComm*, **2006**, *8*, 211;

[87] Lazuen-Garay, A.; Pichon, A.; James, S. L. *Chem. Soc. Rev.*, **2007**, *36*, 846.

[88] van Leeuwen, Piet W. N.; Editor. *Supramolecular Catalysis*, **2008**, Wiley-VCH **:** Weinheim,

[89] Kelly, T. R.; Zhao, C.; Bridger, G. J. A bisubstrate reaction template. *J. Am. Chem. Soc.* **1989**, *111*, 3744.

[90] Bassani, D. M.; Darcos, V.; Mahony, S.; Desvergne, J. *J. Am. Chem. Soc.* **2000**, *122*, 8795.

[91] Toda, F.; Tanaka, K.; Sekikawa, A *J. Chem. Soc., Chem. Commun.* **1987**, 279.

[92] Hirano, S.; Yoshizawa, K.; Toyota, S.; Toda, F.; Urbanczyk-Lipkowska, Z. *Mendeleev Commun.* **2003**, 141-144.

[93] Klosterman, J. K.; Yamauchi, Y.; Fujita, M. *Chem. Soc. Rev.* **2009**, *38*, 1714.

[94] Gale, P. A. *Chem. Commun.* **2008**, 4525.

[95] Prudhomme, M*Curr. Med. Chem.* **2000**, *7*, 1189.

[96] Gale, P. A. *Chem. Commun.* **2008**, 4525-4540.

[97] Banerji, A.; Bandyopadhyay, D.; Basak, B.; Biswas, P. K.; Banerji, J.; Chatterjee, A. Chem. Lett. 2005, 34, 1500.

[98] Ramamurthy, V.; Venkatesan, K. *Chem. Rev.***1987**, *87*, 433.

[99] Berg, J. M.; Tymoczenko, J. L.; Stryer, L. *Biochemistry*, 5th ed.; W. H. Freeman: New York, NY, 2002.

[100] Pietrs, R. J.; Huc, I.; Rebek Jr., J. *Angew. Chem.* **1994**, *106*, 1667.

[101] Pietrs, R. J.; Huc, I.; Rebek Jr., J. *Angew. Chem.* **1994**, *106*, 1667.

[102] Kassiandis, E.; Philp, D. *Chem. Commun.* **2006**, 4072.

[103] Halasz, I. *Cryst. Growth. Des.* **2010**, *10*, 2817.

[104] Frisčić, T.; MacGillivray, L. R. *Chem.Commun.* **2005**, 5748.

[105] Ghosn, M. W.; Wolf C. *J. Org. Chem.*, **2010**, *75*, 6653.

[106] Friscic, T.; MacGillivray, L. R. Chem. Commun. 2009, 773.

[107] Diederich, F.; Stang, P. J., Eds.; *Templated Organic Sthesis;* **2000,** Wiley-VCH: New York

[108] Stryer, L. *Biochemistry,* **1988**, W.H. Freeman and Co.: New York

[109] Leiserowitz, L.; Schmidt, G. M. J. *Acta Cryst.* **1965**, *18*, 1058.

[110] Atkinson, M. B. J.; Bucar, D.; Sokolov, A. N.; Friscic, T.; Robinson, C. N.; Bilal, M. Y.; Sinada, N. G.; Chevannes, A.; MacGillivray, L. R. *Chem. Commun.* **2008**, 5713.

[111] Hamilton, T. D.; Papaefstathiou, G. S.; MacGillivray, L. R. *J. Am. Chem. Soc.* **2002**, *124*, 11606.

[112] Novikov, A. N.; Shapiro, Y. E. *J. Phys. Chem. A*, **2012**, 116, 546.

[113] Friscic, T. *Thesis*, **2006**.

[114] Gordillo, A.; de Jesus, E.; Lopez-Mardomingo, C. *Chem. Commun.* **2007**, 4056.

[115] R. Ahlrichs, M. Baer, M. Haeser, H. Horn, and C. Koelmel Electronic structure calculations on workstation computers: the program system TURBOMOLE Chem. Phys. Lett. 162: 165 (1989).

[116] O. Treutler and R. Ahlrichs Efficient Molecular Numerical Integration Schemes J. Chem. Phys. 102: 346 (1995)

[117] Fully Optimized Contracted Gaussian Basis Sets of Triple Zeta Valence Quality for Atoms Li to Kr. A. Schaefer, C. Huber and R. Ahlrichs; J. Chem. Phys. 100,5829 (1994).

[118] Auxiliary Basis Sets to approximate Coulomb Potentials Chem. Phys. Lett. 240: 283 (1995) K. Eichkorn, O. Treutler, H. Oehm, M. Haeser and R. Ahlrichs Chem. Phys. Lett. 242: 652 (1995) Auxiliary Basis Sets for Main Row Atoms and their Use to approximate Coulomb Potentials K. Eichkorn, F. Weigend, O. Treutler and R. Ahlrichs Theo. Chem. Acc. 97: 119 (1997) Accurate Coulomb-fitting basis sets for H to Rn F. Weigend Phys. Chem. Chem. Phys. 8: 1057 (2006)

[119] S. Grimme. Semiempirical ggc-type density functional constructed with a long-range dispersion contribution. J. Comput. Chem., 27(15), 1787-1799, (2006). S. Grimme; J. Antony; S. Ehrlich; H. Krieg. A consistent and accurate ab initio parametrization of density functional dispersion correction (DFT-D) for the 94 elements H-Pu. J. Chem. Phys., 132, 154104, (2010).

[120] Data obtained from the Alliance for the Responsible Atmospheric policy,

http://www.arap.org/

[121] Adopted quote by Leopold Ružička, 1939 Nobel Prize in Chemistry laureate

[122] James, S. L.; Adams, C. J.; Bolm, C.; Braga, D.; Collier, P.; Friščić, T.; Grepioni, F.; Harris, K.D.M.; Hyett, G.; Jones, W.; Krebs, A.; Mack, J.; Maini, L.; Orpen, A. G.; Parkin, I. P.; Shearhouse, W.C.; Steed, J. W.; Waddell, D.C. *Chem. Soc. Rev.* **2012**, *41*, 413.

[123] Friščić, T.; Hamilton, T. D.; Papaefstathiou, G. S.; MacGillivray, L. R. *J. Chem. Educ.* **2005**, *82*, 1679.

[124] The experiment is an adaptation of the work published in: Chu, Q.; Swenson, D. C.; MacGillivray, L. R. *Angew. Chem.* **2005**, *117*, 3635.

APPENDIX: TABLES OF CRYSTALLOGRAPHIC DATA

Table 1 Relevant Crystallographic parameters for the crystals of (res)·(2,2'-tpcb).

Compound	**(res)·2(2,2'-tpcb)**
Chemical formula	C30 H26 N24 O2
Formula mass	476.6
Crystal system	monoclinic
Space group	$P2_1/n$
a/Å	11.8171(13)
b/Å	15.6944(17)
c/Å	12.8618(157)
α/°	90.00
β/°	93.961(5)
γ/°	90.00
V / Å^3	2527.5(5)
T / K	293(2)
Z	8
Crystal dimensions	.32x.21x.055
Calculated density	1.347
Radiation type	MoK\a
Wavelength	0.71073
θ_{max}	25.00
μ / mm^{-1}	
No. of reflections measured	4433
No. of independent reflections	3387
Parameters	361
R_1 ($I > 2\sigma(I)$)	0.0417
$wR(F^2)$ ($I > 2\sigma(I)$)	0.1263
R_1 (all data)	0.0643
$wR(F^2)$ (all data)	0.1505
Goodness of fit on F^2	0.920

Table 2 Relevant Crystallographic parameters for the crystals of IC, $(IC)_2$(4,4'-bpe)$_2$·2(AcN), $(IC)_2$(4,4'-bpe)$_3$, $(IC)_2$(4,4'-bpe)$_4$, and (IC)(4,4'-tpcb).

Compound	**IC**	**(IC)$_2$(4,4'-bpe)$_2$·2(AcN)**	**(IC)$_2$(4,4'-bpe)$_3$**	**(IC)$_2$(4,4'-bpe)$_4$**	**(IC)(4,4'-tpcb)**
Chemical formula	C18 H12 N2	C32 H25 N5	C72 H54 N10	C42 H32 N6	C42 H32 N6
Formula mass	256.30	479.57	1059.25	620.74	620.74
Crystal system	monoclinic	monoclinic	monoclinic	monoclinic	monoclinic
Space group	$P2_1/c$	$P2_1/n$	$P2_1/c$	$P2_1/c$	$P2_1/c$
a/Å	5.7523(7)	10.4092(11)	25.389(3)	14.9113(16)	16.0937(17)
b/Å	27.213(3)	12.0921(13)	11.4526(12)	10.9827(12)	10.0171(11)
c/Å	16.1851(17)	20.944(3)	19.5016(19)	20.619(3)	21.329(3)
α/°	90.00	90.00	90.00	90.00	90.00
β/°	93.961(5)	102.766(5)	103.813(5)	101.104(5)	107.036(5)
γ/°	90.00	90.00	90.00	90.00	90.00
V / Å^3	2527.5(5)	2571.0(5)	5506.5(10)	3313.5(7)	3287.6(7)
T / K	293(2)	293(2)	293(2)	293(2)	293(2)
Z	8	4	4	4	4
Crystal dimensions	.32x.21x.055	.44x.4x.05	.38x.14x.04	.36x.16x.015	.36x.26x.12
Calculated density	1.347	1.239	1.278	1.244	1.244
Radiation type	MoK\a	MoK\a	MoK\a	MoK\a	MoK\a
Wavelength	0.71073	0.71073	0.71073	0.71073	0.71073
θ_{max}	25.00	25.00	25.00	25.00	25.00
μ / mm^{-1}					
No. of reflections measured	4433	4517	9682	19080	5774
No. of independent reflections	3387	3163	5196	5803	4505
Parameters	361	335	758	442	441
R_1 ($I > 2\sigma(I)$)	0.0417	0.0522	0.0572	0.0874	0.0631
$wR(F^2)$ ($I > 2\sigma(I)$)	0.1263	0.1517	0.1440	0.2177	0.1277
R_1 (all data)	0.0643	0.0857	0.1402	0.2346	0.0631
$wR(F^2)$ (all data)	0.1505	0.1811	0.1854	0.2830	0.1519
Goodness of fit on F^2	0.920	1.038	0.965	0.920	1.160
CCDC number	**940861**	**940862**	**940863**	**940860**	**940859**

Table 3 Relevant crystallographic parameters for the crystals of (cbta)·2(4,4'-bpe), *Form I* and *Form II*, and (cbta)·(4,4'-tpcb).

Compound	**(cbta)·2(4,4'-bpe), *Form I***	**(cbta)·2(4,4'-bpe), *Form II***	**(cbta)·(4,4'-tpcb)**
Chemical formula	C32 H28 N4 O8	C32 H28 N4 O8	C32 H28 N4 O8
Formula mass	596.58	596.58	596.58
Crystal system	monoclinic	triclinic	triclinic
Space group	$P2_1/c$	$P\bar{1}$	$P\bar{1}$
a/Å	7.0625(4)	7.3377(4)	9.131(5)
b/Å	10.8486(6)	11.3673(7)	11.006(6)
c/Å	18.2963(8)	18.0101(11)	15.272(7)
α/°	90.00	74.380(5)	99.50(3)
β/°	94.908(5)	90.072(5)	98.70(2)
γ/°	90.00	70.386(5)	110.13(3)
V / Å^3	1396.69(13)	1355.82(15)	1384.9(12)
T / K	298	130	293
Z	2	2	2
Crystal dimensions	0.39x0.35x0.21	0.4x0.2x0.07	0.18x0.055x0.03
Calculated density	1.419	1.461	1.431
Radiation type	Mo K_α	Mo K_α	Mo K_α
Wavelength	0.7107	0.7107	0.71073
θ_{max}	29.27	29.220	20.000
μ / mm^{-1}	0.104	0.107	0.105
No. of reflections measured	7917	14415	4283
No. of independent reflections	3266	6336	2498
Parameters	207	432	397
R_1 ($I > 2\sigma(I)$)	0.0524	0.0818	0.1189
$wR(F^2)$ ($I > 2\sigma(I)$)	0.1103	0.1994	0.2186
R_1 (all data)	0.0908	0.1213	0.2534
$wR(F^2)$ (all data)	0.1311	0.2291	0.2754
Goodness of fit on F^2	1.017	1.045	1.159
CCDC number	**899403**	**901408**	**901557**

Table 4 Relevant crystallographic parameters for the crystals of 2(4,6-didpe-res)·2(4,4'-bpe), 2(4,6-didpe-res)·2(3,3'-bpe), 2(4,6-didpe-res)·2(2,2'-bpe)

Compound	**2(4,6-didpe)·2(4,4'-bpe)**	**2(4,6-didpe)·2(3,3'-bpe)**	**2(4,6-didpe)·2(2,2-bpe)**
Chemical formula	C92 H80 N4 O4	C92 H80 N4 O4	C92 H80 N4 O4
Formula mass	652.8	652.8	652.8
Crystal system	triclinic	triclinic	monoclinic
Space group	$P\bar{1}$	$P\bar{1}$	$P2_1/c$
a/Å	9.6606(11)	7.3377(4)	21.3040(30)
b/Å	10.5249(12)	11.3673(7)	15.5584(16)
c/Å	18.0016(19)	18.0101(11)	12.2733(13)
α/°	81.978(5)	74.380(5)	90.00
β/°	83.520(5)	90.072(5)	94.668(5)
γ/°	79.00	70.386(5)	90.00
V / Å^3	1773.69(13)	1355.82(15)	4054.57(12)
T / K	298	130	150
Z	2	2	2
Crystal dimensions	0.34x0.18x0.13	0.4x0.2x0.07	0.18x0.05x0.03
Calculated density	1.22	1.461	1.23
Radiation type	Mo K_α	Mo K_α	Mo K_α
Wavelength	0.7107	0.7107	0.7107
θ_{max}	27.88	29.220	20.000
μ / mm^{-1}	0.0744	0.107	0.105
No. of reflections measured	6251	14415	4283
No. of independent reflections	3266	6336	2498
Parameters	451	432	397
R_1 ($I > 2\sigma(I)$)	0.0677	0.0818	0.0542
$wR(F^2)$ ($I > 2\sigma(I)$)	0.1103	0.1994	0.1123
R_1 (all data)	0.01055	0.1213	0.0982
$wR(F^2)$ (all data)	0.2185	0.2291	0.1311
Goodness of fit F^2	1.104	1.045	1.019